MICROWAVE SPECTRA AND MOLECULAR STRUCTURES OF ORGANIC MOLECULES AND HYDROGEN BONDED DIMERS

by

Aaron Matthew Pejlovas

A Dissertation Submitted to the Faculty of the

DEPARTMENT OF CHEMISTRY AND BIOCHEMISTRY

In Partial Fulfillment of the Requirements

For the Degree of

DOCTOR OF PHILOSOPHY

WITH A MAJOR IN CHEMISTRY

In the Graduate College

THE UNIVERSITY OF ARIZONA

2018

THE UNIVERSITY OF ARIZONA

GRADUATE COLLEGE

As members of the Dissertation Committee, we certify that we have read the dissertation prepared by Aaron M. Pejlovas, titled Microwave Spectra and Molecular Structures of Organic Molecules and Hydrogen Bonded Dimers and recommend that it be accepted as fulfilling the dissertation requirement for the Degree of Doctor of Philosophy.

Stephen G. Kukolich Date: April 2, 2018
Dr. Stephen G. Kukolich

Michael F. Brown Date: April 2, 2018
Dr. Michael F. Brown

Dennis L. Lichtenberger Date: April 2, 2018
Dr. Dennis L. Lichtenberger

Lucy M. Ziurys Date: April 2, 2018
Dr. Lucy M. Ziurys

Final approval and acceptance of this dissertation is contingent upon the candidate's submission of the final copies of the dissertation to the Graduate College.

I hereby certify that I have read this dissertation prepared under my direction and recommend that it be accepted as fulfilling the dissertation requirement.

Stephen G. Kukolich Date: April 2, 2018
Dissertation Director: Dr. Stephen G. Kukolich

STATEMENT BY AUTHOR

This dissertation has been submitted in partial fulfillment of the requirements for an advanced degree at the University of Arizona and is deposited in the University Library to be made available to borrowers under rules of the Library.

Brief quotations from this dissertation are allowable without special permission, provided that an accurate acknowledgement of the source is made. Requests for permission for extended quotation from or reproduction of this manuscript in whole or in part may be granted by the head of the major department or the Dean of the Graduate College when in his or her judgment the proposed use of the material is in the interests of scholarship. In all other instances, however, permission must be obtained from the author.

SIGNED: Aaron Matthew Pejlovas

ACKNOWLEDGEMENTS

I want to thank Dr. Stephen G. Kukolich for all his guidance throughout my journey of graduate school. Without his advice and mentorship, I would not be the scientist I have developed into today. I also want to acknowledge all of the professors I have had, in my undergraduate career here at the University of Arizona as well as my graduate career, teaching me the fundamentals of the wonderful field of chemistry.

Additionally, I want to acknowledge the University of Arizona for the great education I received throughout my tenure here. It has been an honor to have been able to complete my graduate degree at the same great university I attended for my Bachelor's. Lastly, I would like to thank the National Science Foundation for the funding to perform the research presented in this dissertation. I look forward to my journey ahead, wherever my career and life may take me.

DEDICATION

For my mom, dad, family, and beautiful loving wife, Rhianna. Thank you all for the support and love that helped me get through this endeavor.

Table of Contents

LIST OF FIGURES

LIST OF TABLES

ABSTRACT

The microwave spectra were measured in the 4-15 GHz regime for cyclopropanecarboxylic acid, 1,2-cyclohexanedione, maleimide, phthalimide, and 4a,8a-azaboranaphthalene. Doubly hydrogen bonded dimers formed with formic acid were also measured with the molecules cyclopropanecarboxylic acid, 1,2-cyclohexanedione, maleimide, and tropolone. Measurements were made using a pulsed beam Fourier transform microwave spectrometer. Rotational and centrifugal distortion constants were determined from the microwave spectra. In the case of the systems that exhibit electric quadrupole coupling interactions, the electric quadrupole coupling strengths were also determined from the analysis of the hyperfine structure in the spectra, yielding additional electronic structure information for the molecules studied. The spectra were also measured for a number of unique, singly substituted isotopologues under natural abundance concentrations. This isotopologue data is crucial in order to obtain key gas phase molecular structure parameters of the molecules and complexes studied. Many theoretical computations, using *ab initio* and DFT methods, were also performed to obtain optimized electronic structures of the systems studied. These computations aid in the search and assignments of the rotational transitions measured. Comparisons between the theory and the experimental results are described in greater detail in the respective chapters for those systems. The experimental results for the organic systems studied agreed well (within a few percent) with the gas phase optimization computations performed.

1. INTRODUCTION

Scientific research has reached a point throughout its inspiring history that making use of theoretical models and computational predictions for molecular systems is of fundamental importance. These models are crucial to chemists such as in the areas of spectroscopy, organic synthesis, or in the development of new catalysts for important industrial applications such as hydrogen production. The high resolution that microwave spectroscopy provides enables this technique to be an invaluable tool in gauging the predictive power of currently existing theoretical models. The gas phase structures determined from the microwave spectra are the best “free molecule” representations of systems, absent of many of the types of interactions that are observed in condensed phases. The types of molecules studied in this dissertation cover a range of organic molecules and hydrogen bonded dimers. These systems provide great benchmarks on which to refine the currently available theoretical methods. The gas phase molecular structures obtained for the systems studied in this dissertation are discussed in the following chapters.

Spectroscopy is the technique in which the energy levels of a molecule are studied with electromagnetic radiation. The radiation excites the molecules from one lower energy state to a higher energy state, as in the case of the absorption, or radiation is emitted when a molecule relaxes from a higher energy state to a lower energy state. In the case of microwave spectroscopy, or rotational spectroscopy, microwave radiation between 1-1000 GHz is used to excite molecules that have permanent electric dipole moments from one rotational (or ro-vibrational) state to another. Valuable information can be gained about the systems studied by measuring the microwave spectra, such as

key gas phase structural parameters, electronic structure information of molecules, and information about the dynamics of some systems, for example concerted double proton tunneling in hydrogen bonded dimers. The microwave spectrometer used to measure the rotational spectra of the molecules studied in this dissertation is described in greater detail in chapter two, but will also be briefly described here. First the molecules are pulsed into the microwave cavity maintained at low pressures of about 10^{-7} Torr using a solenoid pulsed valve. The low pressure in the cavity is achieved using a mechanical fore pump and a diffusion pump. This cavity has two spherical mirrors that can be tuned to resonance. This resonance condition is achieved when there are an integer number of half wavelengths of the radiation radiating between the two mirrors. The microwave pulses are generated and then coupled to the cavity with a small quarter wave antenna protruding from a fixed mirror. This type of microwave cavity with these two spherical mirrors is called a Fabry-Pérot resonator. Shortly after the molecular beam is pulsed into the cavity using the solenoid valve, a one microsecond burst of radiation is generated at the microwave switch and is coupled into the cavity with the antenna. If the frequency of this resonant radiation is within ± 1 MHz of a rotational transition in the molecule, by the uncertainty principle, the sample will become coherently polarized. After a short time the molecules will begin to relax and emit a molecular free induction decay signal, or FID. From the recorded FID signal, a rotational transition frequency is measured.

The theory of quantum mechanics and angular momenta describe the energy levels and assignments of all of the rotational transitions observed in this dissertation. The sources of angular momenta within these individual molecules can arise from the

rotation of the molecule, the nuclear spin, the electronic spin, and also the electronic state of the molecule. Chapter three provides a brief description of the rotational energy level expressions for symmetric and asymmetric top molecules as well as centrifugal distortion corrections. Real molecules are not rigid and this distortion significantly affects the rotational energy levels with large J and K quantum numbers. Chapter three also discusses some of the computational details used in this dissertation, but the details pertaining to the specific systems studied are given in their respective chapters. The optimization of the gas phase molecular structure is one key to analyzing the microwave spectra. Much of the time, the theoretical models used will yield rotational constants in fair agreement with the experimental results, but that is not always the case as is observed for some organometallic systems which may be off by 10% or more. It is crucial to compare the experimental results from these microwave studies to that of theory due to the importance of having accurate models to describe, for instance, the hydrogen bonding and proton tunneling dynamics within large enzymes or in macromolecules such as DNA. Obtaining this information about these small benchmark systems will aid future scientific research in advancing theoretical models, as well as provide chemists with an idea of which models accurately describe systems of interest.

The organic molecules studied in this dissertation are similar to many of the small molecules synthesized for drug-development and used in organic synthesis. The computational theory used in this dissertation can predict structural parameters to within a few percent for some systems, but the larger systems become more difficult to model with the currently available theoretical methods. This is partly due to the lack of computational power to efficiently optimize and determine the structures of the

molecules using high levels of theory. Therefore it is important to study these small organic molecules, as detailed in this dissertation, to provide these benchmarks for theoreticians. Chapter four focuses on the results of simple organic molecules that are considered large in the microwave spectroscopy realm. Examples of the systems studied are cyclopropanecarboxylic acid (CPCA, Figure 1.1) and 1,2-cyclohexanedione (1,2-CDO, Figure 1.2).

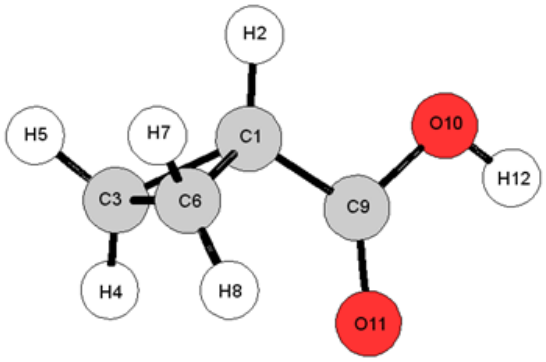

Figure 1.1 Ground state structure of cyclopropanecarboxylic acid.

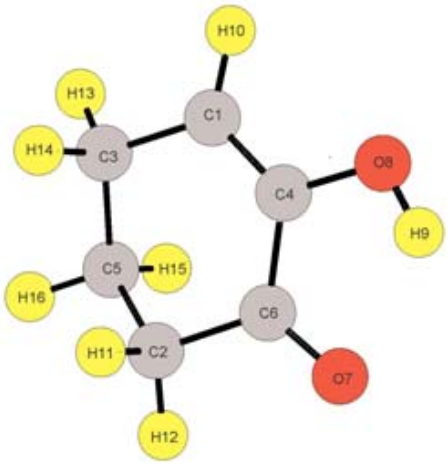

Figure 1.2 Molecular structure of 1,2-cyclohexanedione in its monoenolic form.

In the case of CPCA, the microwave spectra revealed an additional excited state conformer that had not been observed in previous microwave studies. It is important to

measure the spectra of the excited states of molecules as computational theory needs to be put to the test with these excited state structures. It is also important to characterize these excited states as some chemical reactions or enzymatic processes may begin from only the excited state conformer of a substrate. Knowing the structures of these high energy states is essential to determining reaction mechanisms. The study of 1,2-cyclohexanedione revealed that the prominent structure observed in the gas phase was a monoenolic tautomer, as opposed to the dione. The prevalence of this tautomer indicates the enol form is lower in energy, possibly due to the intramolecular hydrogen bond formed by the enol and the remaining ketone, which is similar to the intramolecular interaction observed in molecules such as tropolone.

The complexity of the microwave spectra of the organic molecules studied is increased when organic molecules have nuclei with nuclear spin greater than one half. These nuclei have nonspherical charge distributions and quadrupole moments that generate a measureable hyperfine structure in the microwave spectra. Chapter five discusses the molecules that have one nitrogen nucleus (nuclear spin = 1) in two of the molecules, maleimide and phthalimide, and 4a,8a-azaboranaphthalene where there are both boron and nitrogen nuclei (^{10}B and ^{11}B both have nuclear spins of 3 and 3/2 respectively). These molecules are shown in Figure 1.3 A-C.

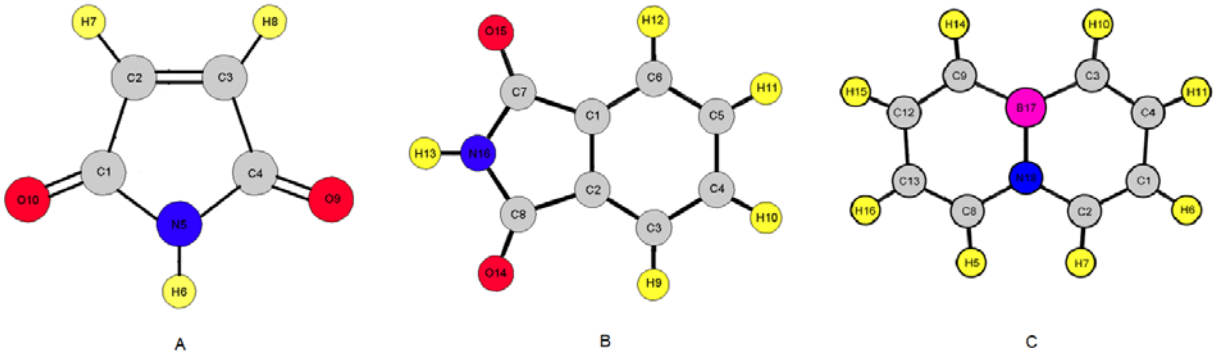

Figure 1.3 Molecular structures of A) maleimide, B) phthalimide, and C) 4a,8a-azaboranaphthalene.

Due to these molecules exhibiting the electric quadrupole hyperfine structure, additional electronic structure information can be gained about these systems. The quadrupole coupling strengths determined from the analysis of the hyperfine structure directly provide electron charge distributions. In the case of 4a,8a-azaboranaphthalene, an extended Townes-Dailey analysis was performed to determine the numbers of electrons in each of the nuclei's (^{11}B and ^{14}N) valence hybridized orbitals, which provides some insight into the extent of the aromatic character exhibited in this molecule.

The pulsed beam microwave technique also provides an efficient method to form and isolate hydrogen bonded systems in the gas phase.[1] The doubly hydrogen bonded dimers formed with formic acid, as studied in this dissertation, represent a class of noncovalent systems whose structures may not be described very well by the theoretical methods available. Some previously studied doubly hydrogen bonded dimers, such as the dimer formed between formic acid and propiolic acid or benzoic acid and formic acid, exhibit a concerted double proton tunneling motion between the two molecules. Spectral splittings are observed in the microwave spectra caused by the

tunneling motion and these splittings are further analyzed to obtain information on the dynamics of this tunneling process, such as the tunneling splitting between the two states involved. Additional information can be deduced about the barrier height in the potential energy surface through simple models of the potential energy surface. As many doubly hydrogen bonded dimers exhibit the concerted tunneling motion, it is crucial to study more hydrogen bonded dimers in order to determine the information about the dynamics of the tunneling process. It seems that the dimers that exhibit this tunneling motion have a C_{2v}(M) symmetry[2] or a C_{2v} symmetry at the transition state (the point where the two protons are equidistant between the two molecules). This symmetry creates a symmetric double well potential energy surface that allows for the tunneling motion to be resolved in the spectra. One question to answer is: how asymmetric can these dimers be and still exhibit the tunneling motion? It would be very important if this tunneling motion is observed in asymmetric dimers to gain the information about the tunneling motion in these dimers with asymmetric potential energy surfaces. Chapter six discusses the results obtained from the dimers studied in great detail.

2. RESEARCH METHODS

2.1 INTRODUCTION

The microwave spectrometers used to measure the high resolution microwave spectra of all the molecules and complexes studied in this dissertation are Flygare-Balle type pulsed beam Fourier transform microwave (PBFTMW) spectrometers. They have very high resolution and sensitivity that allows for the measurement of many singly substituted isotopologues under natural abundance concentrations. The sensitivity is so great that a ^{15}N singly substituted isotopologue was able to be observed in BN-naphthalene discussed in chapter 5.3. This is the largest molecule in which ^{15}N was observed under natural abundance. Successful experiments consist of performing electronic structure computations to optimize the equilibrium gas phase structures followed by introducing the molecules into the gas phase which are then pulsed into the PBFTMW spectrometer with a Ne carrier gas by a solenoid pulsed valve. Following the measurements, the transitions are assigned to the correct rotational energy levels to yield very accurate rotational constants. These rotational constants obtained from the assigned spectra are used further to determine the gas phase structural parameters of the molecule through a nonlinear least squares fitting routine.

2.2 MICROWAVE SPECTROMETER

The PBFTMW spectrometer used in this dissertation has been developed and reported previously.[3,4] The resolution of spectrometer one (SP1) is about 10 kHz and the frequency bandwidth covered for each stimulation frequency is about ±1 MHz, due to the uncertainty principle. A block diagram of this microwave spectrometer is shown

below in Figure 2.2.1. The molecular beam, which includes the neon carrier gas and the gaseous sample, is pulsed transversely into the Fabry-Pérot resonance cavity at a rate of ~2 Hz. Within the Fabry-Pérot cavity, there are two spherical mirrors 30 cm in diameter with a 60 cm radius of curvature. The microwave radiation pulse is coupled to the cavity using a coaxial cable connected to a quarter wave antenna that lies parallel to the mirror's surface. The coupling of the radiation can be adjusted by modifying the distance between the mirror and the antenna. Under the current conditions of the spectrometer, the frequency range of 4-18 GHz is accessible to probe the molecules of interest.

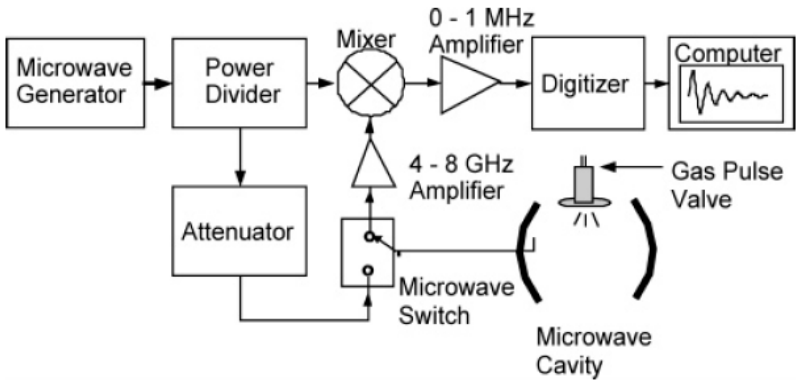

Figure 2.2.1. Block diagram of the electronics for the pulsed-beam Fourier transform microwave spectrometer.

Once the molecular sample has been pulsed into the microwave cavity, a π/4 microwave signal is generated at about 10 dBm (~10 mW) and passed through an attenuator to decrease the power of this signal further. A pulse of this signal is then sent into the cavity, about 1 ms after the molecular beam is pulsed into the cavity. The microwave pulse is generated by sending a 1 μs electrical signal to the fast microwave

switch triggering it, allowing for a 1 μs burst of radiation to couple into the cavity. When the mirrors are tuned to resonance for a specific stimulation frequency, the microwave radiation will resonate between the mirrors and if the stimulation frequency is close to the rotational transition frequency of the molecule (± 1 MHz due to the uncertainty principle), the molecules pulsed into the cavity will be coherently polarized in the resonant electromagnetic beam. After the stimulating microwave pulse decays, the molecular emission signal caused by the relaxation of the coherently polarized sample (free induction decay or FID) is collected for ~100 μs and allowed to pass through a homodyne detection system. The molecular signal is passed through an amplifier (shown as 4-8 GHz in Figure 2.2.1) and mixed with the synthesized stimulation frequency. The mixed signal is passed through a 0-1 MHz amplifier, digitized at 5 MHz, and the FID is recorded with a PICO scope (a multichannel analog to digital converter) that is displayed on the computer through the data collection program which displays the average signal collected. The computer subsequently will perform a Fourier transform on the measured FID to obtain the data in the frequency domain. Successful measurements of rotational transitions depend heavily on the delays between each of the electrical signals that activate the valve, microwave switch and FID data collection. The sequence of each of the pulses in the spectrometer design can be seen in Figure 2.2.2. The top trace shows the signal sent to the solenoid pulsed valve and after the 1 ms delay (indicated by the green dashed line) the short microsecond transmit signal is sent to the microwave switch (bottom trace) that allows the coupling of the radiation into the cavity. After the microwave pulse decays (indicated by the receive delay shown by

the spacing between the blue and red lines) the signal to begin data collection begins (middle trace).

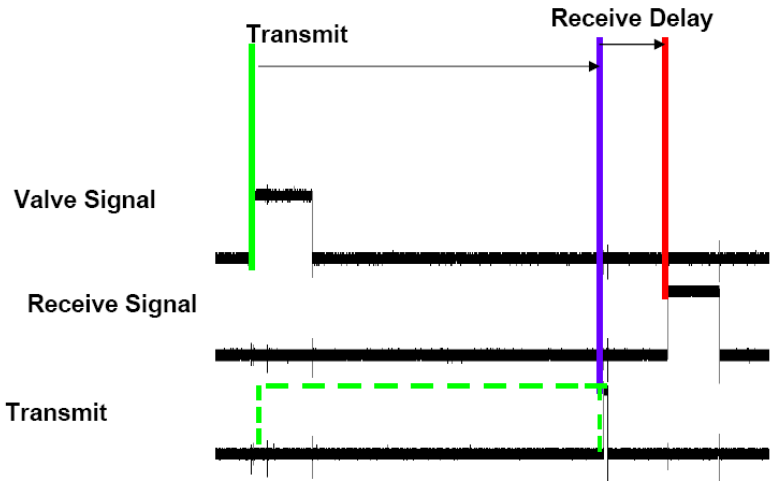

Figure 2.2.2. Pulse sequence of spectrometer. The valve opens and after a 1 ms delay, a short 1 μs pulse of microwave radiation is sent through the microwave switch and the radiation fills the cavity. After a short time, the PICO scope is triggered and 100 μs of data is collected.

To find the resonant mode of the mirrors for a specific stimulating frequency, the reflected signal out of the cavity is monitored using a directional coupler and recorded using a standard 2 channel oscilloscope (Figure 2.2.3). At a given stimulation frequency, a DC motor operated by the user moves the mirrors until the cavity is in resonance. The resonant condition is determined by a decrease in reflected signal recorded from the microwave cavity. The decrease in reflected signal occurs when there are an integral number of half wavelengths of the radiation between the two mirrors. The Q-values, or quality values ($f / \Delta f$), for the resonant condition in the microwave spectrometer are on the order of 30000, indicating a high quality resonant cavity.

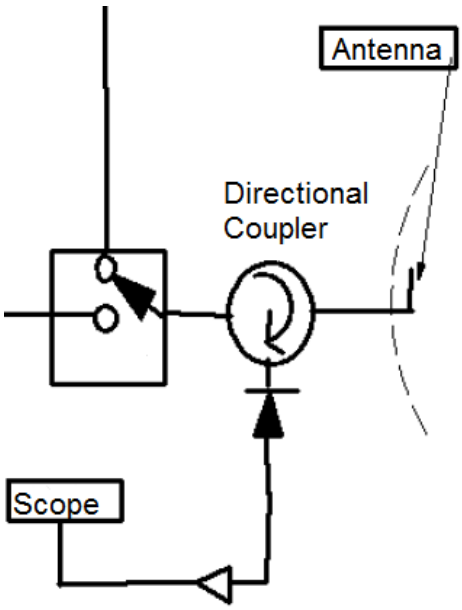

Figure 2.2.3. Diagram showing directional coupler used to monitor reflected microwave signal.

To more efficiently scan frequency ranges of the rotational transitions predicted, an automatic scan program was developed previously for the instrument, called AutoScan 6.0.[5] The AutoScan program allows the computer to control an HP 8673E frequency synthesizer through its general purpose interface bus (GPIB) and track the resonant condition by monitoring the reflected signal. The reflected signal is integrated by a simple op-amp circuit and the integrated signal is sent to the AutoScan program and the minimum reflected signal is found, indicating the cavity is in resonance. To set up the AutoScan program to scan a desired frequency range, the input file is created to contain the starting and ending frequencies. The starting frequency is entered into the HP frequency synthesizer, the resonant condition is found manually, and the program is initiated. The program will undergo a specific number of pulsed beam cycles for a given stimulating frequency, which is also dictated in the input script file. Once the number of

pulses has been met, the program will save the file with the given frequency as the file name and then will move the mirrors slightly, depending on the voltage supplied to the DC motor. The frequency sweeps 1 MHz to find the minimum reflected signal and the frequency is set that corresponds to the minimum. The voltage to the motor is adjusted at a potentiometer control to allow the step sizes in stimulating frequency to be about 200 to 300 kHz, sufficient to save multiple FIDs of one rotational transition. To analyze the files saved during an AutoScan sequence, two complementary programs, written in LabVIEW, have also been previously developed for the research lab. Following the analysis of the data with the LabView programs, the rotational transitions are measured manually to obtain more accurate transition frequencies.

2.3 SAMPLE PREPARATION

Many of the molecules studied were purchased and transferred to a specialized glass sample cell that was designed for the lab. This specialized glass cell is shown below in Figure 2.3.1. Once the sample has been carefully transferred into the cell, the cell is connected to the solenoid pulsed valve with a small piece of Tygon tubing or a Swagelok adapter with Teflon ferrules, depending on what temperature the sample and pulsed valve need to be heated to obtain sufficient vapor pressure of the sample. If the temperature exceeds 50 °C, then the Swagelok adapter is used.

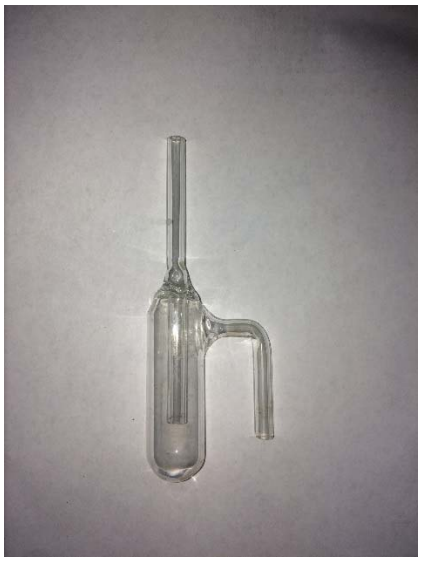

Figure 2.3.1. Specialized glass sample cell used for the microwave experiments in this dissertation.

In the case of some molecules studied, singly deuterated isotopologues were synthesized. These were created by mixing the sample with a deuterated solvent (either D_2O or MeOD) for a few days and the remaining solvent was pumped off under reduced pressure. The deuterated sample was then transferred to the sample cell and the experiment was performed as described.

3. THEORY AND COMPUTATIONS

3.1 THEORY

The rotational quantum number assignments of all the transitions measured in this dissertation can be described with quantum mechanics and the angular momenta within a molecule. The following description will not present all of the mathematics involved in the derivation of rotational energy levels, but will show the important quantum mechanical steps and the final results obtained. The derivations of all solutions presented here are given in great detail in texts by Gordy and Cook[6] and Kroto.[7] The program SPCAT[8] by Dr. Herb Pickett was used to simulate the microwave spectra from the optimization computations. After correctly assigning the rotational energy levels to the transitions measured, these transitions are fit using SPFIT to a set of rotational and centrifugal distortion constants. In the case of the molecules with the electric quadrupole interactions, a set of quadrupole coupling strengths are also determined.

3.1.1 SYMMETRIC TOP ENERGY LEVELS

For a molecule rotating about its center of mass, the generic rotational Hamiltonian can be written as shown below in equation 3.1. The bold letter J represents the quantum mechanical operator for the angular momenta and I_a, I_b, I_c are the moments of inertia with respect to the principal axes in the molecule.

$$\widehat{\boldsymbol{H}} = \left(\frac{\hat{\boldsymbol{J}}_a^2}{2I_a} + \frac{\hat{\boldsymbol{J}}_b^2}{2I_b} + \frac{\hat{\boldsymbol{J}}_c^2}{2I_c}\right) \text{(eq. 3.1)}$$

The components of the angular momenta all lie along the principal axes (denoted a, b, and c). The rotational constants (A, B, and C) are then conveniently defined as:

$$A = \frac{\hbar^2}{2I_a} \text{ (3.2a)}$$

$$B = \frac{\hbar^2}{2I_b} \text{ (3.2b)}$$

$$C = \frac{\hbar^2}{2I_c} \text{ (3.2c)}$$

In the case of a prolate symmetric top, the angular momenta along the b and c principal axes are equivalent. The Hamiltonian can be conveniently written in terms of rotational constants A and B shown in equation 3.3a. After operating on the rotational wavefunction, the energy level expressions are obtained in terms of quantum numbers J and K.

$$\left(B\hat{\boldsymbol{J}}^2 + (A - B)\hat{\boldsymbol{J}}_a^2\right)\psi(\theta, \varphi) = E\psi(\theta, \varphi) \text{ (3.3a)}$$

The other symmetric top case is when the angular momenta along the a and b principal axes are equivalent and this is called an oblate symmetric top. Again, the Hamiltonian can be written in terms of rotational constants B and C shown in equation 3.3b. After operating on the rotational wavefunctions, the energy level expressions are obtained in terms of the quantum numbers J and K.

$$\left(B\hat{\boldsymbol{J}}^2 + (C - B)\hat{\boldsymbol{J}}_a^2\right)\psi(\theta, \varphi) = E\psi(\theta, \varphi) \text{ (3.3b)}$$

The quantum mechanical angular momentum operators $\hat{\mathbf{J}}^2$ and $\hat{\mathbf{J}}_a$ have eigenfunctions which are the associated Legendre polynomials and these eigenfunctions are written in Dirac notation in terms of the quantum numbers J, K, and M as shown in equation 3.4a.

$$| \Psi > = | \mathrm{J\ K\ M} > \text{ (3.4a)}$$

For a symmetric top, K represents the projection of the total angular momentum of the molecule on to the symmetry axis (the a-principal axis for a prolate symmetric top and the c-principal axis for an oblate symmetric top). M is the projection of the total angular momentum on to the laboratory axis, which is usually labeled as z. The projection of the angular momenta on the laboratory axis, M, is important when external electric fields are applied to systems during Stark microwave experiments. These Stark experiments are used to determine electric dipoles of molecules. The eigenvalues for each of the quantum mechanical operators of angular momentum used to derive the rotational energy levels are shown in equations 3.4b-d.

$$< \mathrm{J\ K\ M} \left| \hat{\boldsymbol{J}}^2 \right| \mathrm{J\ K\ M} > = \hbar^2 J(J+1) \quad (3.4b)$$

$$< \mathrm{J\ K\ M} \left| \hat{\boldsymbol{J}}_a \right| \mathrm{J\ K\ M} > = \hbar K \quad (3.4c)$$

$$< \mathrm{J\ K\ M} \left| \hat{\boldsymbol{J}}_z \right| \mathrm{J\ K\ M} > = \hbar M \quad (3.4d)$$

The energy levels for the two symmetric tops can then be derived from equations 3.3 and the eigenvalue results of 3.4b-d. The energy level expressions for the prolate and oblate symmetric top molecules are then written in terms of the rotational constants and the rotational quantum numbers, J and K, shown in equations 3.5a and b.

$$E = (BJ(J+1) + (A-B)K^2) \quad (3.5a)$$

$$E = (BJ(J+1) + (C-B)K^2) \quad (3.5b)$$

The selection rules for the transitions observed for a rigid symmetric top are ΔJ = ±1 and ΔK = 0. These can be derived from the dipole moment matrix elements which will not be discussed here. The change in J can be rationalized in terms of photons possessing unit angular momentum. The selection rule ΔK = 0 can be explained due to

the symmetric top molecules not having a component of the permanent electric dipole perpendicular to the symmetry axis to generate a torque about the axis by interaction with the microwave radiation. There are similarities with the spectrum obtained from a linear molecule, in that the spacing between each transition is equal to 2B. Molecules are, however, not rigid and undergo centrifugal distortion effects that are proportional to J and K and so the spacing between transitions are not uniform. The deviations in the energy levels introduced by centrifugal distortion are very small and are determined using perturbation theory methods, which will be discussed in the following sections.

3.1.2 ASYMMETRIC TOP ENERGY LEVELS

In the case of the asymmetric top molecule, all components of the angular momenta are not equal and so the rotational Hamiltonian cannot be expressed in simple terms of $\mathbf{J}^2$ and only one of the components of **J**. If the asymmetric top is very close to one of the symmetric top limits, then it is useful to write the rotational Hamiltonian in a form that takes advantage of the near symmetric top symmetry. The rotational Hamiltonian for the asymmetric top can then be written as shown in equation 3.6 in which a, b, and c are just parameters related to the rotational constants, depending on the symmetry of the molecule.

$$\widehat{\boldsymbol{H}} = \frac{1}{2}(a+b)(\hat{\boldsymbol{J}}_a^2 + \hat{\boldsymbol{J}}_b^2) + c\hat{\boldsymbol{J}}_c^2 + \frac{1}{2}(a-b)(\hat{\boldsymbol{J}}_a^2 - \hat{\boldsymbol{J}}_b^2) \quad (3.6)$$

The Hamiltonian can then be rewritten in terms of raising and lowering operators shown in equation 3.7,

$$\widehat{\boldsymbol{H}} = \alpha\hat{\boldsymbol{J}}^2 + \beta\hat{\boldsymbol{J}}_c^2 + \gamma(\hat{\boldsymbol{J}}_+^2 + \hat{\boldsymbol{J}}_-^2) \quad (3.7)$$

where $\alpha = \frac{1}{2}(a+b)$, $\beta = c - \frac{1}{2}(a+b)$, and $\gamma = \frac{1}{4}(a-b)$. It is important to know whether the molecule is near-prolate, near-oblate, or very asymmetric as the rotational constants (A, B and C) can be mapped on to a, b and c in six possible ways, but it is useful to use the following mappings listed in Table 3.1.1 in order to facilitate the diagonalization of the Hamiltonian matrix to obtain the rotational energy levels.

Table 3.1.1 Mapping of asymmetric top parameters a, b and c on to rotational constants A, B and C.

Parameter	Near-Prolate	Very Asymmetric	Near-Oblate
a	B	C	A
b	C	A	B
c	A	B	C

In order to solve for the energy level expressions using equation 3.7, the following eigenvalues are needed for the associated operators shown in equations 3.8a-d.

$$< \mathrm{J\ K} \left| \hat{\boldsymbol{J}}^2 \right| \mathrm{J\ K} > = \hbar^2 J(J+1) \quad (3.8a)$$

$$< \mathrm{J\ K} \left| \hat{\boldsymbol{J}}_c^2 \right| \mathrm{J\ K} > = \hbar K^2 \quad (3.8b)$$

$$< \mathrm{J\ K+2} \left| \hat{\boldsymbol{J}}_+^2 \right| \mathrm{J\ K} > = \hbar^2 \sqrt{(J+K)(J-K+1)(J+K-1)(J-K+2)} \quad (3.8c)$$

$$< \mathrm{J\ K-2} \left| \hat{\boldsymbol{J}}_-^2 \right| \mathrm{J\ K} > = \hbar^2 \sqrt{(J-K)(J+K+1)(J-K-1)(J+K+2)} \quad (3.8d)$$

The Hamiltonian matrix for the asymmetric top has dimensions of (2J+1) by (2J+1) due to the degeneracy in J. There are also off-diagonal components that mix K-states that are different by ± 2. The matrix is also symmetric along both of the diagonals, due to the degeneracy in ± K. The rotational Hamiltonian then lends itself to

be transformed to a new representation, using the Wang transformation described in the texts by either Kroto or Gordy and Cook. The resulting basis functions are shown in equation 3.9 after performing the Wang transformation.

$$\frac{1}{\sqrt{2}}\{ |J\ +K> \pm |J\ -K>\} \quad (3.9)$$

Following the Wang transformation and further factorization to diagonalize the Hamiltonian matrix yields rotational energy levels that require a new designation different than just the two quantum numbers J and K as used for the symmetric tops. The new energy levels are assigned to J, K_a, and K_c where J is the total angular momentum of the molecule, K_a is the projection of the angular momentum on to the a-principal axis (or $K_{prolate}$) and K_c is the projection of the angular momentum on to the c-principal axis (or K_{oblate}). The energy levels are obtained in closed form for small values of J, but the solutions for these asymmetric tops require numerical methods for large values of J.

3.1.3 CENTRIFUGAL DISTORTION CORRECTIONS

The molecules studied in this dissertation are not rigid and undergo distortions due to the centrifugal force of the rotating molecule. These distortions within the molecules depend on the quantum numbers J and K. Because molecules are not rigid, this requires corrections to the energy levels derived in the previous sections. Watson proposed two reduced representations to account for these distortion effects, which are the asymmetric (A) and symmetric (S) representations. The terms in the Hamiltonian due to these effects are listed in Table 3.1.2. Pickett's SPCAT and SPFIT programs take into account both of these representations, depending on the molecule and which

is specified. For the molecules studied in this dissertation, all were asymmetric and the A-representation was used to determine the spectroscopic constants in the fitting of the microwave spectra to obtain the rotational and centrifugal distortion constants.

Table 3.1.2 Watson's centrifugal distortion Hamiltonians for the A- and S-representations.

Watson's S-reduced Hamiltonian ($\widehat{H} = \widehat{H}_R + \widehat{H}_d^{(4)} + \widehat{H}_d^{(6)}$)
$\widehat{H}_d^{(4)} = D_J\hat{J}^4 - D_{JK}\hat{J}^2\hat{J}_z^2 - D_K\hat{J}_z^4 + d_1\hat{J}^2\left(\hat{J}_+^2 - \hat{J}_-^2\right) + d_2(\hat{J}_+^4 - \hat{J}_-^4)$
$\widehat{H}_d^{(6)} = H_J\hat{J}^6 - H_{JK}\hat{J}^4\hat{J}_z^2 - H_{KJ}\hat{J}^2\hat{J}_z^4 - H_K\hat{J}_z^6 + 2h_{1j}\hat{J}^4\left(\hat{J}_+^2 - \hat{J}_-^2\right) - h_2\hat{J}^2\left(\hat{J}_+^4 - \hat{J}_-^4\right) + h_3(\hat{J}_x^6 - \hat{J}_y^6)$
Watson's A-reduced Hamiltonian ($\widehat{H} = \widehat{H}_R + \widehat{H}_d^{(4)} + \widehat{H}_d^{(6)}$)
$\widehat{H}_d^{(4)} = \Delta_J\hat{J}^4 - \Delta_{JK}\hat{J}^2\hat{J}_z^2 - \Delta_K\hat{J}_z^4 - \delta_j\hat{J}^2\left(\hat{J}_x^2 - \hat{J}_y^2\right) - \delta_k[\hat{J}_z^2\left(\hat{J}_x^2 - \hat{J}_y^2\right) + (\hat{J}_x^2 - \hat{J}_y^2)\hat{J}_z^2)$
$\widehat{H}_d^{(6)} = \Phi_J\hat{J}^6 - \Phi_{JK}\hat{J}^4\hat{J}_z^2 - \Phi_{KJ}\hat{J}^2\hat{J}_z^4 - \Phi_K\hat{J}_z^6 + 2\phi_j\hat{J}^4\left(\hat{J}_x^2 - \hat{J}_y^2\right) - \phi_{jk}\hat{J}^2[\hat{J}_z^2\left(\hat{J}_x^2 - \hat{J}_y^2\right) + \left(\hat{J}_x^2 - \hat{J}_y^2\right)\hat{J}_z^2] + \phi_k[\hat{J}_z^4\left(\hat{J}_x^2 - \hat{J}_y^2\right) + \left(\hat{J}_x^2 - \hat{J}_y^2\right)\hat{J}_z^4]$

3.1.4 MICROWAVE SELECTION RULES

Spectroscopy involves measuring the differences between energy levels to gain information about the molecules of interest. In the case of microwave spectroscopy, the energy levels probed are the rotational states of the molecule. In order for a rotational transition to be excited, the permanent electric dipole moment within the molecules needs to be nonzero. Depending on which dipole-moment matrix elements are nonzero, there can be a-, b-, or c-type transitions, or a combination of all depending on which dipole moment components are nonzero. The allowed transitions can be determined by the symmetries of the wave functions of the two rotational states involved and the

symmetry of the dipole moment matrix elements by the cross product $\Gamma(\Psi') \times \Gamma(\mu) \times \Gamma(\Psi'')$. The rotational states and dipole moment matrix elements that result in the totally symmetric irreducible representation A are said to be allowed. Table 3.1.3 lists the symmetries of the rotational states for given values of K_a and K_c.

Table 3.1.3 Symmetry of rotational states for given values of K_a and K_c.

K_a	K_c	Symmetry
Even	Even	A
Even	Odd	B1
Odd	Odd	B2
Odd	Even	B3

The selection rules on J, K_a, and K_c are summarized in Table 3.1.4 which give the totally symmetric (A_1) cross product between the rotational states and the dipole moment matrix elements.

Table 3.1.4 Summary of selection rules for an asymmetric top molecule. For all types of transitions $\Delta J = 0, \pm 1$.

Dipole Moment Component	ΔK_a	ΔK_c
$\mu_a \neq 0$	0, ±2, …	±1, ±3, …
$\mu_b \neq 0$	±1, ±3, …	±1, ±3, …
$\mu_c \neq 0$	±1, ±3, …	0, ±2, …

3.1.5 NUCLEAR SPIN ANGULAR MOMENTUM

In the case of closed-shell molecules that have nuclei with nuclear spin > ½, the nuclear spin has an angular momentum that couples with the total angular momentum of the molecule. These nuclei have quadrupole moments and this creates a

nonspherical charge distribution around that nucleus. The nonspherical charge distribution interacts with the electric field gradient of the molecule as the molecule rotates and splits each of the rotational transitions into what is called the hyperfine structure in the microwave spectra. In the case of nuclei with spin ≤ ½, these nuclei are spherically symmetric and thus do not interact with the electric field gradient in the molecule. The Hamiltonian for the electric quadrupole interaction that gives rise to the hyperfine structure in the microwave spectra is shown below in equation 3.10, which is obtained from the Taylor expansion of the potential energy. Q is the nuclear quadrupole moment tensor and V is the electrostatic field-gradient tensor at the nucleus generated from the electrons in the molecule.

$$\widehat{H}_Q = \frac{1}{6}\sum_{ij} V_{ij}^{(2)} Q_{ij}^{(2)} \quad (3.10)$$

The first term from the Taylor expansion of the potential energy represents the nuclear monopole and does not interact with the electric field during the molecular rotation. The second term represents the nuclear dipole and this can be neglected. External electric fields allow the molecular dipole to align with the applied electric field and gives rise to what is known as the Stark effect which introduces additional spectral splittings dependent on the laboratory axes. The Stark effect in rotational spectroscopy is useful for the determination of the molecular electric dipole moments. The third term from the Taylor expansion of the potential energy (eq. 3.10) gives rise to the interaction of the quadrupole moment of the nuclei and the electric field around the nuclei. $V_{ij}^{(2)}$ and $Q_{ij}^{(2)}$ are second rank symmetric tensors that represent the electric field gradient of electrons in non-spherically symmetric orbitals and the nuclear charge distribution. Expanding the above equation and collecting terms yields equation 3.11, shown below

for the electric quadrupole Hamiltonian. Q is the quadrupole moment of the nucleus and q_J is the electric field gradient of the molecule averaged over the ro-vibrational state involved. I is the angular momentum resulting from the nuclear spin and J is the total angular momentum in the molecule.

$$\hat{H}_Q = \frac{eQq_J}{2J(2J-1)I(2I-1)}\left[3\left(\hat{I}\cdot\hat{J}\right)^2 + \frac{3}{2}\hat{I}\cdot\hat{J} - \hat{I}^2\hat{J}^2\right] \text{ (eq. 3.11)}$$

Analyzing the hyperfine structure in the rotational spectra of the molecules that exhibit these electric quadrupole interactions allows one to determine additional electronic structure information about the molecule. The quadrupole coupling strengths obtained from the analysis directly yield the electron distribution around these nuclei and can be used to understand processes such as chemical bonding or reaction rates. These parameters also supply the theoretical chemist and physicists with stringent experimental parameters on which to refine theoretical methods. The calculated parameters obtained from the theory can be different by 50% or more for some nuclei.

3.2 COMPUATIONAL METHODS

Electronic and molecular structure computations are a crucial aspect to the research performed in this dissertation and the importance of such computations is increasing in every aspect of chemistry, physics, and biology. In order to predict the microwave spectra, the structures of these molecules first needs to be predicted, from which moments of inertia and rotational constants can be calculated. From the optimized structures of the molecules, the center of mass is determined and the moments and products of inertia are calculated using equations 3.12-3.17. For the off diagonal products of inertia, I_{xy} is equal to I_{yx} because the tensor is symmetric. The

inertia tensor is then diagonalized using the secular equation and the diagonal components are then equal to the moments of inertia in the molecular principal axis system – from which the rotational constants of the molecule A, B, and C are determined and used to calculate the energy of the rotational levels.

$$I_{xx} = \sum_{\alpha} m_{\alpha}(y_{\alpha}^2 + z_{\alpha}^2)$$ (eq. 3.12)

$$I_{yy} = \sum_{\alpha} m_{\alpha}(x_{\alpha}^2 + z_{\alpha}^2)$$ (eq. 3.13)

$$I_{zz} = \sum_{\alpha} m_{\alpha}(x_{\alpha}^2 + y_{\alpha}^2)$$ (eq. 3.14)

$$I_{xy} = -\sum_{\alpha} m_{\alpha} x_{\alpha} y_{\alpha}$$ (eq. 3.15)

$$I_{xz} = -\sum_{\alpha} m_{\alpha} x_{\alpha} z_{\alpha}$$ (eq. 3.16)

$$I_{yz} = -\sum_{\alpha} m_{\alpha} y_{\alpha} z_{\alpha}$$ (eq. 3.17)

Another way to determine the diagonal moment of inertia tensor is to find the set of Euler angles to rotate the original inertia tensor into the principal axis system yielding the diagonalized inertia tensor. However, since the inertia tensor can be easily diagonalized and the principal moments determined using the secular equation, these Euler angles can be found with the equation $\mathbf{R^{-1}IR = I'}$, where **R** is the 3x3 rotation matrix, $\mathbf{R^{-1}}$ is its inverse, **I** is the non-diagonal 3x3 inertia tensor and **I'** is the diagonalized inertia tensor. One can compute the three angles given the three principal moments of inertia from the diagonalization process. The description of this method is given in great detail in the text by Gordy and Cook.

The microwave spectra is then simulated using Pickett's SPCAT program with the calculated rotational constants from the optimized equilibrium gas phase structure's

diagonal inertia tensor. However, for most molecular systems of interest (more than a few atoms) the exact solutions to the Schrödinger equation cannot be obtained and so obtaining molecular structures with the lowest possible energy becomes quite difficult. The time for each computational method to optimize the electronic structures depends on the number of electrons in the system. *Ab initio* methods such as MP2 and coupled cluster (CC) scale as N^5 and N^7 where N is the number of electrons.[9] These methods sometimes produce more accurate results when compared with density functional theory (DFT) methods, which scale as N^4 and so the results are obtained faster. The speed of DFT computations comes from the way in which electron correlation is handled when solving for the energies. DFT methods assume that the electron density does not vary rapidly throughout the molecule.

Several systems were studied in this dissertation where both MP2 and DFT methods produced similar results and sometimes the DFT methods were closer to the experimentally determined values. All of the computations were performed on the high-performance computing system at the University of Arizona using the Gaussian 09 suite.[10] Details on the electronic structure computations performed for each of the specific systems studied will be given in the respective chapters for those systems. A brief overview of the optimization procedure follows.

To begin the gas phase optimization computations on the molecular species of interest, these systems first need to be constructed in molecular modeling programs. Any molecular modeling software can be used, so long as Cartesian coordinates or a Z-matrix of the molecular structure is obtained. These preliminary structures should be built with some chemical intuition – for example a trans-species is typically lower in

energy than its cis counterpart and so if the ground state is desired, the trans-structure is constructed. This is an important step in the optimization of the molecular systems studied as the structures may be optimized to a local minimum in the potential energy surface as opposed to the global minimum which is desired. Following the construction of the molecular species, the Cartesian coordinates or Z-matrices are used in the Gaussian input file with a specific formatting, shown in the appendix. If a potential energy scan is required for the system, a Z-matrix must be used in order to specify which structural parameters to vary (either bonds, angles, or dihedral angles) – the keywords and examples of these types of calculation are documented well on the Gaussian corporation website. A script file is then created in order to submit the computation to the HPC system at the University of Arizona, also shown in the appendix. The computational power, such as memory and number of nodes, is specified in this script file, as well as the location and name of the input file with the molecular coordinates or Z-matrix.

3.3 LEAST SQUARES STRUCTURE FITTING

The most valuable piece of information that can be determined of molecules by measuring the microwave spectra is the determination of key gas phase molecular structure parameters. These parameters are obtained by measuring the microwave spectra of many singly substituted isotopologues, from which the rotational constants are determined by fitting the assigned spectra using Pickett's SPFIT program. The rotational constants of the most abundant isotopic species and all of the unique singly substituted isotopologues are used in an iterative Fortran program (shown in the

appendix) to determine the important molecular structure parameters. For the isotopologue spectra measured for the molecules described, these isotopic species were measured under natural abundance concentrations.

First the molecular geometry is obtained either from the electronic structure computations or from X-ray crystal structure data published in the literature. The Cartesian coordinates of the atoms are parameterized and the best values of these parameters are obtained through a nonlinear least squares method. The best fit structure obtained using this structure fitting program has calculated rotational constants closest in value to all of the experimentally determined values obtained from the assigned spectra. A standard deviation is reported for the molecular structure fit obtained and is shown below in equation 3.12.

$$\sigma = \sqrt{\sum_i \frac{(Y_i - Y_{calc})}{(N-P)}} \quad \text{(eq. 3.12)}$$

Y_i is the set of experimental rotational constants for each of the isotopologues and Y_{calc} are the calculated values from the best fit structure (with the smallest sum of squares). N is the number of rotational constants determined from the observed microwave spectra for all of the isotopologues measured and P is the number of parameters used to adjust the Cartesian coordinates of the molecular structure.

Once the molecular structure is obtained from the fitting routine, the coordinates, with respect to the molecule's center of mass, are calculated for each of the singly substituted atoms using the Kraitchman equations, which are described well in the text by Gordy and Cook. These Kraitchman calculated substitution coordinates are

compared with the coordinates obtained from the structure fit and the obtained structure is typically accurate to about 0.01 Å and sometimes even better.

4. MICROWAVE MEASUREMENTS AND STRUCTURES OF LARGE ORGANIC MOLECULES

The computational power of current theoretical models decreases in accuracy as the size of the molecules and complexes become larger. Current models scale as a power of the number of electrons within the systems, so it is important to study large molecules and weakly interacting complexes to gauge the accuracy of the currently available theory. The measurement of the microwave spectra of the organic molecules discussed in this chapter aim to provide benchmarks for the theoreticians in order to improve upon the existing theory.

Cyclopropanecarboxylic acid is a carboxylic acid with a cyclopropane ring. Even though it is considered small on most standards, the ability of current available computational methods are still unable to calculate extremely accurately what is observed in the laboratory. Furthermore, molecules like cyclopropanecarboxylic acid undergo some internal motion and excited state conformers are sometimes observed, which was the case for this carboxylic acid. 1,2-cyclohexanedione is another somewhat large molecule and provides another great benchmark for theoretical methods. The case of 1,2-cyclohexanedione was also an interesting one, in that under the experimental conditions the molecule seemed to have completely tautomerized to its monoenolic tautomer, which was observed. Tautomeric species and other conformations, such as the one observed for 1,2-cyclohexanedione, may be elusive and difficult to study by other methods. Microwave spectroscopy lends itself as a great technique to obtain free molecular structure parameters, as well as to observe the dynamics and other elusive excited state structures or complexes.

4.1 CYCLOPROPANECARBOXYLIC ACID

4.1.1 INTRODUCTION

Derivatives of cyclopropanes are versatile compounds in many organic syntheses and are found throughout nature.[11] Specifically, cyclopropanecarboxylic acid (CPCA) is an important biologically active compound due to the hypoglycemic metabolic effects shown in experiments by Duncombe and Rising in several animal species, including humans.[12] CPCA can be synthesized using chiral copper carbenoids[13] and due to the versatility of the cyclopropane ring, geminal dihalides of CPCA can be easily derivatized using a Ni induced reductive carbonylation.[14] Other syntheses of CPCA utilize transition metal catalyzed reactions, cycloaddition of alkenes, sulfoxides and other metal carbenoids.

Potential energy scans of the different conformers of CPCA have been previously performed and predicted, at room temperature, the abundances of the two conformers of CPCA. These conformers were separated in energy by only a few hundred wavenumbers. The predicted abundances from these initial calculations were 85% and 15% for the lower and higher energy conformers, respectively.[15] Additional calculations were performed and these predicted a difference in energy of only 321 cm^{-1}, so it is reasonable that rotational transitions from the excited state conformer should be observed. In the work by Marstokk *et al.*, the high energy conformer was searched for in the 26.5-38.0 GHz range but was not observed, most likely due to the low abundance of the species in addition to the low populations of the large J energy levels. In this study described here, the microwave measurements and determined spectroscopic constants of the low and high energy conformers of CPCA are reported.

The crystal structure of CPCA was determined by Boer and Stam.[16] IR and Raman spectroscopic techniques were utilized by Maillols, Tabacik, and Sportouch[17] to determine some gaseous structural parameters of CPCA. To extend the study on gaseous CPCA, Marstokk, Møllendal, and Samdal[18] performed an electron diffraction experiment, waveguide microwave measurements (in the 26.5-38 GHz regime), and *ab initio* computations. In this study presented here, high resolution pulsed-beam Fourier-transform (PBFT) microwave spectroscopy was used to measure low frequency transitions for the low energy conformer (in the 5-15 GHz regime) of the parent, the unique singly substituted ^{13}C isotopologues, and the –OD isotopologue and key gas phase structural parameters were determined. Additional transitions were also measured and assigned corresponding to the excited state conformer.[19,20]

4.1.2 MICROWAVE MEASUREMENTS

The CPCA sample was purchased from Sigma Aldrich (95%) and was used as received. The deuterated CPCA sample was prepared by mixing equimolar quantities of CPCA (Sigma Aldrich, 95%) and MeOD, or deuterated methanol, (Cambridge Isotope Lab, Inc., 99%) and allowing the H and D to exchange overnight. The remaining MeOH, after the exchange, was removed from the mixture under reduced pressure, leaving the less volatile CPCA-OD behind. Each sample was then transferred into a specialized glass sample cell presented in chapter two. The sample and pulsed-valve (General Valve, series 9) were heated to 45 °C to obtain sufficient vapor pressure of the molecule to provide a strong test signal. The pressure within the microwave cavity was maintained at 10^{-6} to 10^{-7} Torr prior to the pulsed injection of the sample and Ne carrier

gas. The Ne backing pressure was maintained at ~1 atm during microwave measurements.

Table 4.1.1 Parent isotopologue transitions of CPCA. Frequencies are given in MHz.

$J'_{Ka'\ Kc'}$	$J''_{Ka''\ Kc''}$	ν_{obs}	ν_{o-c}
6_{25}	5_{32}	5039.365	0.000
1_{01}	0_{00}	5106.835	-0.006
1_{10}	1_{01}	5242.984	0.001
2_{02}	1_{11}	5296.063	-0.001
2_{11}	2_{02}	5603.069	0.001
3_{12}	3_{03}	6175.152	-0.001
6_{24}	5_{33}	6210.009	0.000
4_{13}	3_{22}	6878.550	-0.001
4_{13}	4_{04}	6995.124	-0.001
5_{14}	5_{05}	8104.475	0.000
2_{12}	1_{11}	9870.926	0.002
1_{11}	0_{00}	10007.086	-0.002
2_{02}	1_{01}	10196.314	0.003
2_{11}	1_{10}	10556.397	0.002
3_{03}	2_{12}	10676.475	0.001
3_{13}	2_{12}	14795.766	-0.002

Table 4.1.2 –OD isotopologue transitions of CPCA. Frequencies are given in MHz.

$J'_{Ka'\ Kc'}$	$J''_{Ka''\ Kc''}$	ν_{obs}	ν_{o-c}
1_{01}	0_{00}	4938.008	0.009
1_{10}	1_{01}	5311.345	0.001
2_{11}	2_{02}	5647.302	-0.009
3_{12}	3_{03}	6178.926	0.005
4_{13}	4_{04}	6937.507	0.003
5_{14}	5_{05}	7960.020	0.001
2_{12}	1_{11}	9555.002	0.012
2_{02}	1_{01}	9860.989	-0.002
2_{11}	1_{10}	10196.945	-0.014

Microwave transitions were measured for the parent isotopologue and the –OD isotopologue in the 5-15 GHz range using a PBFT Flygare-Balle type microwave spectrometer described in chapter two. 16 new transitions have been measured for the

parent and 9 for the –OD isotopologue corresponding to the CPCA molecule shown in Figure 4.1.1 (top). The newly measured rotational transitions for the parent and –OD isotopologues are given in Tables 4.1.1 and 4.1.2 respectively. Additional measurements on the lower energy CPCA conformer, were extended to include all of the unique single ^{13}C substituted positions, with all transitions being measured under natural abundance concentrations. These measured rotational transitions are shown in Table 4.1.4. The numbering scheme for each of the substituted atoms reflects what is shown in Figure 4.1.1. These new ^{13}C measurements were taken at room temperature, as a parent test signal was a very strong after pulsing at a higher temperature (60 °C).

Measurements on the higher energy CPCA conformer, corresponding to the geometry of the CPCA molecule shown in Figure 4.1.1 (bottom), were also taken at room temperature after ~2 hours of pulsing the CPCA sample through the pulsed valve at ~60 °C. The measured transitions of this new conformer are shown in Table 4.1.3.

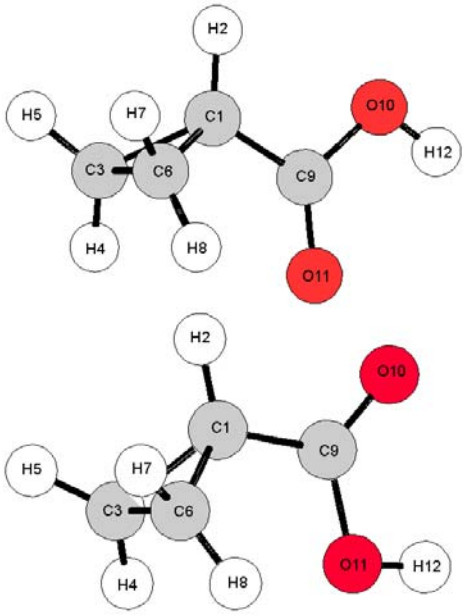

Figure 4.1.1 Structures of the two conformers of CPCA where the top is lower in energy by 373.1 cm^{-1}, obtained from the B3LYP/aug-cc-pVQZ calculation.

Table 4.1.3 Spectral assignments and frequencies for the high energy conformer of CPCA. Frequencies given in MHz.

J'	K_a'	K_c'	J''	K_a''	K_c''	Frequencies (MHz)	o-c
1	1	0	1	0	1	5037.232	-0.004
1	0	1	0	0	0	5204.936	0.004
2	1	1	2	0	2	5433.717	0.006
2	0	2	1	1	1	5725.706	-0.004
3	1	2	3	0	3	6068.218	0.004
4	1	3	4	0	4	6984.654	-0.005
1	1	1	0	0	0	9867.375	-0.004
2	1	2	1	1	1	10035.056	-0.002
2	0	2	1	0	1	10388.154	-0.004
2	0	2	1	1	0	10784.644	0.010

Table 4.1.4 Spectral assignment and frequencies for the ^{13}C isotopologues of CPCA. The observed – calculated (o – c) values are listed in kHz.

J'	K_a'	K_c'	J''	K_a''	K_c''	$^{13}C(3\&6)$	o-c*	$^{13}C(9)$	o-c*	$^{13}C(1)$	o-c
1	0	1	0	0	0	5027.498	2	5092.480	-4	5095.068	2
2	0	2	1	1	1	5152.397	-2	5259.474	2		
1	1	0	1	0	1	5212.357	1	5249.158	0	5203.388	4
2	1	1	2	0	2	5553.572	-1				
1	1	1	0	0	0	9914.347	-3	10000.827	1	9952.100	-4
2	0	2	1	0	1	100039.255	2	10167.814	0	10172.253	4
2	1	1	1	1	0					10536.453	-3

4.1.3 CALCULATIONS

Since previous microwave work was previously performed by Marstokk et. al., the rotational constants obtained in the previous study were used to predict the lower frequency microwave transitions. Measurements of the new experimental transitions were in excellent agreement with the predictions from the initial study. The OD and ^{13}C transitions were predicted by changing the mass of the H or C atom in the initial optimized structure to that of D or ^{13}C, from which preliminary rotational constants of the isotopologues were calculated. The ratios between the calculated rotational constants

from the theory and the experimentally determined rotational constants of the parent isotopologue were used as scale factors and multiplied by the calculated isotopologue rotational constants. These corrected values provided an accurate set of rotational constants for the OD and ^{13}C isotopologues to predict the transitions.

Potential energy scans of the rotation of the carboxylic acid moiety about the C1 – C9 bond of the CPCA monomer were previously performed, resulting in the calculated abundances of each conformer to be 85% and 15% at room temperature. Additional optimization calculations using B3LYP/aug-cc-pVQZ of the two conformers were also performed and the energy difference between the conformers was calculated to be 373.1 cm^{-1}, with the bottom conformer in Figure 4.1.1 having higher energy. The calculated a and b dipoles of this high energy conformer were 2.02 and 1.13 D respectively, so both a and b type transitions were expected to be observed, however the transitions will be weak due to the lower abundance of the higher energy conformer. The calculated values of the rotational constants from the B3LYP calculation compared to the experimentally fit values of this high energy conformer are shown in Table 4.1.5.

Table 4.1.5 Spectroscopic constants for the high energy conformer of cyclopropanecarboxylic acid.

	Experiment	B3LYP/aug-cc-pVQZ	Calculation[15]
A/MHz	7452.3132(57)	7490.121	7451
B/MHz	2789.8602(43)	2770.327	2786
C/MHZ	2415.0725(40)	2399.7699	2411
Δ_J/kHz	0.29(53)		
Δ_{JK}/kHz	2.5(12)		
N	10		
σ/kHz	5		

4.1.4 ROTATIONAL CONSTANTS

The fits to obtain the rotational constants of all species were performed using Pickett's SPFIT program and these results are listed in Table 4.1.6. During the fit of the ^{13}C transitions, the centrifugal distortion constants were held fixed to the values obtained by Marstokk *et al*, due to these constants being thought to be more accurately determined with the measurement of high J and K transitions. Also in Table 4.1.6 are the rotational constants of the best fit structure and the deviation of these constants of the best fit structure from the experimentally determined values (M – C). The calculated rotational constants of the best fit structure had a standard deviation of 0.31 MHz when compared to the experimentally determined values, which is very good when taking into consideration the magnitudes of the rotational constants of CPCA. The previously calculated rotational constants were within <1% of the experimentally fit values and the rotational constants obtained from the current B3LYP/aug-cc-pVQZ were in fair agreement.

Table 4.1.6. Spectroscopic constants for the CPCA low energy conformer from the experiment and the structure fit, shown in MHz.

ISOTOPOLOGUE		MEASURED	CALCULATED	(M – C)
Parent	A	7625.0432(17)	7625.5604	-0.5172
	B	2724.7672(8)	2724.9594	-0.1922
	C	2382.0755(5)	2382.2998	-0.2243
-OD	A	7619.8580(64)	7619.5759	0.2821
	B	2629.4700(14)	2629.0129	0.4571
	C	2308.5301(14)	2308.0919	0.4382
^{13}C3	A	7563.3591(16)	7563.3012	0.0579
	B	2676.4756(9)	2676.4388	0.0368
	C	2351.0216(1)	2350.9624	0.0592
^{13}C6	A	7563.3591(16)	7563.3063	0.0528
	B	2676.4756(9)	2676.3973	0.0783
	C	2351.0216(1)	2351.0214	0.0002
^{13}C9	A	7624.9982(19)	7624.9659	0.0323
	B	2716.6267(19)	2716.7176	-0.0909
	C	2375.8584(19)	2375.9405	-0.0821
^{13}C1	A	7577.7505(38)	7577.6578	0.0927
	B	2720.6834(22)	2720.9473	-0.2639
	C	2374.3843(28)	2374.5590	-0.1747

4.1.5 MOLECULAR STRUCTURE

A nonlinear least squares structure fit was performed on the low energy conformer of CPCA using the rotational constants of all the measured singly substituted isotopologues to obtain key gas phase structure parameters within the cyclopropane ring. In the least squares fit, there were 8 total varied parameters in 3D Cartesian space. 3 of these varied parameters were the movement of C3, H4 and H5 (as one group), 3 were the movement of C6, H7 and H8 (as a second group), and 2 were the movement of C1 and H2 (as a third group) in the a-b plane. Atoms 9-12 were all held fixed to the calculated B3LYP/aug-cc-pVQZ coordinates. C1 and H2 were constrained to be in the a-b plane because the c-coordinates in the calculated structure were very small, indicating these atoms lie mostly within the a-b plane. The standard deviation of

this nonlinear least squares structure fit was 0.31 MHz. A Kraitchman analysis was also performed using the Kiesel KRA program[21] on the low energy CPCA monomer of all the measured isotopologues. The best fit coordinates of the low energy CPCA conformer are shown with the Kraitchman calculated coordinates in Table 4.1.7. Agreement between the structure fit and the Kraitchman calculated values is very good, indicating the best fit structure is a reasonable representation of the molecule in its ground state.

Table 4.1.7 Coordinates of the best fit low energy conformer of CPCA and the ^{13}C isotopically substituted coordinates, calculated by a Kraitchman analysis.

Atom	a	b	c	Krait-|a|	Krait-|b|	Krait-|c|
C1	0.523764	0.650343	0.021147	0.527(12)	0.645(15)	0.050(1)
H2	0.452885	1.726044	0.052516			
C3	1.683716	-0.074816	0.745077	1.678(26)	0.0430(7)	0.747(12)
H4	1.473675	-1.022121	1.218132			
H5	2.345932	0.581808	1.289096			
C6	1.683362	0.036968	-0.747865	1.678(26)	0.0430(7)	0.747(12)
H7	2.346877	0.724213	-1.250935			
H8	1.474560	-0.881056	-1.275993			
C9	-0.753177	-0.072331	-0.001568	0.75(30)	0.011(4)	0.023(9)
O10	-1.808001	0.778661	0.021870			
O11	-0.891655	-1.269858	-0.036844			
H12	-2.608059	0.235118	0.004902	2.598(27)	0.209(2)	0.0654(7)

4.1.6 DISCUSSION

The rotational spectrum for CPCA has been extended to the 5-15 GHz regime, with the new high resolution measurements taken using a PBFT microwave spectrometer. The experimental rotational transitions are shown in Tables 4.1.1 and 4.1.2 and the rotational constants obtained from this study. Measurements were extended for the low energy conformer of CPCA to include all of the singly substituted ^{13}C and singly substituted -OD positions. To perform the fit on the measured transitions

for each of the isotopologues, the centrifugal distortion constants were held fixed to the values obtained in the study by Marstokk *et al.* This was done due to these centrifugal distortion constants being more accurately fit than the distortion constants obtained in this study because of the measurement of large J and K transitions. By measuring rotational transitions with larger J and K values, the distortion with respect to each of these quantum numbers can be more accurately fit, compared to the fit that was limited to low J transitions. A Kraitchman analysis was performed on this CPCA conformer and these Kraitchman coordinates, along with the best fit structure coordinates, are shown in Table 4.1.7. The substituted coordinates from the Kraitchman analysis seem to agree fairly well with the best fit structure obtained from the nonlinear least squares fit. Tables 4.1.8 and 4.1.9 show the key molecular structure parameters of the bond lengths and angles of the B3LYP/aug-cc-pVQZ calculated values compared to the parameters that were obtained during the structure fit.

Table 4.1.8 Bond lengths obtained from the structure fit of CPCA (Å). Unreported bond lengths were fixed at calculated B3LYP/aug-cc-pVQZ values.

Interatomic Distance	Microwave Fit Value (Å)	Calculated Value (Å)
$r(C_1\text{-}C_3)$	1.548	1.517
$r(C_1\text{-}C_6)$	1.521	1.517
$r(C_1\text{-}C_9)$	1.467	1.478
$r(C_3\text{-}C_6)$	1.497	1.486

Table 4.1.9 Angles obtained from the structure fit of CPCA (°). The last 2 listed angles are dihedral angles, indicating the non-planarity of carbon atoms 3 and 6. Unreported angles were held fixed to calculated B3LYP/aug-cc-pVQZ values.

Angle	Microwave Fit Value(°)	Calculated Value(°)
$<(C_3\text{-}C_1\text{-}C_6)$	58	59
$<(C_6\text{-}C_3\text{-}C_1)$	60	61
$<(C_1\text{-}C_6\text{-}C_3)$	62	61
$<(C_1\text{-}C_9\text{-}O_{10})$	112	112
$<(C_1\text{-}C_9\text{-}O_{11})$	126	126
$<(C_3\text{-}C_1\text{-}C_9\text{-}O_{10})$	148	146
$<(C_6\text{-}C_1\text{-}C_9\text{-}O_{10})$	-146	-146

It can be seen that the cyclopropane ring does not have equal $C_1 – C_3$ and $C_1 – C_6$ bond lengths as the B3LYP/aug-cc-pVQZ calculation predicted. The greatest change in bond length compared to the calculated value was the C_1-C_3 bond changing by ~0.03 Å. The bond angles in the ring remained fairly constant, with the angles changing by only 1°. The bond lengths within the cyclopropane ring also agree fairly well with previous structural work. Differences between these structures most likely arise from the combination of the microwave data with electron diffraction work as molecules may have slightly different structures in the gas phase.

After searching for transitions corresponding to the higher energy conformer with the geometry shown in Figure 4.1.1 (bottom) of CPCA, 10 weak rotational transitions were measured and definitively assigned to be from this conformer. The experimentally fit rotational constants agreed within 1% of the rotational constants obtained from the B3LYP calculations and <1% with previous calculations. The intensities of the measured transitions of this high energy conformer seemed to reflect the abundances of the two conformers somewhat that was calculated under equilibrium conditions at room

temperature, 85% and 15%. However it seemed the abundance was lower for the high energy conformer in the gas phase under the experimental conditions. The intensities of the 0_{00} to 1_{01} transitions for each of the conformers can be observed in Figure 4.1.2 taken after the same number of pulsed beam cycles. The high energy conformer was similar to the ^{13}C signals of the low energy conformer, representing 1% natural abundance, so from this comparison we concluded the abundance of this high energy conformer in the gas phase was ~ 1%.

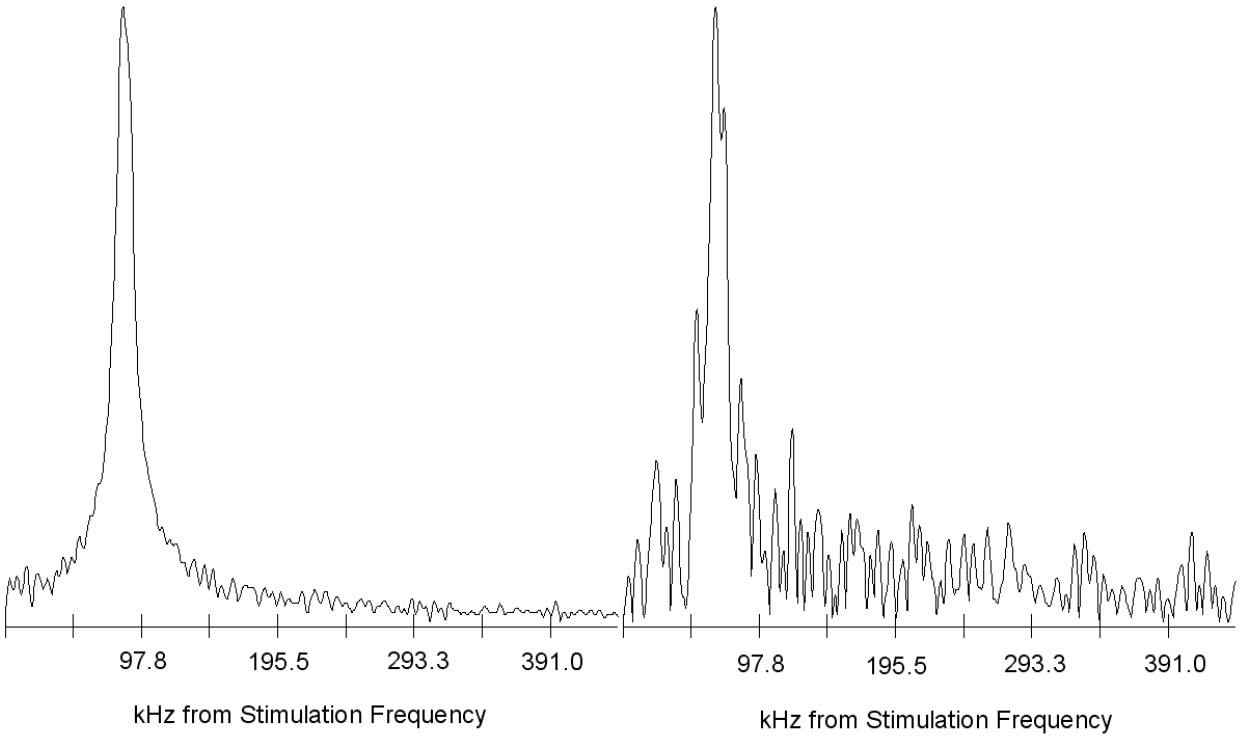

Figure 4.1.2 Example transitions of the low energy conformer (left) and higher energy conformer (right) taken of the 0_{00} to 1_{01} transition. Both transitions were recorded after ~230 pulsed-beam cycles.

4.2 1,2-CYCLOHEXANEDIONE

4.2.1 INTRODUCTION

The important organic compound 1,2-cyclohexanedione (CDO) is widely used in organic syntheses and has many industrial applications. It can be prepared by a number of different reactions. One method of CDO preparation is by the ring-opening of epoxides, which are versatile organic intermediates, easily prepared from olefins or carbonyl compounds using Bi catalysts.[22,23] It can also undergo many organic reactions, including a Michael addition of CDO to β-nitrosytrenes.[24] It is also added to a number of different consumer products to alter the scent and flavor, such as food products, perfumes, and tobacco products.[25,26] CDO has gained attention in biological chemistry, as it was found to selectively and reversibly modify arginine residues in proteins at the guanidino group,[27] allowing for primary protein sequences to be determined.[28]

CDO is a solid at room temperature and melts at about 35 °C into a yellow liquid. The vapor pressure was sufficiently high at 35 °C that strong signals of the parent isotopologue could be obtained by pulsed-beam Fourier transform (PBFT) microwave spectroscopy. CDO can exist in either the diketo or monoenol forms,[29] but in the gas phase it is mostly monoenolic (Figure 4.2.1). Searches for rotational transitions for the diketo form were not successful. The gas phase structure of the monoenolic form of CDO has been previously determined using electron diffraction methods.[30] Since there are limitations (in the sense that the structures are distorted) to electron diffraction data, it is beneficial to measure microwave data also for this molecule. Infrared spectroscopy and quantum chemistry computations for CDO were reported by Chakraborty et al.[31]

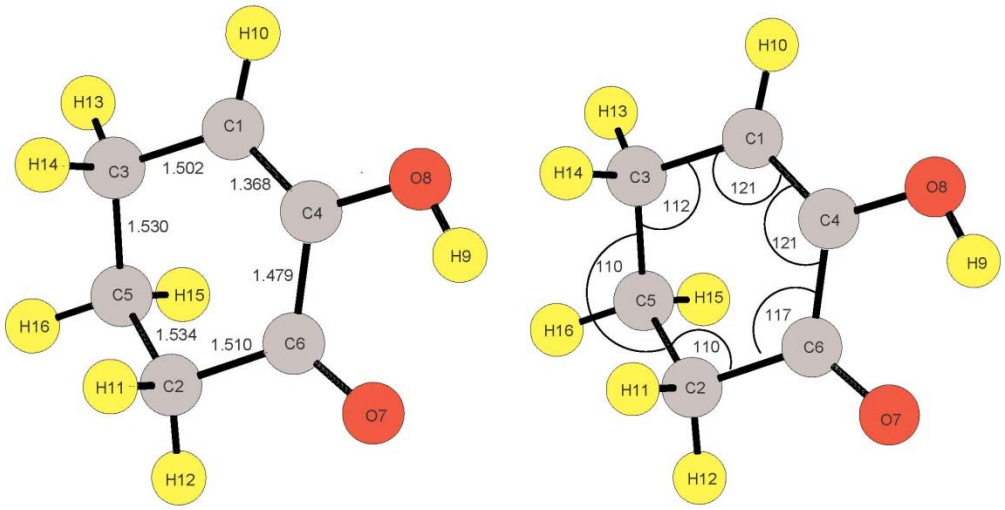

Figure 4.2.1 The best fit structure of 1,2-cyclohexanedione (enol tautomer) showing the best fit bond lengths (Å) and the bond angles (degrees) for the cyclohexane ring. The C3-C5-C2 bond angle passes over the C5-H16 bond. All C-H bond lengths are 1.09(1) Å.

4.2.2 MICROWAVE MEASUREMENTS

The microwave spectrum was measured for the parent isotopologue, all singly substituted ^{13}C isotopologues (under natural abundance), and a deuterium substituted isotopologue at H9 in the 4-14 GHz region using a PBFT-type spectrometer described in chapter two. There were 72 transitions measured in total, 16 for the parent isotopologue, 14 for the deuterium substitution at H9, and 7 for each single substituted ^{13}C isotopologue. The numbering scheme used in the analysis is given in Figure 4.2.1.

The sample was purchased from Sigma Aldrich (97%) and was used without further purification. It was loaded into a glass sample cell and attached to a pulsed valve (General Valve series 9). The sample cell and valve were heated to ~35 °C to obtain

sufficient vapor pressure of the sample in the neon gas stream. The pressure inside the spectrometer was maintained at 10^{-6} to 10^{-7} Torr prior to the pulsed injection of the gaseous molecular sample and the Ne carrier gas. The Ne backing pressure was maintained at ~1 atm during the microwave measurements. The signal strength was sufficiently strong that the singly substituted ^{13}C isotopologue transitions were measured under the same conditions in 100 beam pulse cycles under natural abundance of ^{13}C.

A deuterated sample of 1,2-cyclohexanedione was prepared by mixing equimolar amounts of 1,2-cyclohexanedione (Sigma Aldrich, 97%) and CH_3OD (Cambridge Isotope Laboratories, Inc., 99%) overnight. The remaining CH_3OH was removed under reduced pressure and the deuterated 1,2-cyclohexanedione was crystallized and transferred to a small vial. Similar instrumental conditions were used to measure the deuterated transitions. All measured transitions are shown in Tables 4.2.1-3.

Table 4.2.1 Results of the measurements and least squares fit calculations for CDO parent isotopologue transitions. The standard deviation of the fit is 0.002 MHz. Frequencies are given in MHz.

$J'_{Ka' Kc'}$	$J''_{Ka'' Kc''}$	ν_{obs}	ν_{o-c}
1_{11}	0_{00}	4482.397	-0.001
2_{02}	1_{11}	5484.907	0.000
2_{12}	1_{11}	6063.935	0.001
2_{21}	2_{02}	6101.431	0.001
2_{02}	1_{01}	6544.965	0.001
2_{12}	1_{01}	7123.990	-0.001
2_{11}	1_{10}	7625.426	0.002
3_{03}	2_{02}	9277.312	-0.001
2_{11}	1_{01}	9466.226	0.000
2_{21}	1_{10}	10805.592	0.000
2_{20}	1_{10}	11105.305	-0.002
3_{21}	2_{20}	11256.720	0.000
2_{21}	1_{11}	11586.341	0.005

4_{04}	3_{03}	11850.350	0.000
2_{20}	1_{11}	11886.047	-0.004
3_{12}	2_{02}	14118.823	0.000

Table 4.2.2 Results of the measurements and least squares fit calculations for D-CDO isotopologue transitions. The standard deviation of the fit is 0.005 MHz. Frequencies are given in MHz.

$J'_{Ka' Kc'}$	$J''_{Ka'' Kc''}$	ν_{obs}	ν_{o-c}
2_{02}	1_{11}	5318.014	0.002
2_{12}	1_{11}	5948.716	-0.002
2_{02}	1_{01}	6426.843	0.000
2_{12}	1_{01}	7057.545	-0.003
4_{13}	4_{04}	7169.658	0.005
2_{11}	1_{10}	7448.654	0.001
3_{03}	2_{12}	8504.260	0.008
3_{13}	2_{12}	8775.248	-0.003
3_{03}	2_{02}	9134.961	0.004
3_{13}	2_{02}	9405.953	-0.003
3_{22}	2_{21}	10048.019	-0.007
3_{12}	2_{11}	10958.520	0.000
3_{21}	2_{20}	10961.087	-0.008
4_{04}	3_{03}	11672.237	0.007

		^{13}C1		^{13}C2		^{13}C3		^{13}C4		^{13}C5		^{13}C6	
$J'_{Ka' Kc'}$	$J''_{Ka'' Kc''}$	ν_{obs}	ν_{o-c}	ν_{obs}	ν_{o-c}	ν_{obs}	ν_{o-c}	ν_{obs}	ν_{o-c}	ν_{obs}	ν_{o-c}	ν_{obs}	ν_{o-c}
2_{12}	1_{11}	6037.642	-0.001	6031.021	0.000	5990.835	0.000	6051.833	0.000	5991.664	-0.001	6051.919	0.002
2_{02}	1_{01}	6513.195	0.002	6506.678	-0.002	6468.898	0.001	6531.595	0.000	6469.952	0.001	6531.386	0.003
2_{11}	1_{10}	7611.114	-0.001	7598.334	0.000	7520.632	0.000	7612.600	0.000	7515.111	0.000	7614.246	-0.001
3_{13}	2_{12}	8888.752	0.003	8880.426	0.001	8830.809	-0.001	8915.280	0.002	8833.774	-0.001	8914.873	-0.001
3_{03}	2_{02}	9218.580	-0.001	9212.411	0.001	9179.673	0.000	9256.690	-0.005	9185.286	-0.001	9255.227	-0.001
4_{14}	3_{13}	11628.328	-0.002	11618.853	-0.001	11563.428	0.001	11668.618	0.005	11569.157	0.001	11667.542	0.000
4_{04}	3_{03}	11773.636	0.001	11766.207	0.000	11726.815	-0.001	11823.708	-0.003	11735.216	0.000	11821.705	0.000

Table 4.2.3 Results of the measurements and least squares fit calculations for ^{13}C isotopologues of 1,2-CDO. The standard deviation of each of the fits (in order of numbering in Figure 1) are 0.002 MHz, 0.001 MHz, 0.001 MHz, 0.004 MHz, 0.001 MHz, and 0.002 MHz. Frequencies are given in MHz.

4.2.3 CALCULATIONS

Ab initio calculations were performed to obtain initial values of rotational constants for 1,2-cyclohexanedione using the Gaussian 09 suite with MP2/6-311++G**. The calculations predicted the lowest energy structure to be the enol tautomer. This was determined to be true, due to the intense signals observed for the rotational transitions corresponding with the enol structure, as well as the strong signals observed with each of the singly substituted ^{13}C isotopologues. Predicted transitions were not observable for the diketo structure after significantly searching. Comparisons of the structural parameters with those determined from the least squares structure fit are given in Tables 4.2.4 and 4.2.5.

Table 4.2.4 Bond distances obtained from the fit. Bond lengths are in Å. Starred bond lengths(*) were fixed at calculated (Gaussian) values.

Interatomic Distance	Microwave Fit Value (Å)	Calculated Value (Å)
$r(C_1\text{-}C_4)$	1.368	1.353
$r(C_1\text{-}C_3)$	1.502	1.505
$r(C_3\text{-}C_5)$	1.530*	1.530
$r(C_5\text{-}C_2)$	1.534	1.530
$r(C_2\text{-}C_6)$	1.510	1.509
$r(C_6\text{-}C_4)$	1.479	1.485
$r(C_6\text{-}O_7)$	1.229*	1.229
$r(C_4\text{-}O_8)$	1.356*	1.356
$r(C_1\text{-}H_{10})$	1.088*	1.088
$r(C_3\text{-}H_{13})$	1.096*	1.096
$r(C_3\text{-}H_{14})$	1.101*	1.101
$r(C_5\text{-}H_{15})$	1.097*	1.097
$r(C_5\text{-}H_{16})$	1.095*	1.095
$r(C_2\text{-}H_{11})$	1.100*	1.100
$r(C_2\text{-}H_{12})$	1.094*	1.094
$r(O_8\text{-}H_9)$	0.971*	0.971

Table 4.2.5 Angles obtained by fitting the experimental and rotational constants for eight isotopologues. Angles are listed in degrees. The last 2 listed angles are dihedral angles, indicating the non-planarity of the cyclohexane skeleton.

Angle	Microwave Fit Value(°)	Calculated Value(°)
$<(C_4\text{-}C_1\text{-}C_3)$	121	122
$<(C_1\text{-}C_3\text{-}C_5)$	112	111
$<(C_3\text{-}C_5\text{-}C_2)$	110	110
$<(C_5\text{-}C_2\text{-}C_6)$	110	111
$<(C_2\text{-}C_6\text{-}C_4)$	117	117
$<(C_6\text{-}C_4\text{-}C_1)$	121	122
$<(C_1\text{-}C_3\text{-}C_5\text{-}C_2)$	53	
$<(C_1\text{-}C_4\text{-}C_6\text{-}C_2)$	-17	

4.2.4 ROTATIONAL CONSTANTS

The experimental rotational and centrifugal distortion constants for the parent isotopologue were determined using a least squares fitting program, FITSPEC[32], and are given in Table 4.2.6.

Table 4.2.6 MEASURED rotational constants and the “best fit” CALCULATED values for rotational constants obtained from the structure fit, given in MHz. The centrifugal distortional constants (D_J and D_K) were obtained from the microwave fit of the parent isotopolgue and are D_J=0.04355 KHz and D_K=0.4358 KHz. The distortion constants were held fixed to these values when obtaining the microwave fit for each of the other isotopologues. The standard deviation for the structure fit is 0.18 MHz.

ISOTOPOLOGUE		MEASURED	CALCULATED	(M. – C.)
Parent	A	3161.6006(12)	3161.7844	-0.1838
	B	2101.5426(3)	2101.6104	-0.0678

	C	1320.7976(4)	1320.8582	-0.0606
DCDO	A	3158.4864(27)	3158.0533	0.4331
	B	2049.6554(5)	2049.6654	-0.0100
	C	1299.6880(3)	1299.5564	0.1316
^{13}C1	A	3120.0650(59)	3119.8658	0.1992
	B	2099.4632(7)	2099.4394	0.0238
	C	1312.7269(4)	1312.6387	0.0882
^{13}C2	A	3122.1020(33)	3122.1785	-0.0765
	B	2095.4979(4)	2095.3309	0.1670
	C	1311.8413(2)	1311.9275	-0.0862
^{13}C3	A	3147.0237(31)	3147.2021	-0.1785
	B	2071.3833(3)	2071.4420	-0.0586
	C	1306.4843(2)	1306.5140	-0.0296
^{13}C4	A	3152.2477(119)	3152.1881	0.0596
	B	2098.2463(13)	2098.0731	0.1731
	C	1317.8627(7)	1317.8290	0.0337
^{13}C5	A	3152.8131(30)	3152.9266	-0.1135
	B	2069.2089(3)	2069.3500	-0.1411
	C	1307.4857(2)	1307.5010	-0.0153
^{13}C6	A	3149.7990(51)	3149.9345	-0.1355
	B	2098.8533(6)	2098.9441	-0.0908
	C	1317.6887(3)	1317.7380	-0.0493

Similar analyses were carried out for all singly substituted isotopologues, but the centrifugal distortion constants were held fixed to the values obtained from the parent isotopologue for each fit. The deviations (ν_{o-c}) between the best fit calculated (c) and observed (o) frequencies are listed in Tables 4.2.1-3. The J and K values for reported transitions ranged from 0 to 4 and this range is believed to be sufficient to obtain fair values for the distortion constants. Higher J-values could be obtained to refine the parameters, but signal strength would be lower.

4.2.5 MOLECULAR STRUCTURE

The rotational constants obtained for each isotopologue from fitting the measured rotational transitions were used in a nonlinear least squares fit program to determine the

best fit coordinates of the atoms in 1,2-cyclohexanedione relative to the parent isotopologue's center of mass. During the least squares fit, all hydrogen atom coordinates were held fixed relative to the atom it was bonded to, as was determined from the Gaussian 09 calculation. The coordinates of atoms C1, C6, and O7 were also held constant. The carbon atoms at positions 3 and 5 were varied using the same variable parameters as well as the group with atoms C4, O8, and H9. With these constraints, only 9 variable parameters remained and were precisely determined from the least squared structure fitting analysis. The variable parameters were the a, b, and c Cartesian coordinates in the principal axes system for C2, C3 and C5, and C4.

Table 4.2.7 Atom Cartesian coordinates in a, b, c system for the best fit structure of CDO, and the Kraitchman determined values (Krait.).

Atom	a	b	c	|a| -Krait.	|b| -Krait.	|c| -Krait.
C1	0.4778	1.4682	-0.1001	0.476(3)	1.462(1)	0.083(18)
C2	0.7998	-1.4119	-0.2573	0.793(2)	1.413(1)	0.230(7)
C3	1.8673	0.8779	-0.1244	1.8613(8)	0.866(2)	0.160(9)
C4	-0.6310	0.6956	-0.0366	0.615(2)	0.692(2)	0.01*i(25)
C5	1.9001	-0.5610	0.3943	1.8996(8)	0.553(3)	0.397(4)
C6	-0.5477	-0.7772	-0.0307	0.553(3)	0.776(2)	0.047(32)
O7	-1.5905	-1.4249	0.0310			
O8	-1.8784	1.2095	0.1026			
H9	-2.4687	0.4386	0.0942	2.4653(6)	0.392(4)	0.126(12)
H10	0.3583	2.5496	-0.0755			
H11	0.9674	-1.4238	-1.3445			
H12	0.7767	-2.4494	0.0880			
H13	2.5752	1.4986	0.4362			
H14	2.2008	0.8976	-1.1734			
H15	1.7254	-0.5529	1.4772			
H16	2.8826	-1.0125	0.2208			

The experimental A, B, and C rotational constants and the deviations of the "best fit" calculated values from the experimental values are listed in Table 4.2.6. Values of

the atomic coordinates obtained in the structural fit are listed in Table 4.2.7. Coordinates for the substituted atoms were also obtained by performing Kraitchman analyses, using the Kiesel KRA program, and these values are also shown in Table 4.2.7. Agreement between the structural fit values and Kraitchman values is very good, with the exception of several of the c-coordinates as these substituted atoms lie close to the principal axis and are not as reliable.

4.2.6 DISCUSSION

The rotational spectrum of 1,2-cyclohexandione has been measured using PBFT microwave spectroscopy and all of the measured lines were assigned. The experimental rotational transitions of all the isotopologues are listed in Tables 4.2.1-3, as well as the best fit structural parameters given in Tables 4.2.4 and 4.2.5. The best fit structure obtained from microwave data (Figure 4.2.1) is in good agreement with the structure obtained from the electron diffraction data. The C-C bond lengths also agreed well with values calculated from Gaussian 09. An exception is the C1-C4 bond length which was 0.025 Å larger than the calculated value. The dihedral angles for the best fit structure are $<(C_1\text{-}C_3\text{-}C_5\text{-}C_2) = 53°$ and $<(C_1\text{-}C_4\text{-}C_6\text{-}C_2) = -17°$, an indication of the non-planarity of the molecule. Carbon atoms C_1, C_2, C_3, C_4, and C_6 are all nearly in the same plane, with only C_5 being significantly out of plane. A more distorted structure was found for 1,2-cyclohexanedione by Hedberg, et, al.[33] using electron diffraction. That structure exhibited a mixture of a chair form of C_{2h} symmetry and a twisted boat form of D_2 symmetry which will account for the differences in the present microwave structure. Obtaining more accurate microwave values for the 1,2-cyclohexandione bond lengths

and angles would require measurements of significantly more rotational transitions for additional substituted isotopologues.

5. MICROWAVE MEASUREMENTS ON MOLECULES WITH ELECTRIC QUADRUPOLE INTERACTIONS

Electric quadrupole interactions between the quadrupole moments of nuclei and the electric field gradients within molecules adds to the complexity of the observed microwave spectra, yielding a very rich spectra full of rotational transitions. The analysis of the rich spectra yields important information about the electronic structure of the molecule which may lead to some insight into bonding and chemical reactivity. This chapter focuses on the molecules maleimide, a related molecule phthalimide, and 4a,8a-azaboranaphthalene. The quadrupole coupling strengths were determined for the quadrupolar nuclei in each system yielding important electronic structure information about these molecules in addition to the molecular structure parameters that are typically obtained from these microwave studies. In the case of 4a,8a-azaboranaphthalene, the aromatic character was determined from an extended Townes-Dailey analysis which will be described in more detail in the respective section. This analysis allows for the determination of the electron occupancies in the valence hybridized orbitals in each of the quadrupolar nuclei, ^{11}B and ^{14}N.

Microwave spectroscopy is a valuable tool to determine the electric quadrupole coupling strengths in molecules due to the low rotational states that are able to be probed with extremely high resolution. The determination of the electric quadrupole coupling strengths is an important parameter to identify different isomers present of a molecule[34] or even a different but related structure,[35] as well as characterizing the ionic character[36] in some systems. This chapter details the experiment and the results obtained for maleimide, phthalimide, and 4a,8a-azaboranaphthalene.

5.1 MALEIMIDE

5.1.1 INTRODUCTION

Maleimide (Mal) and its derivatives are important compounds in biological chemistry and in other types of applications, such as in biotechnology and organic synthesis. Fluorescent Mal derivatives are used to study the *in vivo* processes of intracellular trafficking, membrane association, and auto toxicity.[37,38] These Mal compounds are also the backbone of some enzyme inhibitors.[39] In organic synthesis, Mal and its derivatives play an important role in the protection of amino groups.[40] Bismaleimide resins are important in industrial applications due to the high temperature performance, toughness, and low cost in products such as tires.[41,42,43] Polyethylene glycol (PEG)-Mal compounds are often used to attach proteins to surfaces or PEG to different amino acid residues.[44,45] Synthesis of Mal is achieved with copolymers of styrene and maleic anhydride while reacting with gaseous NH_3 at elevated temperatures under low pressure environments.[46] Mal can also be prepared from dimethyl maleate through the Rinkes method.[47]

Maleimide or 2,5-pyrroledione (IUPAC), has a slight yellow crystalline appearance. The melting point of Mal is 92-95 °C[48] and the vapor pressure at 70 ºC is sufficient to measure the pure rotational spectrum by pulsed-beam microwave spectroscopy. Mal has been studied by X-ray diffraction[49], electron diffraction[50], and IR spectroscopic techniques. In order to obtain accurate gas phase structural parameters of Mal, the rotational spectrum should be measured for this molecule. This study extends the structural parameters of Mal to include these gas phase microwave measurements, which are important as structures may be distorted in solid phases

when compared to structural parameters obtained in the gas phase from microwave studies.

5.1.2 MICROWAVE MEASUREMENTS

The Mal sample was purchased from Sigma Aldrich (99%) and was used without further purification. All measurements were made in the 5 – 12 GHz range using a Flygare-Balle type pulsed-beam Fourier transform microwave spectrometer that has been previously described. The measured rotational transitions for the parent are listed in Table 5.1.1.

Table 5.1.1 Measured rotational transitions of the parent isotopologue of Maleimide, shown in MHz.

J′ Ka' Kc' F'	J″ Ka" Kc" F"	ν_{obs}	ν_{o-c}
1 1 0 1	1 0 1 1	5059.705	-0.002
1 1 0 1	1 0 1 2	5060.191	-0.000
1 1 0 2	1 0 1 1	5060.769	-0.001
1 1 0 1	1 0 1 0	5060.917	-0.001
1 1 0 2	1 0 1 2	5061.257	0.002
1 1 0 0	1 0 1 1	5062.367	0.003
2 1 1 2	2 0 2 2	5725.561	0.003
2 1 1 2	2 0 2 3	5726.190	0.005
2 1 1 3	2 0 2 3	5726.808	0.003
2 1 1 1	2 0 2 1	5727.498	-0.001
3 1 2 3	3 0 3 3	6827.303	0.002
3 1 2 4	3 0 3 3	6827.774	0.004
3 1 2 2	3 0 3 3	6827.938	0.002
3 1 2 3	3 0 3 4	6828.111	-0.002
3 1 2 3	3 0 3 2	6828.403	0.005
3 1 2 4	3 0 3 4	6828.586	0.003
3 1 2 2	3 0 3 2	6829.038	0.005
3 0 3 2	2 1 2 2	8214.566	0.003
3 0 3 3	2 1 2 2	8215.661	0.000
3 0 3 4	2 1 2 3	8215.991	0.005
3 0 3 2	2 1 2 1	8216.337	0.002

3	0	3	3	2	1	2	3	8216.799	-0.001
4	1	3	4	4	0	4	4	8466.040	-0.005
4	1	3	5	4	0	4	5	8467.432	-0.007
4	1	3	3	4	0	4	3	8467.795	-0.002
1	1	1	0	0	0	0	1	8568.683	-0.004
1	1	1	2	0	0	0	1	8569.553	-0.001
1	1	1	1	0	0	0	1	8570.125	-0.007
5	2	3	5	5	1	4	5	11862.727	0.002
5	2	3	6	5	1	4	6	11862.762	-0.004
4	0	4	4	3	1	3	3	12726.967	-0.002
4	0	4	5	3	1	3	4	12727.283	-0.003
4	0	4	3	3	1	3	2	12727.493	0.001
4	2	2	3	4	1	3	3	12191.258	0.004
4	2	2	5	4	1	3	5	12191.292	0.005
4	2	2	4	4	1	3	4	12191.410	-0.007

Prior to the pulse of the molecular beam, the pressure inside the vacuum cavity was maintained at 10^{-6} to 10^{-7} Torr. Ne was used as the carrier gas and the backing pressure was maintained at ~1 atm. In order to obtain sufficient vapor pressure of the solid Mal sample, the pulsed valve and sample cell were heated to ~70 °C as this temperature provided a strong parent test signal that can be seen in one pulsed beam cycle. The ^{13}C isotopologues were measured under natural abundance, using the same method as was used to measure the parent transitions. A –ND isotopologue sample was prepared and its transitions were also measured. The –ND isotopologue was prepared by dissolving equimolar amounts of both Mal and D_2O and allowing to mix and exchange H for D over several days. Most of the remaining water was removed under reduced pressure by pumping on the –ND sample for several hours at ~ 30 °C. All of the isotopologue transitions are listed in Table 5.1.2. The labeling scheme for each of the substituted atoms can be seen in the best fit structure, shown in Figure 5.1.1. There was a small amount of line broadening observed for the –ND isotopologue transitions.

This is most likely caused by the D quadrupole coupling, but there was no attempt to assign the D quadrupole splitting as these hyperfine splittings were not resolved.

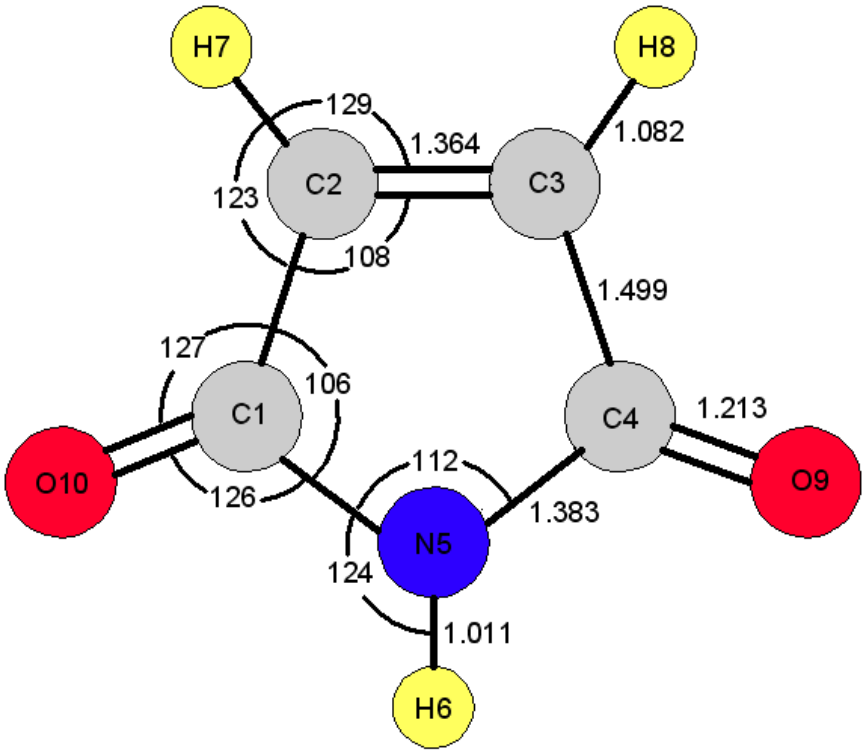

Figure 5.1.1 Best fit structure of Maleimide showing the fit bond lengths (Å) and angles (°). The bond lengths and angles are equivalent on the corresponding side across the symmetry axis.

Table 5.1.2 Measured rotational transitions of each unique ^{13}C isotopologue and the –ND isotopologue, shown in MHz.

Rotational Transitions		$^{13}C1\&4$		$^{13}C2\&3$		-ND	
J′ Ka′ Kc′ F′	J″ Ka″ Kc″ F″	ν_{obs}	ν_{o-c}	ν_{obs}	ν_{o-c}	ν_{obs}	ν_{o-c}
1 1 0 1	1 0 1 1	5066.350	-0.001	4925.181	0.004		
1 1 0 1	1 0 1 2	5066.836	0.003	4925.664	-0.001		
1 1 0 2	1 0 1 1	5067.408	-0.006	4926.245	0.000		
1 1 0 1	1 0 1 0	5067.557	-0.000				
1 1 0 2	1 0 1 2	5067.899	0.002	4926.732	-0.000		
1 1 0 0	1 0 1 1	5069.015	0.005				

2	1	1	2	2	0	2	2					5456.652	-0.002
2	1	1	2	2	0	2	3					5457.303	0.006
2	1	1	1	2	0	2	1					5458.627	-0.004
3	1	2	2	3	0	3	3	6813.879	0.004				
3	1	2	4	3	0	3	3			6725.419	-0.006		
3	1	2	3	3	0	3	2	6814.322	-0.004				
3	1	2	2	3	0	3	2			6726.713	0.006		
1	1	1	0	0	0	0	1	8559.294	0.002	8408.939	-0.001	8225.167	-0.002
1	1	1	2	0	0	0	1	8560.161	-0.002	8409.807	-0.003	8226.051	0.003
1	1	1	1	0	0	0	1	8560.735	-0.008	8410.388	-0.002	8226.633	-0.001
3	0	3	3	2	1	2	2					8451.905	-0.003
3	0	3	2	2	1	2	1					8452.558	0.003
2	1	2	1	1	0	1	1	12051.583	-0.001			11689.513	0.002
2	1	2	3	1	0	1	2	12052.704	0.005	11893.164	0.005	11690.633	-0.004
2	1	2	2	1	0	1	1			11893.816	0.001	11691.298	-0.001
2	1	2	2	1	0	1	2			11894.299	-0.004	11691.790	0.004

5.1.3 CALCULATIONS

Ab initio calculations were performed to predict the structure of MaI using the Gaussian 09 suite, on the HPC system at the University of Arizona. The calculations were performed using an MP2 method with the 6-311++G** basis set. The Gaussian calculated rotational and quadrupole coupling constants were used in Pickett's SPCAT program to predict the b-type rotational transitions expected to be observed, as the calculated Gaussian structure had a large b-dipole of ~1.6 D. To predict the isotopologue rotational constants, a set of scale factors – the ratios between the experimental rotational constants of the parent and their corresponded *ab initio* values, were used to provide reasonable predictions. From the *ab initio* parent isotopologue molecular structure, the mass of the substituted atom was changed and the moments of inertia and corresponding rotational constants were recalculated using Kisiel's PMIFST program. These calculated rotational constants were multiplied by the scale factors obtained from the parent to obtain corrected rotational constants for each of the singly

substituted isotopologues. These scaled rotational constants were used in the SPCAT program, along with the experimentally determined quadrupole coupling constants of the parent, to predict the isotopologue rotational transitions. The experimental results agreed with those scaled values very well, within 1%.

5.1.4 ROTATIONAL CONSTANTS

The rotational constants, quadrupole coupling constants and centrifugal distortion constants were all determined from the measured rotational transitions using Pickett's SPFIT program and all the fit values are shown in Table 5.1.3. During the fits of the isotopologue rotational and quadrupole coupling constants, the centrifugal distortion constants were held fixed to what was obtained from the parent. The rotational constants obtained from the best fit gas phase structure are shown with the experimentally fit values, along with their differences (M – C) in Table 5.1.4. The calculated rotational constants from the best fit structure had a standard deviation of 0.285 MHz from the experimental values.

Table 5.1.3 Fit and calculated spectroscopic constants of the isotopologues.

	Parent	MP2/6-311++G**	B3LYP/aug-cc-pVTZ	^{13}C(1&4)	^{13}C(2&3)	-ND
A/MHz	6815.3251(12)	6818.4054	6848.9871	6813.9509(16)	6668.1911(18)	6493.8111(13)
B/MHz	2361.85011(64)	2340.2953	2364.7515	2347.6975(18)	2356.7728(19)	2361.90584(80)
C/MHZ	1754.32750(64)	1742.2867	1757.8263	1746.3107(10)	1741.7171(10)	1732.33683(56)
D_J/kHz	0.232(24)			0.232*	0.232*	0.232*
D_{JK}/kHz	0.546(54)			0.546*	0.546*	0.546*
$1.5\chi_{aa}$/MHz	2.4227(53)	2.4996	2.4968	2.4130(87)	2.437(12)	2.436(11)
$0.25(\chi_{bb}-\chi_{cc})$/MHz	1.3679(15)	1.4520	1.4156	1.3702(30)	1.3731(32)	1.3826(24)
N	36			13	12	12
σ/kHz	3			4	3	3

* Centrifugal distortion constants were held fixed to the parent during fits of ^{13}C isotopologues

Table 5.1.4 Measured rotational constants compared to the rotational constants calculated of the best fit structure, also showing the difference (M – C), shown in MHz. The standard deviation of the best fit structure was 0.285 MHz.

ISOTOPOLOGUE		MEASURED	CALCULATED	(M – C)
Parent	A	6815.3251	6815.8202	-0.4951
	B	2361.8501	2362.1247	-0.2746
	C	1754.3275	1754.1855	0.1420
^{13}C1	A	6813.9509	6814.1430	-0.1921
	B	2347.6975	2347.7251	-0.0276
	C	1746.3107	1746.1215	0.1892
^{13}C4	A	6813.9509	6814.1430	-0.1921
	B	2347.6975	2347.7251	-0.0276
	C	1746.3107	1746.1215	0.1892
^{13}C2	A	6668.1911	6667.8319	0.3592
	B	2356.7728	2356.9009	-0.1281
	C	1741.7171	1741.3722	0.3449
^{13}C3	A	6668.1911	6667.8319	0.3592
	B	2356.7728	2356.9009	-0.1281
	C	1741.7171	1741.3722	0.3449
-ND	A	6493.8111	6493.7284	0.0827
	B	2361.9058	2362.1247	-0.2189
	C	1732.3368	1732.0744	0.2624

5.1.5 MOLECULAR STRUCTURE

A best fit gas phase structure, which is an averaged structure of both equilibrium and ground state coordinates, was obtained for MaI using a nonlinear least squares fitting program with the measured rotational constants from each of the isotopologues. The fitting program varies the Cartesian coordinates of the atoms within the molecule and a “best fit” structure is determined. This best fit structure yields calculated moments of inertia closest to the experimentally obtained values (smallest deviations). From the MP2 calculation, the structure was predicted to be planar with C_{2v} symmetry. The inertial defect calculated using the experimental parent rotational constants was Δ = -0.0536 amu Å^2, confirming that the actual structure of MaI is indeed planar with a value

very close to zero. The slight negative value of the inertial defect indicates Mal exhibits out of plane vibrations.[51] The Kraitchman determined c-coordinates of H6 are small (Table 5.1.5) further supporting a planar structure of Mal, and indicating no large amplitude motions of H6.

In the structure fit, there were a total of 4 varied parameters representing the movement of the carbon atoms in the a-b plane. With the Mal structure being planar, all c-coordinates were set to zero. Assuming that the C_{2v} symmetry is maintained, the varied parameters in the fit were the same for corresponding atoms on each side of the line of symmetry, with the exception of the varied parameters in the a-direction which were opposite for each corresponding atom. The only fixed atoms in the fit were the N and H atoms forming the imide group, so the N-H bond length was fixed to the calculated equilibrium value. The H and O atoms bonded to the C atoms in the ring were varied by the same parameters as the carbon atom it is bonded to, resulting in the C-H and C=O bond lengths to be fixed to calculated equilibrium values. With these constraints and varied parameters, the standard deviation of this nonlinear least squares structure fit was 0.285 MHz.

A Kraitchman analysis was also performed on all isotopically substituted atoms using the Kisiel KRA program. The best fit structure coordinates as well as the Kraitchman determined coordinates for each substituted atom is shown in Table 5.1.5. The coordinates from the best fit structure and Kraitchman analysis seem to agree very well with the exception of the a-coordinate of H6, shown as an imaginary number. This substituted atom lies on the b-axis, thus making the Kraitchman determined coordinate unreliable.

Table 5.1.5 Principle a and b coordinates (Å) of the best fit structure compared to the coordinates of the unique singly substituted ^{13}C substituted and –ND isotopologues determined from a Kraitchman analysis. The Kraitchman coordinates only show the magnitude of the substituted coordinates.

Atom	a	b	Krait-|a|	Krait-|b|
C1	1.1452	-0.1362	1.1474(13)	0.123(12)
C2	0.6820	1.2894	0.6689(23)	1.2856(12)
C3	-0.6820	1.2894	0.6689(23)	1.2856(12)
C4	-1.1452	-0.1362	1.1474(13)	0.123(12)
N5	0.0000	-0.9108		
H6	0.0000	-1.9216	0.119*i(13)	1.91988(78)
H7	1.3659	2.1285		
H8	-1.3659	2.1285		
O9	-2.2886	-0.5401		
O10	2.2886	-0.5401		

The structural parameters obtained from the nonlinear least squares fit and the Gaussian calculation are shown in Tables 5.1.6 (bond lengths) and 5.1.7 (angles). Figure 5.1.1 shows the structural parameters obtained from the structure fit. Because Mal has C_{2v} symmetry, only half of the bond lengths and angles are shown in the figure because these values are exactly equal on the corresponding side across the symmetry axis. The double C2 – C3 bond increased by 0.044 Å from the calculation whereas the single bonds decreased by 0.002 Å from the calculated values. Most angles changed by 1° in the fit from the calculation with the exception of three of the angles that had the same values as in the calculation.

Table 5.1.6 Microwave fit values for bond lengths (in angstroms) compared to MP2/6-311++G** calculated values. Corresponding bond lengths across line of symmetry are equal.

Interatomic Distance	Microwave Fit Value (Å)	Calculated Value (Å)
$r(C_2\text{-}C_3)$	1.364	1.345
$r(C_3\text{-}H_8)$	1.082*	1.082
$r(C_3\text{-}C_4)$	1.499	1.502
$r(C_4\text{-}O_9)$	1.213*	1.213
$r(C_4\text{-}N_5)$	1.383	1.396
$r(N_4\text{-}H_6)$	1.011*	1.011

*Values were fixed to Gaussian calculated equilibrium values

Table 5.1.7 Microwave fit values for angles (in degrees) compared to MP2/6-311++G** calculated values. Corresponding angles across line of symmetry are equal.

Angle	Microwave Fit Value	Calculated
$<(H_7\text{-}C_2\text{-}C_3)$	129	129
$<(H_7\text{-}C_2\text{-}C_1)$	123	122
$<(C_1\text{-}C_2\text{-}C_3)$	108	109
$<(C_2\text{-}C_1\text{-}O_{10})$	127	128
$<(C_2\text{-}C_1\text{-}N_5)$	106	105
$<(O_{10}\text{-}C_1\text{-}N_5)$	126	127
$<(C_1\text{-}N_5\text{-}C_4)$	112	112
$<(C_1\text{-}N_5\text{-}H_6)$	124	124

5.1.6 DISCUSSION

The pure rotational spectrum of MaI was measured in the 5-12 GHz range using a Flygare-Balle type microwave spectrometer and all measured transitions were assigned for the first time, providing experimentally determined rotational, centrifugal distortion, and quadrupole coupling constants. Two unique singly substituted ^{13}C isotopologues and an –ND isotopologue were also measured and the respective

rotational and quadrupole coupling constants were determined. The nonlinear least squares structure fit performed with the rotational constants of all the measured isotopologues had a standard deviation of 0.285 MHz, providing the first gas phase structure of this molecule with high accuracy. The best-fit experimental bond lengths were close (~0.01 Å) to values from the Gaussian calculations. The greatest difference in bond length being the C2 – C3 bond (~0.04 Å different). The best-fit experimental bond angles deviated by 1° from the Gaussian calculations. These differences between the experiment and the calculations are most likely caused from the calculated structures being an equilibrium structure whereas the experimental structure is a vibrationally averaged ground state structure.

The structure obtained from the electron diffraction study was similar to the structure obtained in the present work. The largest differences between the current microwave and previous electron diffraction structures were seen in the bonds of C2 – C3 and C4 – N5, which deviated by 0.03 and 0.02 Å. The C2 – C3 bond is larger and the C4 – N5 bond is smaller than in the electron diffraction study. To obtain a more complete and accurate gas phase structure and fit the remaining bond lengths and angles, a unique single D substitution at H7, a unique ^{18}O single substitution and ^{15}N isotopologues will need to be measured. Even though the structure determined for Mal is an averaged structure made up from both equilibrium (r_e) and ground (r_0) state atomic coordinates of the different isotopologues, these differences are small and so the determined structure is an excellent representation of the vibrationally averaged ground state.

5.2 PHTHALIMIDE

5.2.1 INTRODUCTION

Phthalimide (PhI) and its derivatives are important compounds widely utilized in industry as well as in medicinal chemistry, due to the biological activity of PhI and its derivatives. Derivatives of PhI have been used in medicinal chemistry and have been found to have a wide range of biological activities, including antitumor, anti-inflammatory, and antimicrobial properties.[52] PhI derivatives are also used to interact with liver receptors that are involved in the regulation of cholesterol, lipid and glucose metabolism.[53] In industry, PhI is used in plastics, plasticizers, and is also used in the synthesis of peptides and as a masked source for amines.[54]

Phthalimide, $C_6H_4(CO)_2NH$, or isoindole-1,3-dione (IUPAC) has a melting point of 237-238 °C.[55] PhI is a solid white crystal and can be obtained by heating phthalic anhydride with ammonia or another amine source, such as ammonium carbonate or ammonium acetate.[56] The vapor pressure of PhI at 90°C is ~0.01 Torr[57], sufficient to measure the rotational transitions using pulsed-beam Fourier transform (PBFT) microwave spectroscopy. The crystal structure of PhI was initially determined by Matzat using data collected from the mineral kladnoite[58] and the IR spectrum was measured by Binev *et al.*[59] In order to gain further insight into the molecular structure, Glidewell et al. performed an X-ray crystallography analysis on PhI that was crystallized with pyridine.[60] However, due to the packing effects and distortions within crystal structures of molecules, it is important to measure the pure rotational spectrum of PhI in an attempt obtain accurate gas phase structure.

5.2.2 MICROWAVE MEASUREMENTS

The phthalimide sample was purchased from Sigma Aldrich (99%) and was used without further purification. A pulsed-beam Fourier transform microwave spectrometer, described previously, was used to make microwave measurements in the 4.8–9.5 GHz range for the parent isotopologue and these transitions are shown in Table 5.2.1.

Table 5.2.1 Measured rotational transitions of the parent isotopologue shown in MHZ.

J′ Ka′ Kc′ F′	J″ Ka″ Kc″ F″	ν_{obs}	ν_{o-c}
3 1 3 4	2 1 2 3	4885.647	-0.001
3 1 3 2	2 1 2 1	4885.773	0.002
3 1 3 3	2 1 2 2	4885.932	-0.004
3 1 3 3	2 1 2 3	4887.012	-0.002
3 0 3 2	2 0 2 2	5057.851	-0.004
3 0 3 4	2 0 2 3	5059.259	-0.002
3 0 3 2	2 0 2 1	5059.336	0.008
3 0 3 3	2 0 2 2	5059.637	0.010
3 0 3 3	2 0 2 3	5060.568	-0.005
4 2 3 4	4 0 4 4	5076.449	-0.003
4 2 3 5	4 0 4 5	5077.656	-0.005
4 2 3 3	4 0 4 3	5077.972	0.000
3 2 2 2	2 2 1 1	5730.793	-0.006
3 2 2 4	2 2 1 3	5731.123	0.000
3 2 2 3	2 2 1 3	5731.123	0.000
3 2 2 3	2 2 1 2	5731.703	-0.002
3 2 2 2	2 2 1 2	5731.703	-0.002
3 1 2 2	2 1 1 1	6285.845	-0.002
3 1 2 4	2 1 1 3	6286.060	0.000
3 1 2 3	2 1 1 2	6286.374	0.002
4 1 4 5	3 1 3 4	6368.981	-0.005
4 1 4 3	3 1 3 2	6369.065	0.002
4 1 4 4	3 1 3 3	6369.185	0.003
3 2 1 2	2 2 0 1	6402.812	-0.000
3 2 1 4	2 2 0 3	6403.096	0.005
3 2 1 3	2 2 0 2	6403.328	-0.002
4 0 4 5	3 0 3 4	6437.139	-0.004
4 0 4 3	3 0 3 2	6437.206	0.003
4 0 4 4	3 0 3 3	6437.383	-0.002
2 2 0 1	1 0 1 1	7194.918	0.001
2 2 0 3	1 0 1 2	7194.940	0.005

4	2	3	3	3	2	2	2	7468.723	0.008
4	2	3	3	3	2	2	3	7468.723	0.008
4	2	3	5	3	2	2	4	7468.799	-0.005
4	2	3	4	3	2	2	3	7469.146	-0.003
4	2	3	4	3	2	2	4	7469.146	-0.003
5	1	5	6	4	1	4	5	7813.517	-0.002
5	1	5	4	4	1	4	3	7813.568	-0.005
5	1	5	5	4	1	4	4	7813.672	0.009
5	0	5	6	4	0	4	5	7834.351	0.000
5	0	5	4	4	0	4	3	7834.396	-0.005
5	0	5	5	4	0	4	4	7834.499	-0.010
4	1	3	3	3	1	2	2	7993.887	0.005
4	1	3	3	3	1	2	4	7993.953	0.003
4	1	3	5	3	1	2	4	7993.988	-0.005
4	1	3	4	3	1	2	3	7994.350	-0.004
5	2	4	4	4	2	3	3	9088.837	0.009
5	2	4	6	4	2	3	5	9088.871	0.007
5	2	4	5	4	2	3	4	9089.131	-0.000
6	1	6	7	5	1	5	6	9242.336	-0.000
6	1	6	5	5	1	5	4	9242.377	-0.001
6	1	6	6	5	1	5	5	9242.445	-0.000
6	0	6	7	5	0	5	6	9247.940	0.003
6	0	6	5	5	0	5	4	9247.975	-0.003
6	0	6	6	5	0	5	5	9248.051	0.002

Ne was used as the carrier gas and the backing pressure was set to ~ 1 atm. Prior to the pulsed injection of the gaseous sample, the pressure inside the microwave cavity was maintained at 10^{-6} to 10^{-7} Torr and the pulsed valve was heated to ~125 – 130 °C in order to obtain sufficient vapor pressure of the sample to obtain a parent test signal in one pulsed-beam cycle. The unique ^{13}C isotopologues of PhI were measured in the same way as the parent in the 4.8 – 6.5 GHz range. The labeling scheme used to describe the isotopic substitutions is shown in Figure 5.2.1 and the measured rotational transitions of all the ^{13}C isotopologues are shown in Table 5.2.2.

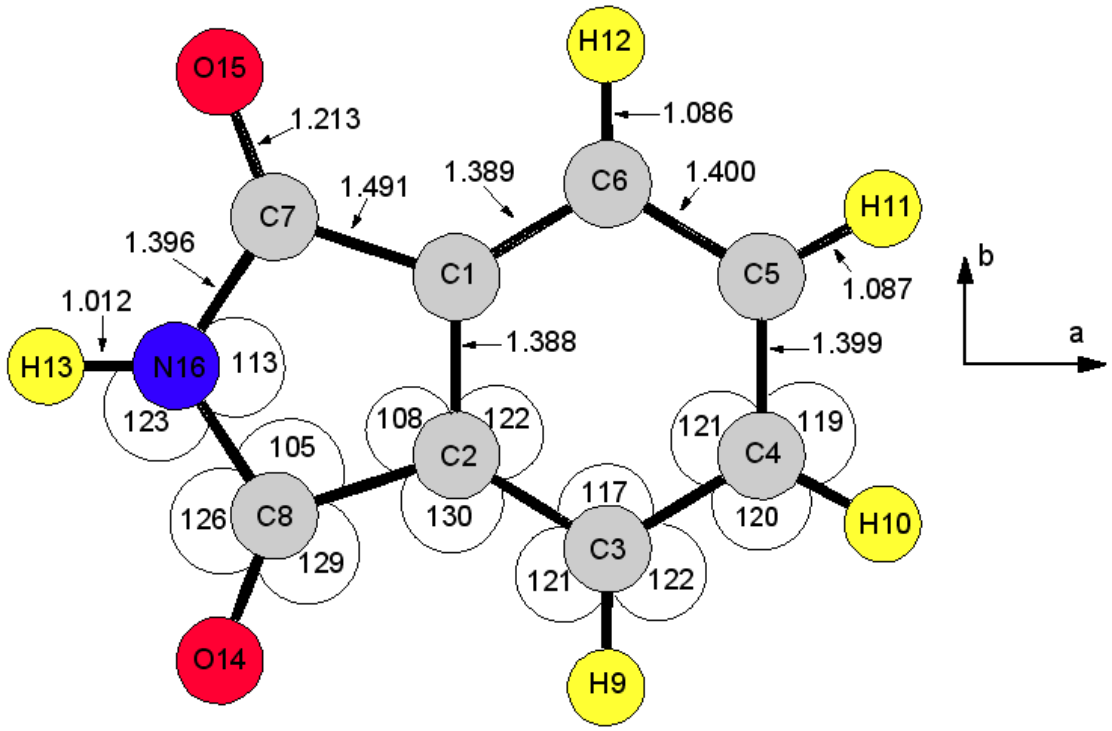

Figure 5.2.1 Best fit structure showing fit bond lengths (top, in Å) and angles (bottom, in °). Also shown are the a and b principle axes within the molecule.

Table 5.2.2 Measured rotational transitions of each unique ^{13}C isotopologue shown in MHz.

Rotational Transitions		^{13}C 1&2		^{13}C 3&6		^{13}C 4&5		^{13}C 7&8	
J′ Ka′ Kc′ F′	J″ Ka″ Kc″ F″	ν_{obs}	ν_{o-c}	ν_{obs}	ν_{o-c}	ν_{obs}	ν_{o-c}	ν_{obs}	ν_{o-c}
3 1 3 4	2 1 2 3	4882.766	0.001	4859.367	0.001	4831.116	0.001	4867.167	0.001
3 1 3 2	2 1 2 1	4882.887	0.000	4859.490	0.003	4831.235	-0.002	4867.290	0.000
3 1 3 3	2 1 2 2	4883.056	-0.004	4859.655	-0.005	4831.403	-0.001	4867.456	-0.004
3 0 3 4	2 0 2 3	5055.325	-0.002	5030.741	-0.004	5011.206	0.000	5039.398	-0.001
3 0 3 2	2 0 2 1	5055.406	0.005	5030.821	0.003	5011.273	-0.000	5039.472	0.004
3 0 3 3	2 0 2 2	5055.692	0.001	5031.106	0.001	5011.570	0.001	5039.767	-0.001
4 1 4 5	3 1 3 4	6364.763	-0.002	6334.076	-0.006	6302.040	-0.005	6344.535	-0.003
4 1 4 3	3 1 3 2	6364.848	0.002	6334.165	0.005	6302.129	0.007	6344.619	0.003
4 1 4 4	3 1 3 3	6364.964	-0.003	6334.282	0.002	6302.241	-0.000	6344.740	0.003
4 0 4 5	3 0 3 4	6432.188	-0.004	6400.922	-0.001	6375.781	-0.000	6411.909	0.000
4 0 4 3	3 0 3 2	6432.255	0.003	6400.988	0.003	6375.841	0.000	6411.965	-0.005
4 0 4 4	3 0 3 3	6432.426	0.003	6401.160	-0.002	6376.023	-0.002	6412.155	0.003

5.2.3 CALCULATIONS

Ab initio and DFT calculations were performed using the Gaussian 09 suite on the high performance computing system at the University of Arizona to obtain an optimized gas phase equilibrium structure which was used to predict the rotational transitions of PhI. Calculations were performed using MP2 and B3LYP methods with 6-311++G** and aug-cc-pVQZ basis sets respectively for each method. The calculated rotational and quadrupole coupling constants of each calculation were used in Pickett's SPCAT program to predict the rotational transitions of the parent isotopologue.

In order to predict the rotational constants of all the unique ^{13}C isotopologues, first the ratios between the experimentally determined parent rotational constants and the MP2/6-311++G** calculated rotational constants were determined. After changing the mass of the ^{13}C atom within the molecular structure and recalculating the rotational constants of the new structure, these rotational constants of the isotopologue were multiplied by the previously determined experimental/calculated ratio to obtain corrected rotational constants of the ^{13}C isotopologues, which were within <1% of the final experimentally fit values. These corrected rotational constants and the quadrupole coupling constants of the parent were used in the SPCAT program to predict the ^{13}C isotopologue rotational transitions.

5.2.4 ROTATIONAL CONSTANTS

The rotational constants for the parent and all unique ^{13}C isotopologues were determined using Pickett's SPFIT program and these results are shown in Table 5.2.3. While fitting the measured rotational transitions of the unique ^{13}C isotopologues, the centrifugal distortion constants (D_J and D_{JK}) were held fixed to what was obtained from

the fit for the parent. The rotational constants obtained from the best fit gas phase structure are shown with the experimentally fit rotational constants of all the isotopologues and the measured – calculated differences (M – C) of these values in Table 5.2.4. The calculated rotational constants of the best fit structure and its isotopologues had a standard deviation of 0.14 MHz. THE B3LYP/aug-cc-pVQZ calculated rotational constants were also much closer to the experimentally determined values compared to the MP2/6-311++G** values, which can also be seen in Table 5.2.3.

Table 5.2.3 Fit rotational, centrifugal distortion and quadrupole coupling constants of the parent and unique ^{13}C isotopologues, as well as the MP2/6-311++G** calculated values for the parent.

	Parent	MP2/6-311++G**	B3LYP/aug-cc-pVQZ	^{13}C(1&2)	^{13}C(3&6)	^{13}C(4&5)	^{13}C(7&8)
A/MHz	1745.66545(95)	1731.668	1753.935	1742.7830(93)	1733.751(10)	1742.8865(81)	1737.6542(82)
B/MHz	1199.33090(54)	1194.126	1202.057	1199.2423(53)	1193.7412(60)	1180.4406(45)	1195.2699(47)
C/MHZ	711.08644(29)	706.758	713.239	710.5795(10)	707.1382(11)	703.94653(92)	708.32901(94)
D_J/kHz	0.0120(65)			0.0120*	0.0120*	0.0120*	0.0120*
D_{JK}/kHz	-0.050(81)			-0.050*	-0.050*	-0.050*	-0.050*
$1.5\chi_{aa}$/MHz	2.719(10)	2.9207	2.9480	2.875(67)	2.856(76)	2.785(59)	2.790(60)
$0.25(\chi_{bb}- \chi_{cc})$/MHz	1.2363(37)	1.2916	1.2745	1.222(12)	1.222(13)	1.231(10)	1.248(10)
N	55			12	12	12	12
σ/kHz	4			3	3	3	3

* Centrifugal distortion constants were held fixed to the parent during fits of ^{13}C isotopologues

Table 5.2.4 Measured rotational constants compared to the rotational constants calculated of the best fit structure, also showing the difference (M – C).

ISOTOPOLOGUE		MEASURED	CALCULATED	(M – C)
Parent	A	1745.6654	1745.6989	-0.0334
	B	1199.3309	1199.4121	-0.0812
	C	711.0864	710.9451	0.1413
^{13}C1&2	A	1742.7830	1742.8085	-0.0255
	B	1199.2423	1199.2756	-0.0333
	C	710.5795	710.4174	0.1621
^{13}C3&6	A	1733.7512	1733.7742	-0.0230
	B	1193.7412	1193.7870	-0.0458
	C	707.1382	706.9902	0.1480
^{13}C4&5	A	1742.8865	1742.9089	-0.0224
	B	1180.4406	1180.4885	-0.0479
	C	703.9465	703.7989	0.1476
^{13}C7&8	A	1737.6542	1737.6740	-0.0198
	B	1195.2699	1195.3256	-0.0557
	C	708.3290	708.1781	0.1509

5.2.5 MOLECULAR STRUCTURE

To obtain a best fit gas phase structure of the PhI molecule, which is a vibrationally averaged structure consisting of equilibrium and ground state bond lengths and angles, a nonlinear least squares fit was performed using the measured rotational constants from each of the isotopologues. In the least squares fit, there were a total of 8 varied parameters in 2D Cartesian space. From the B3LYP/aug-cc-pVQZ calculation, the structure of PhI was planar with C_{2v} symmetry and to reduce the number of parameters in the fit from 3D to 2D Cartesian space, the PhI molecule was restricted to only be in the a-b plane. The inertial defect calculated from the experimental rotational constants of the parent isotopologue was Δ = -0.175 amu Å^2, confirming that the structure of PhI is indeed planar with the calculated value close to zero. The negative

nonzero value indicates there are some slight out of plane vibration modes within PhI. During the structure fit, all C – H and C = O bonds were fixed to the Gaussian calculated equilibrium values and atoms H13 and N16 were held fixed to their calculated equilibrium a-b coordinates fixing the N – H bond to its equilibrium value. Due to the C_{2v} symmetry in the molecule, each corresponding atom on opposite sides of the symmetry axis (a-axis) were varied by the same variable a and b parameters, with the exception of the parameter in the b-direction being varied by exactly opposite. With these constraints and variable parameters set, the structure fit produced a best fit structure with a standard deviation of only 0.14 MHz. A Kraitchman analysis was performed for all the ^{13}C isotopologues using the Kiesel KRA program. The best fit structure coordinates of the parent are compared to the ^{13}C coordinates determined by the Kraitchman analysis in Table 5.2.5. The agreement between the Kraitchman coordinates and best fit structure coordinates is very good, with the exception of the a-coordinate of C1 which is different by ~0.04 Å and this difference can be accounted for the atom being closer to the center of mass in the molecule, making the Kraitchman coordinates less reliable.

Table 5.2.5 Principle a and b coordinates of the best fit structure compared to the coordinates of the unique ^{13}C substituted atoms determined from a Kraitchman analysis.

Atom	a	b	Krait-|a|	Krait-|b|
C1	-0.218960	0.694229	0.17(8)	0.69(31)
C2	-0.219010	-0.694261		
C3	-1.400780	-1.424120	1.40(33)	1.42(34)
C4	-2.598847	-0.699165	2.60(94)	0.70(25)
C5	-2.598787	0.699354		
C6	-1.400659	1.424193		
C7	1.196171	1.164577	1.19(505)	1.16(493)
C8	1.196067	-1.164748		
H9	-1.389308	-2.510437		

H10	-3.546617	-1.230599
H11	-3.546506	1.230883
H12	-1.389086	2.510510
H13	2.978304	-0.000169
O14	1.623990	-2.299981
O15	1.624171	2.299778
N16	1.966051	0.000168

The structural parameters obtained from the structure fit are shown in Tables 5.2.6 (bond lengths) and 5.2.7 (angles) compared to the B3LYP/aug-cc-pVQZ calculated values, and these bond lengths and angles correspond to what is shown in Figure 5.2.1. Because of the C_{2v} symmetry of PhI, only the bond lengths and angles for one side of the symmetry axis are shown, since the corresponding bond lengths and angles for the opposite side of the a-axis are equal. The fit bond lengths and angles compared to the B3LYP calculation are very close, only differing by ~0.005 Å for the bond lengths and are exactly equal for all angles, with the exception of $<(C_1\text{-}C_2\text{-}C_3)$ which increased by 1° from the calculation. Even though the determined gas phase structure is vibrationally averaged between the equilibrium and ground state structures, the differences are small and so the fit structure is an excellent representation of phthalimide.

Table 5.2.6 Microwave fit values for bond lengths (in angstroms) compared to B3LYP/aug-cc-pVQZ calculated values.

Interatomic Distance	Microwave Fit Value (Å)	Calculated Value (Å)
$r(C_1\text{-}C_2)$	1.388	1.392
$r(C_1\text{-}C_6)$	1.389	1.381
$r(C_1\text{-}C_7)$	1.491	1.493
$r(C_7\text{-}N_{16})$	1.396	1.398
$r(C_5\text{-}C_6)$	1.400	1.395
$r(C_4\text{-}C_5)$	1.399	1.394

Table 5.2.7 Microwave fit values for angles (in degrees) compared to B3LYP/aug-cc-pVQZ calculated values.

Angle	Microwave Fit Value	Calculated
$<(C_1\text{-}C_2\text{-}C_3)$	122	121
$<(C_1\text{-}C_2\text{-}C_8)$	108	108
$<(C_3\text{-}C_2\text{-}C_8)$	130	130
$<(N_{16}\text{-}C_8\text{-}C_2)$	105	105
$<(N_{16}\text{-}C_8\text{-}O_{14})$	126	126
$<(C_2\text{-}C_8\text{-}O_{14})$	129	129
$<(C_7\text{-}N_{16}\text{-}C_8)$	113	113
$<(H_{13}\text{-}N_{16}\text{-}C_8)$	123	123
$<(C_2\text{-}C_3\text{-}C_4)$	117	117
$<(C_2\text{-}C_3\text{-}H_9)$	121	121
$<(H_9\text{-}C_3\text{-}C_4)$	122	122
$<(C_5\text{-}C_4\text{-}C_3)$	121	121
$<(C_5\text{-}C_4\text{-}H_{10})$	119	119
$<(H_{10}\text{-}C_4\text{-}C_3)$	120	120

5.2.6 DISCUSSION

The rotational spectrum of PhI was measured in the 4.8 to 9.5 GHz range using pulsed-beam Fourier transform microwave spectroscopy. The rotational transitions measured for the parent and all unique ^{13}C isotopologues are given in Tables 5.2.1 and 5.2.2. Using the rotational constants determined from each of the measured

isotopologues, a vibrationally averaged ground state gas phase structure was determined and is shown in Figure 5.2.1. Tables 5.2.5 – 5.2.7 show the best fit a-b principle axes coordinates, the interatomic distances, and angles respectively. The best fit structure obtained of PhI is in very good agreement with the crystal structure data obtained previously, with the bond lengths only deviating by ~0.01 Å and angles varying by ~0.1°. Obtaining a more complete gas phase structure will require the measurement of deuterium substituted isotopologues.

5.3 4a,8a-AZABORANAPHTHALENE

5.3.1 INTRODUCTION

Interest has been growing in the amine-borane functional groups because of the potential of this group to act as a hydrogen storage material.[61,62] This group stems from the ammonia borane molecule which is an air-stable solid with 19.6% (by weight) of hydrogen. This groups ability to thermally[63] and catalytically[64] desorb H_2 has been significantly studied. The addition of carbon atoms to the amine-borane groups (CBN materials) are currently being studied and have been shown to possess improved thermal stability[65] leading to improved efficiency[66] as well as room temperature liquid-phase behavior[67] and facile regeneration.[68] Aromatic hydrocarbons are of interest because of the well-defined π-conjugation which can be utilized in areas such as organic semiconductors[69] and sensors.[70] The insertion of the B-N group into aromatic hydrocarbons is gaining interest because it provides different electronic properties.[71,72] These molecules can be used for a number of different cross-coupling reactions and also act as fluorophores with a distinct response to certain ions, enabling them to act as chemosensors.[73]

Gas phase microwave spectroscopy provides an accurate method to determine molecular structures. It also allows for identification of compounds and additional understanding of the electronic charge distribution in molecules from the analysis of the hyperfine structure, resulting in the nuclei's electric quadrupole coupling strengths. BN-cyclohexane is a cyclic CBN material with one BN substitution within the cyclohexane ring.[74] Recently, an attempt to determine the structural information of BN-cyclohexane was carried out by microwave spectroscopy. Under the experimental conditions (heating

of sample and pulsed-valve in a Ne gas stream prior to a supersonic expansion of the gaseous sample into a vacuum cavity) there was a loss of H_2 and BN-cyclohexene was produced and the spectra observed.[75] Substituting the BN group into the quintessential molecule benzene yields 1,2-dihydro-azaborine which has also been studied by gas phase microwave spectroscopy.[76] Structural studies regarding B-N bond distances of substituted 1,2-azaborine derivatives using X-ray diffraction have shown that these azaborine compounds have delocalized electronic structures consistent with aromatic character.[77] The experimental determination of nuclear quadrupole coupling strengths allows for the determination of the valence p-orbital electron occupations on the B and N nuclei using an extended Townes – Daily model.[78,79] This results from this model provides information about the aromatic character of these molecules by comparing the determined electron occupations with the calculated natural bond orbital (NBO) occupations for boron and nitrogen. Other molecules studied by microwave spectroscopy containing the B-N substitution are N-Et-1,2-azaborine,[80] aziridine-borane,[81] H_3N-BF_3,[82,83] ammonia-borane,[84] aminoborane,[85,86] aminodifluoroborane,[87] diaminoborane,[88] and a van der Waals complex with HCN-BF_3.[89] The present work extends the BN-substituted molecules studied to include yet another quintessential BN substituted molecule, BN-naphthalene (4a,8a-azaboranaphthalene). A disordered X-ray crystal structure was determined previously so the accuracy of the current structure is limited.[90] It would be important to determine accurate structural parameters and characterize the aromatic character of BN-naphthalene using gas phase microwave spectroscopy.

5.3.2 CALCULATIONS

A DFT computation was performed for BN-naphthalene to obtain an optimized equilibrium structure using a B3LYP method with an aug-cc-pVTZ basis. This computation was performed using the Gaussian 09 suite at the University of Arizona. The calculated dipole moment was 1.6 D oriented along the b-axis. The calculated rotational constants of the optimized equilibrium structure were used in Pickett's SPCAT program to obtain the predicted frequencies of the b-type transitions expected to be observed due to the large b-dipole moment component. Once the rotational constants were determined for the most abundant $^{11}B^{14}N$ isotopologue, a set of scale factors were determined from the ratio of the experimentally determined rotational constants with the optimized, calculated values. To predict the $^{11}B^{13}C$ isotopologue rotational constants, first the moments of inertia were recalculated for the isotopologue after changing one of the masses of ^{12}C to that of ^{13}C using Kisiel's PMIFST program. These rotational constants were multiplied by the set of scale factors determined from the $^{11}B^{14}N$ isotopologue to obtain the predicted set of $^{11}B^{13}C$ isotopologue rotational constants. These predicted rotational constants were within 1% of the final experimentally determined values after the assignments of the rotational energy levels to the transitions measured.

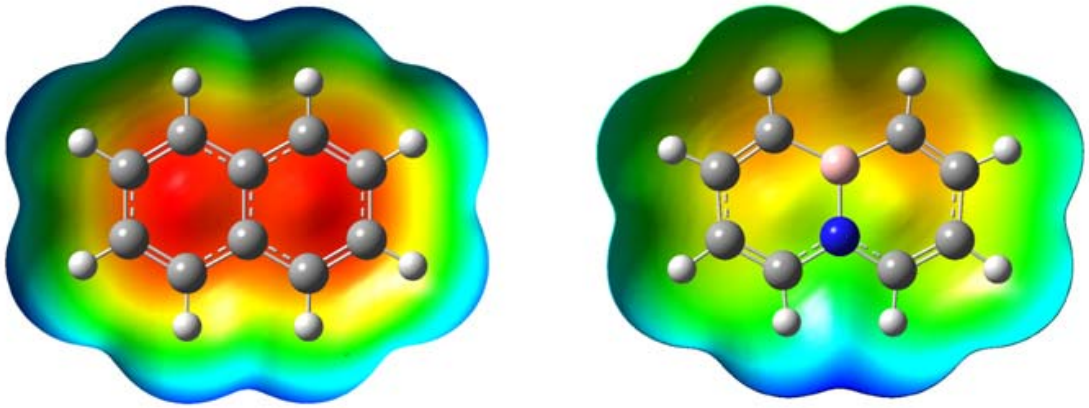

Figure 5.3.1 Electron density mapped with the electrostatic potential (Iso Val = 0.0004) of A) naphthalene and B) BN-naphthalene from the total SCF density using B3LYP/aug-cc-pVTZ. Red is the most electron rich and blue is electron deficient.

Qualitative results regarding the electronic charge distribution of BN-naphthalene were obtained by using the optimized B3LYP/aug-cc-pVTZ structure to calculate the isosurface of total electron density (Iso Val = 0.0004) mapped with the electrostatic potential onto the molecule using B3LYP/aug-cc-pVTZ on the Gaussian 09 suite. To directly compare with its hydrocarbon analog, a similar calculation was carried out for naphthalene. The electrostatic potentials mapped with electron density for naphthalene and BN-naphthalene are shown in Figure 5.3.1A and 5.3.1B respectively. The color scheme is such that the red indicates the most negative (or electron rich) and blue represents the most positive (electron deficient) regions within the molecule. Boron's valence typically has three electrons which are capable of making three sigma bonds using the three valence sp^2 hybridized orbitals, leaving the p-orbital unoccupied. Nitrogen's valence has five electrons, making three sigma bonds with its sp^2 hybridized orbitals and a lone pair in the p-orbital. Since the electric field gradients in molecules

mostly depend on the p-electron density, useful information about the aromatic character of BN-naphthalene is determined from the calculations and directly from the experimentally determined quadrupole coupling strengths of ^{14}N and ^{11}B using the extended Townes-Dailey analysis (more in section 5.3.4).

5.3.3 MICROWAVE MEASUREMENTS

The BN-naphthalene sample was synthesized at the University of Michigan using the experimental details published by the Ashe lab.[91] Microwave measurements on the synthesized sample of BN-naphthalene were made in the 2-10.4 GHz range using a Flygare-Balle type pulsed-beam Fourier transform microwave spectrometer that has been described previously and also the large cavity Flygare-Balle type microwave spectrometer capable of measuring transitions down to 1 MHz.[92] Before the pulse of the molecular sample, the pressure inside the vacuum cavities of the spectrometers were maintained at 10^{-6} to 10^{-7} Torr. Ne was used as the carrier gas and before passing over the molecular sample, the Ne was passed through an OMI-1 purifier tube that was purchased from Sigma Aldrich. The backing pressure of the Ne was maintained at about 1 atm.

Table 5.3.1 Measured rotational transitions of the $^{11}B^{14}N$ isotopologue. Values shown in MHz.

		$^{11}B^{14}N$	
J′ K_a′ K_c′ F_1′ F′	J″ K_a″ K_c″ F_1″ F″	ν_{obs}	ν_{o-c}
1 1 0 3 2	1 0 1 1 1	2179.7240	-0.0060
1 1 0 1 1	1 0 1 3 2	2179.7813	0.0018
1 1 0 1 1	1 0 1 2 1	2179.9329	0.0030
1 1 0 3 2	1 0 1 3 3	2179.9571	-0.0024

1	1	0	2	3	1	0	1	1	2	2180.2341	0.0042
1	1	0	3	4	1	0	1	3	4	2180.3198	-0.0030
1	1	0	3	4	1	0	1	2	3	2180.8807	-0.0018
1	1	0	2	3	1	0	1	3	2	2181.1696	-0.0017
2	0	2	2	1	1	1	1	3	2	2246.0699	-0.0032
2	0	2	3	4	1	1	1	3	4	2246.1470	-0.0066
2	0	2	2	3	1	1	1	2	3	2246.6648	0.0018
2	0	2	2	2	1	1	1	1	1	2246.7358	-0.0098
2	0	2	4	4	1	1	1	3	4	2247.3151	-0.0041
2	0	2	1	2	1	1	1	1	1	2247.4661	0.0022
2	1	1	4	3	2	0	2	1	2	2562.9129	0.0016
2	1	1	2	3	2	0	2	1	2	2563.1467	0.0018
2	1	1	2	3	2	0	2	4	4	2563.3627	-0.0046
2	1	1	3	4	2	0	2	4	5	2563.9003	0.0000
2	1	1	3	2	2	0	2	2	3	2563.9272	0.0047
2	1	1	3	2	2	0	2	2	1	2563.9517	-0.0026
2	1	1	1	2	2	0	2	2	3	2563.9928	0.0004
2	1	1	3	3	2	0	2	4	3	2564.0394	0.0022
2	1	1	3	4	2	0	2	2	3	2564.1451	-0.0002
2	1	1	2	3	2	0	2	3	2	2564.7382	0.0036
2	1	1	3	3	2	0	2	3	3	2564.8827	-0.0048
1	1	1	3	3	0	0	0	2	2	3904.6352	0.0008
1	1	1	2	2	0	0	0	2	3	3904.6973	0.0078
1	1	1	2	3	0	0	0	2	2	3904.9352	-0.0005
1	1	1	3	4	0	0	0	2	3	3905.0188	0.0059
1	1	1	3	2	0	0	0	2	3	3905.4868	-0.0068
3	0	3	3	2	2	1	2	2	1	4484.1528	0.0077
3	0	3	4	5	2	1	2	3	4	4484.4399	-0.0025
3	0	3	5	4	2	1	2	4	3	4484.5142	-0.0083
3	0	3	4	4	2	1	2	3	3	4484.5903	0.0047
3	0	3	2	2	2	1	2	1	1	4484.6792	0.0038
3	0	3	3	2	2	1	2	3	2	4484.7446	-0.0005
5	2	3	4	4	5	1	4	4	4	5011.6021	-0.0026
5	2	3	6	7	5	1	4	7	8	5011.7275	-0.0038
5	2	3	6	5	5	1	4	7	6	5011.7778	0.0046
3	2	1	2	2	3	1	2	2	3	5248.8096	-0.0009
3	2	1	4	4	3	1	2	4	3	5249.3145	0.0027
6	2	4	5	4	6	1	5	5	4	5302.4146	-0.0023
6	2	4	8	9	6	1	5	8	9	5302.4692	-0.0028
2	2	0	1	2	2	1	1	2	1	5562.0176	-0.0065
2	2	0	4	4	2	1	1	3	3	5562.1392	0.0001
2	2	0	1	1	2	1	1	1	2	5562.2998	0.0046
2	2	0	1	1	2	1	1	3	2	5562.3691	0.0040
2	2	0	4	3	2	1	1	3	3	5562.4224	-0.0033
2	2	0	1	1	2	1	1	1	1	5562.4722	-0.0009
2	2	0	4	4	2	1	1	4	3	5562.7515	-0.0044

2 2 0 2 1	2 1 1 2 1	5563.0088	-0.0030
2 1 2 2 3	1 0 1 3 2	5629.4268	0.0047
2 1 2 4 4	1 0 1 3 4	5629.6841	0.0023
3 2 2 2 3	3 1 3 2 2	7076.6250	0.0006
3 2 2 2 3	3 1 3 2 3	7076.8428	0.0010
3 1 3 3 3	2 0 2 2 3	7201.3242	0.0023
3 1 3 2 2	2 0 2 1 2	7201.3672	-0.0037
4 2 3 4 5	4 1 4 3 4	7800.8184	0.0009
4 2 3 4 3	4 1 4 3 2	7800.9487	0.0058
4 1 4 4 4	3 0 3 5 4	8675.9053	-0.0028
4 1 4 3 2	3 0 3 2 1	8676.3770	0.0084
5 1 5 5 5	4 0 4 4 4	10128.1406	-0.0007
5 1 5 6 5	4 0 4 5 4	10128.2158	0.0030
5 1 5 4 4	4 0 4 3 4	10128.6934	0.0012
5 1 5 7 6	4 0 4 5 5	10128.7666	-0.0065
5 3 3 6 7	5 2 4 7 6	10397.6445	-0.0022
5 3 3 4 4	5 2 4 4 3	10397.6816	-0.0061
5 3 3 6 6	5 2 4 6 6	10397.8994	-0.0002
5 3 3 7 6	5 2 4 5 6	10397.9766	0.0064
5 3 3 5 4	5 2 4 5 4	10398.0127	-0.0002
5 3 3 5 5	5 2 4 5 6	10398.0547	-0.0078
5 3 3 6 7	5 2 4 6 7	10398.0947	0.0073

Table 5.3.2 Measured rotational transitions of the $^{10}B^{14}N$ isotopologue. Values shown in MHz.

		$^{10}B^{14}N$	
J′ Ka’ Kc’ F1’ F’	J″ Ka” Kc” F1” F”	ν_{obs}	ν_{o-c}
1 1 1 3 2	0 0 0 3 3	3917.3203	0.0078
1 1 1 4 3	0 0 0 3 2	3917.4241	-0.0007
1 1 1 4 5	0 0 0 3 4	3917.7371	0.0000
1 1 1 2 3	0 0 0 3 2	3918.1902	-0.0061
3 0 3 4 5	2 1 2 5 5	4476.5693	-0.0024
3 0 3 4 3	2 1 2 2 2	4476.7778	-0.0086
3 0 3 5 6	2 1 2 5 5	4476.6436	-0.0060
3 0 3 3 3	2 1 2 1 2	4476.6709	0.0005
3 0 3 3 4	2 1 2 5 5	4476.7007	0.0077
3 0 3 4 3	2 1 2 2 2	4476.7778	-0.0086
3 0 3 3 4	2 1 2 2 3	4476.8572	-0.0052
3 0 3 2 2	2 1 2 1 1	4476.8945	-0.0085
3 0 3 2 2	2 1 2 1 2	4476.9370	0.0053
3 0 3 5 5	2 1 2 5 6	4476.9839	0.0012
3 0 3 4 3	2 1 2 3 3	4477.0952	0.0027
3 0 3 4 5	2 1 2 3 4	4477.1748	-0.0064

3 0 3 2 3	2 1 2 1 2	4477.2212	-0.0042
3 0 3 2 1	2 1 2 2 1	4477.2598	-0.0063
3 0 3 2 2	2 1 2 2 1	4477.3032	-0.0042
3 0 3 6 7	2 1 2 5 6	4477.3418	-0.0044
3 0 3 5 6	2 1 2 4 5	4477.3799	-0.0066
2 1 2 4 3	1 0 1 2 2	5643.2259	-0.0052
2 1 2 4 5	1 0 1 4 4	5643.3608	0.0010
2 1 2 3 2	1 0 1 2 2	5643.4510	-0.0021
2 1 2 4 3	1 0 1 4 3	5643.8789	0.0049
2 1 2 3 3	1 0 1 4 3	5644.0732	-0.0012
2 1 2 4 4	1 0 1 3 4	5644.1519	-0.0085
4 0 4 2 1	3 1 3 0 1	6686.6099	0.0033
4 0 4 6 5	3 1 3 3 4	6686.7041	0.0049
4 0 4 5 5	3 1 3 6 6	6686.7754	0.0019
4 0 4 4 5	3 1 3 3 4	6686.8633	0.0021
4 0 4 6 6	3 1 3 6 7	6686.9263	-0.0025
4 0 4 2 1	3 1 3 1 1	6686.9819	-0.0040
4 0 4 4 4	3 1 3 3 4	6687.0615	-0.0017
4 0 4 2 1	3 1 3 2 1	6687.2593	0.0042
3 1 3 5 5	2 0 2 5 6	7218.1172	0.0032
3 1 3 2 1	2 0 2 1 0	7218.2871	0.0032
3 1 3 6 6	2 0 2 5 5	7218.4150	-0.0073
4 1 4 5 4	3 0 3 2 3	8694.4141	-0.0004
4 1 4 3 2	3 0 3 1 2	8694.7432	0.0038
4 1 4 4 3	3 0 3 4 4	8694.8789	0.0041
4 1 4 3 2	3 0 3 2 3	8695.0029	-0.0039
4 1 4 6 5	3 0 3 5 5	8695.1221	0.0000
4 1 4 5 5	3 0 3 4 4	8695.2275	-0.0028
4 1 4 7 6	3 0 3 6 5	8695.4561	-0.0089
5 0 5 5 6	4 1 4 6 7	8805.0645	0.0050
5 0 5 7 8	4 1 4 6 7	8805.1650	0.0075
5 0 5 4 5	4 1 4 4 5	8805.3037	0.0026

Sufficient vapor pressure was obtained of the BN-naphthalene sample at room temperature and this provided a single shot signal of the 0 to 1 b-type rotational transition of the $^{11}B^{14}N$ isotopologue; these isotopologue transitions are shown in Table 5.3.1. The transitions from the $^{10}B^{14}N$ isotopologue were also measured at room temperature and these transitions are shown in Table 5.3.2. $^{13}C^{11}B$ transitions were measured at room temperature and the $^{11}B^{15}N$ transitions were measured at

temperature of 35 °C; these transitions are shown in Tables 5.3.3 and 5.3.4 respectively. All transitions were measured under natural abundance concentrations of each isotope and an example of transitions from the $^{10}B^{14}N$, $^{11}B^{13}C4$ or $^{13}C12$, and $^{11}B^{15}N$ isotopologues are shown in Figure 5.3.2.

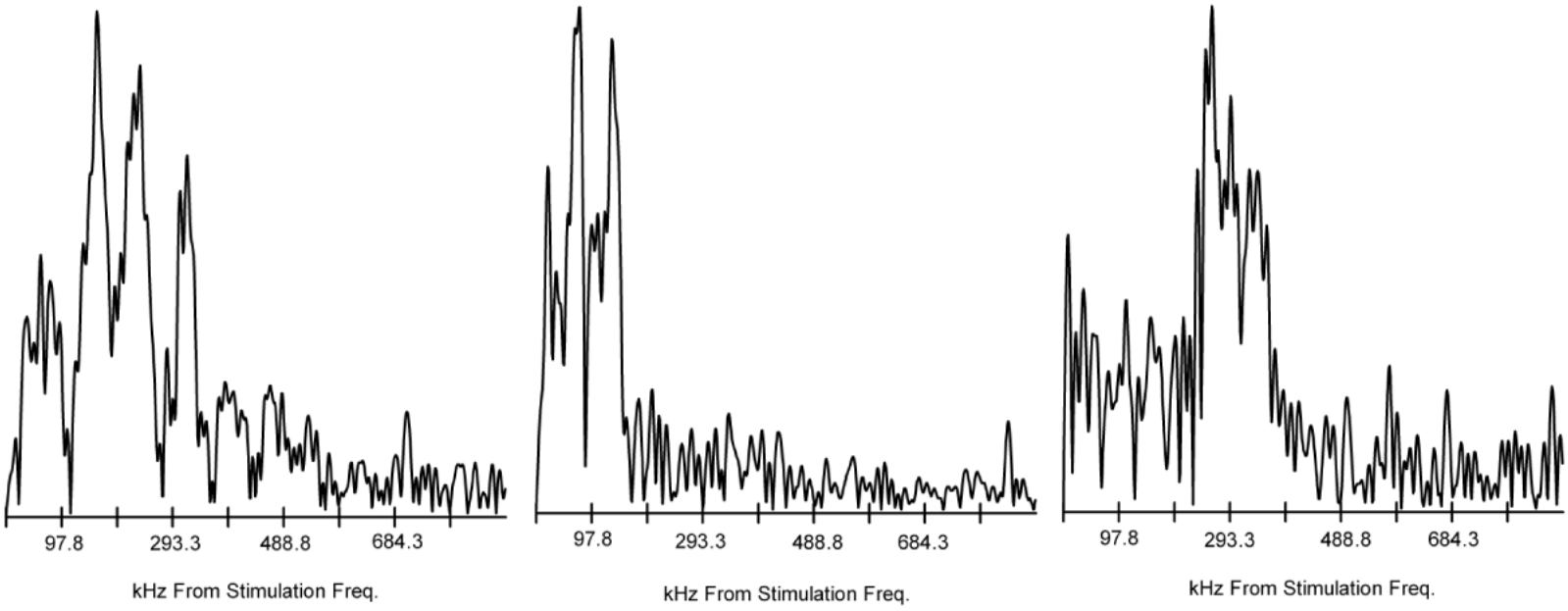

Figure 5.3.2 Example transitions showing the hyperfine splitting from the $^{10}B^{14}N$ (stimulation at 5643.680 MHz, 129 pulsed beam cycles), $^{11}B^{13}C4$ or $^{13}C12$ (stimulation at 3887.160 MHz, 2436 pulsed beam cycles), and $^{11}B^{15}N$ (stimulation at 5619.530 MHz, 7803 pulsed beam cycles) isotopologues.

Table 5.3.3 Measured rotational transitions of the singly substituted $^{13}C^{11}B$ isotopologues. Values shown in MHz.

Energy Level Assignments		$^{11}B^{13}C$1&13		$^{11}B^{13}C$2&8		$^{11}B^{13}C$3&9		$^{11}B^{13}C$4&12	
J′ K_a’ K_c’ F_1’ F’	J″ K_a” K_c” F_1” F”	ν_{obs}	ν_{o-c}	ν_{obs}	ν_{o-c}	ν_{obs}	ν_{o-c}	ν_{obs}	ν_{o-c}
1 1 1 3 3	0 0 0 2 3	3885.691	-0.003						
1 1 1 2 3	0 0 0 2 2	3885.994	-0.001						
1 1 1 2 2	0 0 0 2 3					3860.496	-0.000		
1 1 1 1 2	0 0 0 2 3	3886.059	0.004						
1 1 1 2 2	0 0 0 2 1			3866.099	-0.000				
1 1 1 3 4	0 0 0 2 3							3887.025	0.006
1 1 1 1 1	0 0 0 2 1							3887.091	-0.006
2 1 2 1 1	1 0 1 1 1			5581.264	0.001				
2 1 2 2 1	1 0 1 2 1			5581.341	0.001				
2 1 2 3 3	1 0 1 2 3							5591.966	-0.007
2 1 2 2 1	1 0 1 3 2							5592.029	-0.002
2 1 2 2 3	1 0 1 3 4	5592.112	-0.009						
2 1 2 2 2	1 0 1 2 1							5592.212	-0.018
2 1 2 2 3	1 0 1 3 2	5592.240	0.003			5573.487	0.003		
2 1 2 1 2	1 0 1 1 1	5592.273	-0.006						
2 1 2 4 5	1 0 1 3 4	5592.323	0.004			5573.567	0.001		
2 1 2 4 4	1 0 1 3 4					5573.734	-0.009		
2 1 2 3 2	1 0 1 2 2			5581.576	0.004			5592.395	-0.018
3 1 3 3 4	2 0 2 3 3			7143.693	-0.005				
3 1 3 4 3	2 0 2 2 2	7147.654	0.005						
3 1 3 3 3	2 0 2 1 2	7147.700	0.005						
3 1 3 3 3	2 0 2 3 3			7143.865	-0.007			7147.979	-0.003
3 1 3 2 2	2 0 2 4 3			7144.029	0.003				
3 1 3 3 3	2 0 2 3 2			7144.100	-0.002				
3 1 3 3 3	2 0 2 3 4					7134.095	-0.001	7148.014	0.004
3 1 3 5 4	2 0 2 3 3							7148.221	-0.002
3 1 3 5 4	2 0 2 4 5	7148.648	0.000						
3 1 3 2 2	2 0 2 1 2	7148.691	-0.009						
3 1 3 2 3	2 0 2 4 4					7133.712	-0.006		
3 1 3 3 2	2 0 2 3 3					7133.783	0.008		
3 1 3 3 4	2 0 2 3 4					7133.929	0.005		
3 1 3 2 3	2 0 2 4 3	7148.987	-0.003			7134.008	0.003		
4 1 4 3 3	3 0 3 2 2							8606.540	0.000
4 1 4 4 3	3 0 3 2 2	8607.016	-0.005						
4 1 4 4 5	3 0 3 4 5	8608.798	-0.003						
4 1 4 6 5	3 0 3 4 4					8598.618	0.003		
4 1 4 6 5	3 0 3 3 4	8608.899	-0.007	8610.130	0.000				
4 1 4 3 4	3 0 3 3 3			8610.332	0.005				
4 1 4 6 5	3 0 3 4 5	8609.342	-0.005						

Table 5.3.4 Measured rotational transitions of the $^{11}B^{15}N$ isotopologue. Values shown are in MHz.

J′ Ka' Kc' F'	J″ Ka" Kc" F"	ν_{obs}	ν_{o-c}
1 1 1 3	0 0 0 2	3896.0701	0.0000
2 1 2 4	1 0 1 3	5619.2651	-0.0002
3 1 3 2	2 0 2 1	7189.5835	0.0003
4 1 4 3	3 0 3 2	8663.3870	0.0025
4 1 4 3	3 0 3 3	8664.1787	-0.0027
5 1 5 4	4 0 4 4	10115.7393	0.0000

5.3.4 ROTATIONAL AND QUADRUPOLE COUPLING CONSTANTS

The rotational constants, centrifugal distortion constants and quadrupole coupling strengths were determined using Pickett's SPFIT program. The results are listed in Table 5.3.5. The assignments of the transitions with either ^{10}B or ^{11}B and ^{14}N are assigned using the quantum numbers $|J\ K_a\ K_c\ F_1\ F>$. These quantum numbers arise from the angular momentum coupling scheme $I_B + J = F_1$ and $F_1 + I_N = F$. For ^{11}B, I=3/2, the Pickett notation rounds the spin up to 2 which gives the integer numbers for F_1 and F in Tables 5.3.1, 5.3.3 and 5.3.4. In the case of ^{15}N, the N quadrupole moment collapses and the quantum numbers used in the energy level assignments are $|J\ K_a\ K_c\ F>$ where the angular momentum coupling is $J + I_B = F$. The inertial defect calculated from the experimental rotational constants of the $^{11}B^{14}N$ isotopologue is Δ = -0.159 amu Å^2 which is consistent with a planar structure. The small negative nonzero value of the inertial defect indicates the presence of out of plane vibrational modes within the molecule. Its magnitude is larger than what was obtained for 1,2-dihydro-1,2-azaborine (Δ = 0.02 amu Å^2), which may affect the aromatic character of BN-naphthalene when it deviates from planarity.

Table 5.3.5 Experimentally determined rotational, quadrupole coupling and centrifugal distortion constants of all measured isotopologues.

	$^{11}B^{14}N$	$^{10}B^{14}N$	$^{11}B^{13}C$1&13	$^{11}B^{13}C$2&8	$^{11}B^{13}C$3&9	$^{11}B^{13}C$4&12	$^{11}B^{15}N$
A/MHz	3042.71275(43)	3054.3775(21)	3032.8954(44)	3008.9390(65)	3004.3924(83)	3034.4177(80)	3034.4868(27)
B/MHz	1202.70657(35)	1202.72868(79)	1186.525(12)	1198.597(16)	1197.557(22)	1185.175(23)	1202.6225(95)
C/MHZ	862.22013(35)	863.26917(36)	853.0973(17)	857.4037(23)	856.3471(30)	852.5212(31)	861.5671(11)
B 1.5χ_{aa}/MHz	-3.9221(75)	-3.809(21)	-3.9221*	-3.9221*	-3.9221*	-3.9221*	-3.8933**
B 0.25(χ_{bb}-χ_{cc})/MHz	-0.9069(24)	-1.0013(60)	-0.9069*	-0.9069*	-0.9069*	-0.9069*	-0.8129**
N 1.5χ_{aa}/MHz	2.5781(61)	2.6324(99)	2.5781*	2.5781*	2.5781*	2.5781*	-
N 0.25(χ_{bb}-χ_{cc})/MHz	-0.1185(17)	-0.0987(27)	-0.1185*	-0.1185*	-0.1185*	-0.1185*	-
D_J/kHz	0.0565(96)	0.0565*	0.0565*	0.0565*	0.0565*	0.0565*	0.0565*
N	72	48	16	10	10	10	6
σ/kHz	4	5	5	4	5	6	2

* Quadrupole coupling and distortion constants were held fixed to the $^{11}B^{14}N$ isotopologue.

** Quadrupole coupling constants were held fixed to the B3LYP/aug-cc-pVTZ calculation for the $^{11}B^{15}N$ isotopologue

A B3LYP/aug-cc-pVTZ calculation was performed with BN-naphthalene to determine the natural bond orbital electron occupancies of ^{14}N and ^{11}B. These orbital electron populations are shown in Tables 5.3.6 and 5.3.7 for ^{14}N and ^{11}B respectively. From the experimentally determined quadrupole coupling strengths of ^{14}N and ^{11}B, the orbital occupations can be directly determined through the extended Townes-Dailey analysis using sp^2 hybridized orbitals around the nuclei. In order to perform the Townes-Dailey analysis in BN-naphthalene, it is necessary to know the atomic quadrupole coupling constants for the ^{14}N and ^{11}B atoms due to one unpaired electron in the p-orbital. These values are listed in Gordy and Cook and are -11.2 MHz for ^{14}N and -5.4 MHz for ^{11}B. In order to calculate the orbital occupations, a value for the occupation of the p_c-orbital needs to be chosen (which is chemically reasonable and should not exceed more than 2 for the p-orbital). From following the mathematics in the extended analysis described in the literature, the occupations of either N_B, number of electrons in the valence of N in the N-B σ-bond (in the case of N), or N_N, number of electrons in the valence of B in the N-B σ-bond and the sum of the occupations of the adjacent C atoms (N_C+N_C) next to either the N or B nucleus are calculated. The results from the Townes-Dailey analysis from ^{14}N and ^{11}B are shown with the NBO calculated results in Tables 5.3.6 and 5.3.7 respectively.

Table 5.3.6 Townes-Daily determined and NBO calculated (using B3LYP/aug-cc-pVTZ) electron orbital occupancies for N using sp^2 hybridized orbitals. The bolded values are the best agreement between the NBO calculation and the Townes-Dailey analysis.

Orbital Occupations	Townes-Dailey							NBO
N p_c	1.2	1.3	**1.4**	1.45	1.5	1.6	1.7	**1.4**
N_B (sp^2)	1.3	1.4	**1.5**	1.6	1.6	1.7	1.8	**1.5**
N_C+N_C								**2.5**
(sp^2+sp^2)	2.1	2.3	**2.5**	2.6	2.7	2.9	3.1	
N_{total}	4.6	5.0	**5.4**	5.6	5.8	6.2	6.6	**5.4**
Charge	0.37	0.0	**-0.43**	-0.63	-0.83	-1.2	-1.6	**-0.43**

Table 5.3.7 Townes-Daily determined and NBO calculated (using B3LYP/aug-cc-pVTZ) electron orbital occupancies for B using sp^2 hybridized orbitals. The bolded values are the best agreement between the NBO calculation and the Townes-Dailey analysis.

Orbital Occupations	Townes-Dailey							NBO
N p_c	0.00	0.10	**0.20**	0.30	0.40	0.50	0.60	**0.23**
N_N (sp^2)	0.32	0.42	**0.52**	0.62	0.72	0.82	0.92	**0.46**
N_C+N_C								**1.4**
(sp^2+sp^2)	**1.4**	1.6	1.8	2.0	2.2	2.4	2.6	
N_{total}	1.7	**2.1**	2.5	2.9	3.3	3.7	4.1	**2.1**
Charge	1.3	**0.87**	0.47	0.10	-0.33	-0.73	-1.1	**0.89**

5.3.5 GAS PHASE STRUCTURE

Gas phase structural parameters were obtained for BN-naphthalene using a nonlinear least squares fitting program with the rotational constants determined from the seven unique isotopologues measured. This structure fitting program varies the Cartesian coordinates of the atoms within the molecule and a “best fit” structure is

obtained. The best fit structure is determined when the structure fit yields calculated rotational constants closest to the experimentally fit values. From the B3LYP/aug-cc-pVTZ calculation of BN-naphthalene, the structure was predicted to be planar with C_{2v} symmetry. The calculated inertial defect from the experimentally determined rotational constants is Δ = -0.159 amu Å^2 confirming that the structure is indeed planar with some out of plane vibrational motion.

In the structure fit, there were a total of 10 variable parameters representing small changes in select atomic Cartesian coordinates in the a-b plane. The best fit structure was fixed to be planar by setting all c-coordinates equal to zero due to the experimental value of the inertial defect. It was assumed that the symmetry of BN-naphthalene molecule is maintained and so the varied coordinates in the fit were equivalent for corresponding atoms across the symmetry axis (B-N bond), with the exception of the varied parameters in the a-direction which were opposite sign for each corresponding C atom. The only fixed atom in the structure fit was N and the B atom was varied by its own a and b variable parameters. The H atoms bonded to the C atoms within the ring were varied by the same variable parameters as the C atom it was bonded to, resulting in the C-H bond lengths to be fixed to optimized equilibrium values. With these constraints and varied parameters set, the standard deviation of the structure fit was 0.151 MHz. The best fit structure showing the bond lengths and angles is shown in Figure 5.3.3.

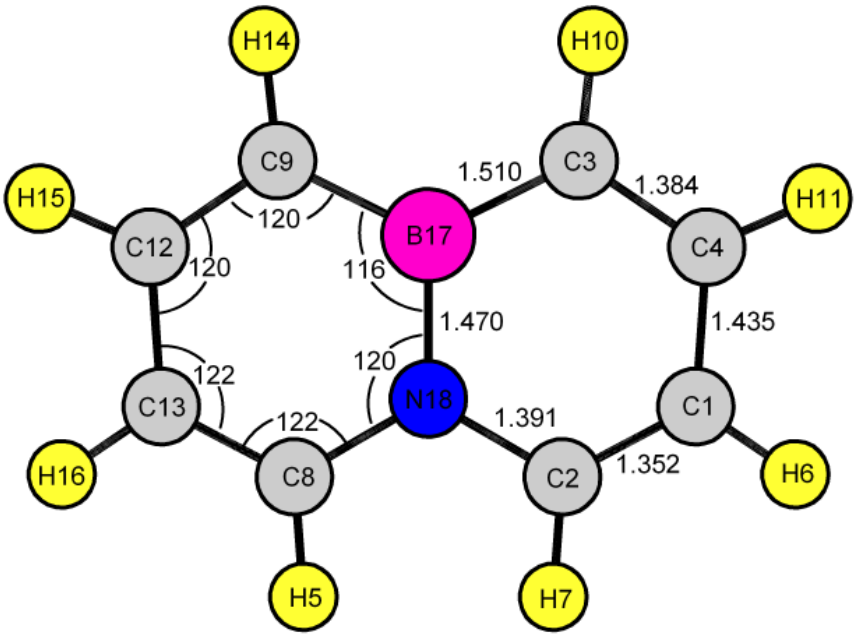

Figure 5.3.3 Best fit structure showing bond lengths (Å) and angles (º). Only half of the bond lengths and angles are shown in the cyclic ring structure due to the symmetry of the molecule. All C-H bond lengths were held fixed to calculated equilibrium values and so are not shown.

A Kraitchman analysis was also performed on all the isotopically substituted atoms using the Kisiel KRA program. The atomic coordinates of the best fit structure and of each isotopically substituted atom are shown in Table 5.3.8. The Kraitchman determined coordinates agree very well with the coordinates obtained from the best fit structure, with the exception of the a-coordinate of both the B and N atoms. These atoms lie along the b-axis, thus making the Kraitchman calculated coordinates unreliable. The differences between the experimentally determined rotational constants are compared with the calculated best fit structure values from each isotopologue in the

in Table 5.3.9. A comparison of the B-N bond length in BN-naphthalene and other B-N substituted molecules are shown in Table 5.3.10.

Table 5.3.8 Principle axes coordinates of the best fit structure being compared with the Kraitchman determined coordinates for each of the isotopically substituted atoms. Values shown are in Å.

Atom	a	b	Krait-|a|	Krait-|b|
C1	-2.400	-0.743	2.39654(71)	0.7431(20)
C2	-1.203	-1.373	1.1933(14)	1.3723(11)
C3	-1.354	1.466	1.3762(13)	1.4642(10)
C4	-2.499	0.689	2.49610(75)	0.6835(22)
C8	1.203	-1.373	1.1933(14)	1.3723(11)
C9	1.354	1.466	1.3762(13)	1.4642(10)
C12	2.499	0.689	2.49610(75)	0.6835(22)
C13	2.400	-0.743	2.39654(71)	0.7431(20)
H5	1.122	-2.451		
H6	-3.294	-1.349		
H7	-1.122	-2.451		
H10	-1.476	2.543		
H11	-3.492	1.125		
H14	1.476	2.543		
H15	3.492	1.124		
H16	3.294	-1.350		
B17	0.000	0.796	0.2790(54)	0.7947(19)
N18	0.000	-0.674	0.078*i(20)	0.6746(22)

Table 5.3.9 Comparison of rotational constants obtained from the best fit structure compared with the experimentally determined values for each isotopologue and their differences. The standard deviation of the structure fit was 0.151 MHz. Values shown are in MHz.

ISOTOPOLOGUE		MEASURED	CALCULATED	(M – C)
$^{11}B^{14}N$	A	3042.7128	3042.7609	-0.0482
	B	1202.7066	1202.8299	-0.1233
	C	862.2201	862.0529	0.1672
$^{10}B^{14}N$	A	3054.3775	3054.4633	-0.0858
	B	1202.7287	1202.8299	-0.1012
	C	863.2692	862.9896	0.2796
$^{11}B^{13}C1$	A	3032.8954	3032.9559	-0.0605
	B	1186.5250	1186.6062	-0.0812
	C	853.0973	852.9142	0.1831
$^{11}B^{13}C13$	A	3032.8954	3032.9562	-0.0608
	B	1186.5250	1186.6062	-0.0812
	C	853.0973	852.9142	0.1831
$^{11}B^{13}C2$	A	3008.9390	3008.9715	-0.0325
	B	1198.5970	1198.6875	-0.0905
	C	857.4037	857.2026	0.2011
$^{11}B^{13}C8$	A	3008.9390	3008.9718	-0.0328
	B	1198.5970	1198.6873	-0.0903
	C	857.4037	857.2026	0.2011
$^{11}B^{13}C3$	A	3004.3924	3004.3468	0.0456
	B	1197.5570	1197.5846	-0.0276
	C	856.3471	856.2633	0.0838
$^{11}B^{13}C9$	A	3004.3924	3004.3479	0.0445
	B	1197.5570	1197.5832	-0.0262
	C	856.3471	856.2627	0.0844
$^{11}B^{13}C4$	A	3034.4177	3034.3442	0.0735
	B	1185.1750	1185.2602	-0.0852
	C	852.5212	852.3281	0.1931
$^{11}B^{13}C12$	A	3034.4177	3034.3442	0.0735
	B	1185.1750	1185.2595	-0.0845
	C	852.5212	852.3277	0.1935
$^{11}B^{15}N$	A	3034.4868	3034.5579	-0.0711
	B	1202.6225	1202.8299	-0.2074
	C	861.5671	861.3932	0.1739

5.3.6 DISCUSSION

The microwave spectra were measured for seven unique isotopologues of BN-naphthalene using pulsed beam Fourier transform microwave spectroscopy. From the best fit structure, bond lengths and angles of the ring system were determined. Even though the C-H bond lengths were held fixed to optimized equilibrium values, the structure obtained is a reasonably accurate representation of the molecule in its ground state. The B-N bond length determined from the structure fit was 1.470 Å. This bond length agrees fairly well with the X-ray determined B-N length of 1.461 Å, only differing by about 0.01 Å. Comparing the remaining bond lengths of the rings in the microwave and X-ray structures, the C1-C2, C1-C4 and C3-C4 bond lengths also all agree fairly well with the X-ray structure, again only deviating by about 0.01 Å. The C3-B17 bond in the microwave structure has the largest deviation when compared with the X-ray structure with a difference of 0.055 Å. The differences between these two structures arise most likely due to the X-ray crystal structure being an averaged structure of the disordered BN-naphthalene molecules within the crystal.

Table 5.3.10 A comparison of B-N bond distances of BN-naphthalene and other previously studied molecules containing the B-N bond.

r(B-N) Interatomic Distances	Microwave Fit Value (Å)	Calculated Value (Å)
BN-naphthalene[a]	1.470	1.475
BN-cyclohexene[b]	-	1.40
1,2-dihydro-azaborine[c]	1.45	1.437
H_3NBF_3[d]	1.59	-
BH_3NH_3[e]	1.6576	-
H_2NBH_2[f]	1.391	-
HCN-BF_3[g]	2.47	-

[a] This work

[b] Reference 75, calculated value obtained using B3LYP/aug-cc-pVTZ

[c] Reference 76, calculated value obtained using MP2/6-311+G(d,p)

[d] Reference 83

[e] Reference 84

[f] Reference 85

[g] Reference 89

When comparing the B-N bond lengths of the different types of molecules with B-N substitutions, listed in Table 5.3.10, the microwave structure bond length of BN-naphthalene agrees with the other B-N bond lengths where there is some π-donation from the N p-orbital to the empty p-orbital on B. As a result there is some double bond character between the B and N, which shortens the bond length. The boron nucleus has an empty p orbital within the π-system that can accept electron density to maintain its aromatic character within BN-naphthalene. As the donation of this lone pair on nitrogen becomes less, the bond length increases which can be seen in the molecules H_3NBF_3, BH_3NH_3, and a van der Waals complex HCN-BF_3. Because the bond length determined

for BN-naphthalene (1.47 Å) is intermediate between H_2NBH_2 (1.391 Å, double bond) and BH_3NH_3 (1.6576 Å, single bond), it can be concluded there is some aromatic bond character between the B and N in BN-naphthalene. Another criteria for the aromatic character in molecules, the planarity, can be directly determined from the analysis of the microwave spectra by calculating the inertial defect using the experimental rotational constants. BN-naphthalene has a larger magnitude inertial defect (Δ = -0.159 amu Å^2) when compared with 1,2-dihydro-1,2-azaborine (Δ = 0.02 amu Å^2). This is likely due to BN-naphthalene being a much more extended molecule, so the out of plane amplitudes for the bending vibrations will be greater than for 1,2-azaborine. Regardless of the larger magnitude inertial defect for BN-naphthalene, the value is still close enough to zero indicating a fairly planar structure.

Since the bond length obtained from the best fit structure supports the assumption that there is some π-character between B and N, natural bond orbital and extended Townes-Dailey analyses were performed to determine the extent of π-donation from the N to the empty p-orbital on the B. The electron occupations determined from the NBO analysis for N are 1.4 in the p-orbital, 1.5 in the sp^2 hybridized orbital making the σ-bond with B (N_B) , and 2.5 for the sum of the electrons in the two sp^2 hybridized orbitals making the σ-bonds with the adjacent C atoms (N_C+N_C). With these occupations the total valence around nitrogen was calculated to be 5.4 electrons with a charge of -0.43. These NBO calculations agree very well with the Townes-Dailey determined occupations when the occupation of the p-orbital on ^{14}N was chosen to be 1.4 and this comparison is shown in Table 5.3.6. The orbital electron occupations of N in BN-naphthalene is very similar to the occupations determined for 1,2-dihydro-1,2-

azaborine, which was shown to have similar properties when compared to other aromatic N-containing molecules, such as pyrrole.[93]

The values of orbital occupations obtained by the NBO analysis of B are 0.23 electrons in the p-orbital, 0.46 electrons in the sp^2 hybridized orbital making the σ-bond with N (N_N), and 1.4 electrons in the two sp^2 hybridized orbitals making the σ-bonds with the adjacent C atoms (N_C+N_C). With these occupations on B, the total valence was calculated to be 2.1 electrons with a charge of +0.89. The agreement of the NBO calculation with the extended Townes-Dailey analysis performed for ^{11}B does not agree as well as with ^{14}N. It can be seen by the bolded values in Table 5.3.7 that the NBO analysis agrees with occupations from the Townes-Dailey analysis when there are between 0-0.2 electrons in the p-orbital. The sum of the N_B and N_N from the sigma bond electron occupancies equal $2.02e^-$ which is consistent with the bond population. Using this as a constraint across the two analyses gives additional support to the designation of 0.2 e^- in the valence p_c-orbital for boron. There may be some disagreement between the NBO calculation and the extended Townes-Dailey analysis for ^{11}B because of the possibility of the B nucleus to also accept π-electron density from the adjacent carbon atoms, which was not taken into account in the NBO calculation as this was calculated for one resonance structure. It can be seen from the electrostatic potential map of BN-naphthalene in Figure 5.3.1B that there is a build-up of negative charge in the π-system adjacent to the B nucleus. If the aromatic character in the molecule is maintained, then there will also be donation of electrons into the empty p-orbital on B, which will change the orbital electron occupancies and thus affect the analysis.

6. MICROWAVE SPECTRA OF DOUBLY HYDROGEN BONDED DIMERS

Hydrogen bonds are important interactions in biological and chemical processes. The determination of gas phase molecular structures of heterodimers is crucial to testing the predictive power available for these noncovalent interactions. For example, the hydrogen bonding seen in DNA is important for the proper translation of the information stored in DNA into functioning proteins. Furthermore, the secondary and tertiary structures of proteins is largely dependent upon these hydrogen bonding interactions. Studying these types of systems is important to obtain these benchmarks so the theory can be improved upon and agree more accurately with experiment. Hydrogen bonding is also observed in catalysis and many chemical reactions. Understanding these interactions is critical so that synthetic chemists, for example, are able to formulate and synthesize catalysts with increased enzymatic activity.

The proton tunneling dynamics between the two molecules in the dimer can be studied using gas phase microwave spectroscopy. This proton tunneling phenomenon can be observed in the microwave spectra in terms of splittings of transitions. These splittings are similar to what is observed in the inversion of ammonia. Research suggests that it is this proton tunneling motion in DNA base pairs that may give rise to spontaneous point mutations, which may cause disease. Furthermore, microwave spectroscopy is one of the best techniques to analyze this tunneling motion in molecules due to the high resolution available. The importance of hydrogen bonding interactions, accurate molecular structures and describing the dynamics in these systems is of fundamental importance in all of chemistry and biochemistry and so studying these small benchmarks is crucial to advance our understanding.

6.1 CYCLOPROPANECARBOXYLIC ACID – FORMIC ACID DIMER

6.1.1 INTRODUCTION

There has been recent interest growing in doubly and triply hydrogen bonded complexes. These complexes are simple prototypes of doubly and triply hydrogen bonded DNA base pairs, adenine – thymine and guanine – cytosine. The dynamics of hydrogen bonding is also involved in the intricate formation of protein secondary structures as well as in the most basic proton transfer within solutions. These hydrogen bonded dimers are not static and some previously studied dimers have been shown to exhibit proton tunneling dynamics, which may be associated with some types of genetic mutations and disease.[94,95] The dynamics of this proton tunneling process are best observed and characterized through the analysis of the rotational spectrum measured by microwave spectroscopy. Some of these previously studied hydrogen bonded dimers by microwave spectroscopy include dimers formed between propiolic acid – formic acid,[96,97,98] acetic acid – formic acid,[99] and the monoenolic tautomer of 1,2-cyclohexanedione – formic acid (discussed in the next section).[100] In the case of propiolic acid – formic acid, proton tunneling was observed and details about the dynamics were characterized. The tunneling may be due to the C_{2V}(M) symmetry which creates a symmetric double well potential energy surface allowing for the tunneling motion to occur. Studying these carboxylic acid doubly hydrogen bonded dimers may allow for more insight into this tunneling process and give better quantitative predictions for the tunneling phenomena.

The simplest of these doubly hydrogen bonded systems is the formic acid homodimer.[101] The two equivalent forms of this dimer were found to interconvert through a concerted tunneling motion of the two acidic protons. The potential energy surface for this system has a classic double well potential, similar to that of ammonia inversion and the systems of single proton tunneling as in malonaldehyde[102,103,104,105] and tropolone.[106,107] Microwave spectroscopy is the most suitable technique to study the molecular structure and dynamics of many systems, but is restricted to molecules and complexes with permanent electric dipoles, or in heterodimers of two carboxylic acids as in the case of the dimer cyclopropanecarboxylic acid – formic acid (CPCA – FA) discussed here.

6.1.2 MICROWAVE MEASUREMENTS

The rotational spectra was measured in the 4-11 GHz region for the doubly hydrogen bonded dimer CPCA-FA. Microwave measurements were made using a Flygare-Balle type pulsed-beam Fourier transform (PBFT) microwave spectrometer. The CPCA (95 %) and FA (98 %) samples were purchased from Sigma Aldrich and the FA-d_1 (99.2% d) was purchased from CDN isotopes; each sample was used without further purification. The samples were transferred to separate glass sample cells. The glass sample cell containing the CPCA was connected directly to the pulsed-valve (General Valve series 9) and was heated to ~70 °C. The cell containing the FA was placed in the Ne gas line leading to the CPCA sample and the pulsed valve, seeding the FA vapor into the carrier gas. This FA and Ne gas was pulsed into the cavity, picking up CPCA vapor just before reaching the cavity. The FA sample (and also FA-d_1) was first cooled

to about -8 °C before connecting to the gas line and the sample temperature was maintained using a Peltier cooling device. The pressure inside the microwave cavity was maintained at 10^{-6} to 10^{-7} Torr prior to the molecular beam pulse into the cavity. The Ne carrier gas backing pressure was maintained at ~ 1 atm. The valve was set to pulse at ~ 2 Hz. All measured transitions of the CPCA – FA dimer are given in Table 6.1.1 and examples of observed transitions from the ^{13}C isotopologues are shown in Figure 6.1.1. The labeling scheme used for the atoms in the dimer is shown in Figure 6.1.2.

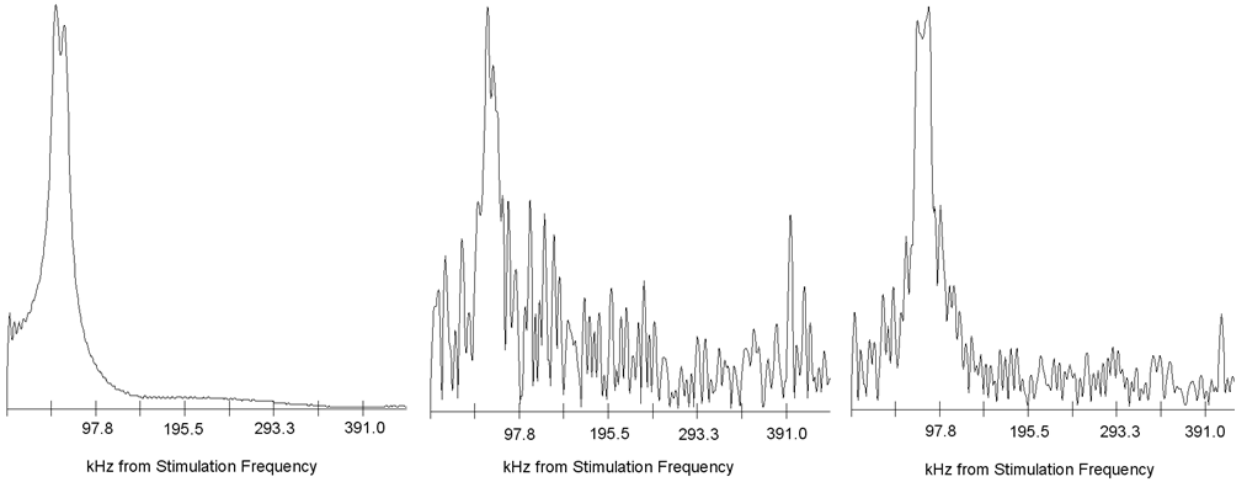

Figure 6.1.1 Example transitions of the parent isotopologue (6965.580 MHz stimulation), the ^{13}C isotopologue at the C16 position (6876.240 MHz stimulation), and the ^{13}C isotopologue at the equivalent positions of C3 and C6 (6878.020 MHz stimulation) of the 404 – 505 transition (from left to right) taken at 300 pulsed-beam cycles for each transition shown.

Table 6.1.1 Spectral assignment and frequencies for parent and ^{13}C isotopologues of the cyclopropanecarboxylic acid-formic acid dimer.

J'	K_a'	K_c'	J''	K_a''	K_c''	Parent	o-c*	$^{13}C(16)$	o-c*	$^{13}C(3\&6)$	o-c*	$^{13}C(1)$	o-c*	$^{13}C(9)$	o-c*	D(17)	o-c*
										a-type transitions							
3	0	3	2	0	2	4191.421	0										
3	2	2	2	2	1	4197.447	1										
3	2	1	2	2	0	4203.475	1										
3	1	2	2	1	1	4319.526	5	4261.910	2	4262.330	1	4291.032	1	4316.691	4		
4	1	4	3	1	3	5429.595	0	5361.166	0	5362.955	-1	5394.770	1	5425.831	0	5305.745	12
4	0	4	3	0	3	5581.547	0	5509.598	1	5510.783	2	5545.365	-1	5577.765	1	5451.427	-1
4	2	3	3	2	2	5595.418	1										
4	3	2	3	3	1	5599.555	6										
4	3	1	3	3	0	5599.648	-5										
4	2	2	3	2	1	5610.463	0										
4	1	3	3	1	2	5757.559	3	5680.834	0	5681.396	0	5719.599	-2	5753.775	0		
5	1	5	4	1	4	6784.273	-1	6698.874	-1	6701.116	0	6740.787	0	6779.566	0	6629.704	3
5	0	5	4	0	4	6965.732	0	6876.372	0	6877.861	0	6920.702	1	6960.994	0	6804.090	-1
5	2	4	4	2	3	6992.377	0										
5	3	3	4	3	2	7000.724	-1										
5	3	2	4	3	1	7001.087	-2										
5	2	3	4	2	2	7022.376	0										
5	1	4	4	1	3	7193.992	0	7098.244	-1	7098.947	-2	7146.600	1	7189.260	-3		
6	1	6	5	1	5	8137.229	-3									7952.096	-10
6	0	6	5	0	5	8342.650	-2									8150.128	1
6	2	5	5	2	4	8388.072	-5										
6	3	4	5	3	3	8402.670	2										
6	2	4	5	2	3	8440.285	0										
6	1	5	5	1	4	8628.358	-2										

7	1	7	6	1	6	9488.217	2			
7	0	7	6	0	6	9711.186	0		9488.486	1
8	1	8	7	1	7	10837.018	3			
8	0	8	7	0	7	11070.533	-1			
								b-type transitions		
1	1	1	0	0	0	4703.986	0			
6	0	6	5	1	5	5569.666	0			
2	1	2	1	0	1	6021.120	0			

*observed-calculated frequencies in kHz

Rotational transitions from five ^{13}C isotopologues of the CPCA – FA dimer were measured under natural abundance which include the parent and four single ^{13}C substitutions at all unique carbon atom positions within the dimer. The ^{13}C substitutions at carbon atoms 3 and 6 were calculated to be equivalent, which would result in an increased intensity in the observed transitions. These two positions are indeed equivalent and a comparison of signal intensities of some isotopologue transitions are shown in Figure 6.1.1.

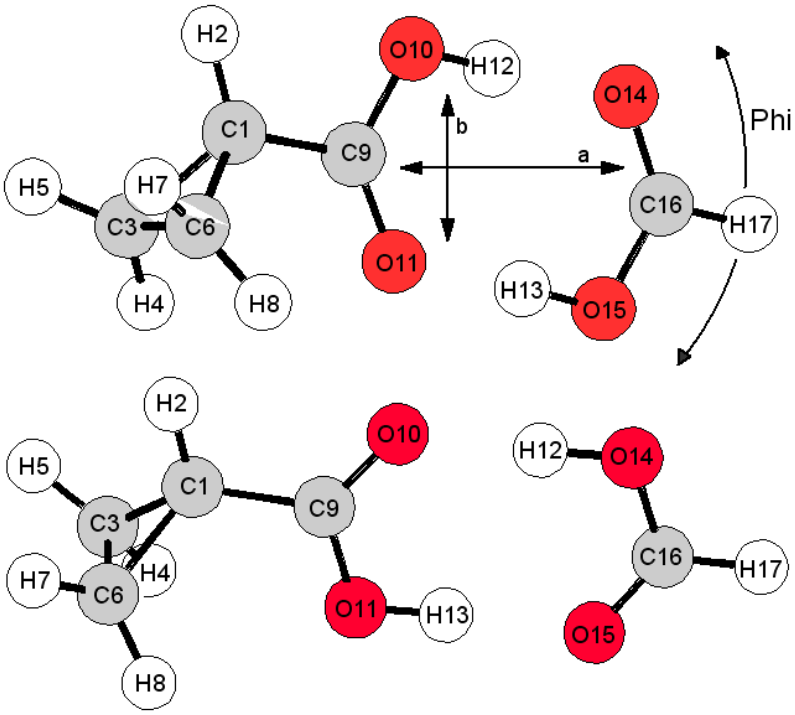

Figure 6.1.2 Calculated structures of the low energy (top) and higher energy (bottom) CPCA-FA conformers using B97D with aug-cc-pVTZ basis. Also shown superimposed on the low energy conformer are the a and b principle axes and the visualization of the parameter φ (phi) used in the structure fit.

There were 51 total rotational transitions measured for the lower energy conformer shown in Figure 6.1.2 (top); 28 a-type transitions and 3 b-type transitions were measured for the parent isotopologue and 7 a-type transitions were measured for each of the four uniquely substituted ^{13}C and deuterated isotopologues. The small splittings observed in the transitions shown in Figure 6.1.1 were determined to be a result of the Doppler Effect and not the proton tunneling motion. Rotational transitions were searched for corresponding to the high energy conformer in Figure 6.1.2 (bottom), however after significant scanning, transitions from this conformer not observed.

6.1.3 CALCULATIONS

Ab initio and DFT calculations to obtain an optimized equilibrium structure of the low energy CPCA – FA conformer were performed using the Gaussian 09 suite using B97D/aug-cc-pVTZ and MP2/aug-cc-pVTZ methods. The calculated a and b dipole moments for this conformer shown in Figure 6.1.2 (top) were 1.4 and 0.2 D respectively from the MP2 calculation. Due to the magnitudes of the dipole moment components, it was expected that the a-type transitions would be the strongest. The calculated rotational constants from the optimized equilibrium structure for this conformer were used in the Pickett program, SPCAT, to calculate the a and b-type rotational transitions. The values of the rotational constants from the optimized structure are shown in Table 6.1.2, along with the experimentally fit constants determined from the measured transitions. A Kraitchman analysis using the Kisiel KRA program was performed on each of the isotopically ^{13}C and deuterium substituted atoms in the CPCA – FA dimer.

These Kraitchman coordinates are shown in Table 6.1.3, compared with the best fit gas phase structure coordinates.

Table 6.1.2 *Ab initio* (MP2/aug-cc-pVTZ and B97D/aug-cc-pVTZ) spectroscopic constants and dipole moments of the cyclopropanecarboxylic acid - formic acid dimer.

Type	B97D/aug-cc-pVTZ	MP2/aug-cc-pVTZ	Experiment
A/MHz	4068.66	4038.00	4045.42
B/MHz	732.32	747.56	740.58
C/MHz	652.25	663.19	658.57
μ_a(Debye)	1.7	1.4	
μ_b(Debye)	0.2	0.2	
μ_c(Debye)	0.0	0.0	

Table 6.1.3 Structural coordinates of the CPCA – FA (low energy) dimer in Å from the nonlinear least squares fit with a standard deviation of 1.13 MHz. Also shown are the Kraitchman determined coordinates for each of the isotopically ^{13}C substituted atoms.

Atom	a	b	c	Krait-|a|	Krait-|b|	Krait-|c|
C1	2.154	0.509	0.021	2.1464(11)	0.5447(42)	0.03*i(8)
H2	2.478	1.537	0.053			
C3	2.972	-0.587	0.745	2.9923(8)	0.4674(53)	0.7440(34)
H4	2.433	-1.394	1.218			
H5	3.827	-0.215	1.289			
C6	3.012	-0.483	-0.748	2.9923(8)	0.4674(53)	0.7440(34)
H7	3.880	-0.083	-1.251			
H8	2.485	-1.263	-1.276			
C9	0.701	0.299	-0.002	0.661(5)	0.3354(97)	0.04(9)
O10	0.027	1.474	0.022			
O11	0.139	-0.767	-0.037			
H12	-4.022	0.506	0.006	4.1468(13)	0.476(12)	0.282(20)
H13	-0.915	1.258	0.005			
O14	-2.840	-1.325	-0.001			
O15	-2.209	0.833	-0.001			
C16	-3.022	0.085	0.001	3.08253(72)	0.190(12)	0.02(13)
H17	-1.935	-1.645	0.012			

A separate B97D/aug-cc-pVTZ calculation was performed to optimize the high energy conformer's geometry. Comparing two B97D calculations of each of the conformers, the energy separation of the two was determined to be 219 cm^{-1}, less than what was calculated to be the energy separation of the CPCA monomers (~ 300 cm^{-1}). The energy separation between the two conformers of the CPCA monomer was small enough so these transitions from this other conformer were observed previously. Based on these calculations and previous results from the monomer, it was expected that the high energy CPCA – FA conformer would be observed. However, after performing the predictive calculations for rotational constants and transitions, no transitions were observed after significant searching for these high energy conformer transitions.

6.1.4 ROTATIONAL CONSTANTS

The experimental rotational and centrifugal distortion constants for the parent low energy conformer of the dimer, Figure 6.1.2 (top), were determined using the Pickett's program SPFIT and are given in Table 6.1.4. A similar analysis was carried out for all remaining singly substituted ^{13}C and deuterium substituted isotopologues. The centrifugal distortion constants obtained from the parent were held fixed in the fits for the ^{13}C and D isotopologues. These results are also given in Table 6.1.4. The rotational constants from the calculations and the experiment are compared in Table 6.1.2. The MP2 calculation with the aug-cc-pVTZ basis yielded rotational constants within 1% of the experimental results.

Table 6.1.4 Spectroscopic constants for the parent and ^{13}C isotopologues of the CPCA – FA dimer.

	Parent	$^{13}C(16)$	$^{13}C(3\&6)$	$^{13}C(1)$	$^{13}C(9)$	D(17)
A/MHz	4045.4193(16)	4044.16(21)	4021.03(25)	4035.98(22)	4041.76(37)	4035.84(66)
B/MHz	740.58380(14)	730.45455(16)	730.44765(18)	735.63679(17)	740.11049(30)	722.3152(32)
C/MHZ	658.56760(23)	650.51344(17)	650.81382(20)	654.40357(19)	658.09839(33)	643.9651(12)
Δ_J/kHz	0.0499(16)	0.0499*	0.0499*	0.0499*	0.0499*	0.0499*
Δ_{JK}/kHz	0.108(14)	0.108*	0.108*	0.108*	0.108*	0.108*
N	31	7	7	7	7	7
σ/kHz	2	1	1	1	2	6

* fixed at the values for the parent isotopologue

6.1.5 MOLECULAR STRUCTURE

A nonlinear least squares fit was performed to obtain a best fit gas phase structure of the low energy conformer of the CPCA – FA dimer using the rotational constants from the parent and each of the measured isotopologues. The input is the set of Cartesian coordinates of the atoms within the structure of the dimer. These Cartesian coordinates of the atoms are varied to produce a structure with rotational constants closest to the experimental results, so the derived structure assumes a rigid rotor approximation that is vibrationally averaged, due the C – H bond lengths being fixed to optimized equilibrium values within the monomer structure. The standard deviation for this structure fit on the CPCA – FA dimer was 1.13 MHz. In the fit, the coordinates of all atoms for each monomer unit were held fixed to previously obtained structural values for CPCA (discussed in chapter) and FA.[108] There were only two variable parameters used in the structure fit for this dimer, which represented the movement of the fixed structure of the FA moiety in the a-b plane relative to the fixed center of mass of CPCA.

A third parameter, φ, is the angle of rotation in the a-b plane for the FA coordinates using a standard rotation matrix. Figure 6.1.2 shows the relative motion the angle φ invokes on the FA moiety. The angle φ was not a variable parameter in the fit, but different trial values were tested. The structure with the smallest standard deviation (the minimum in Figure 6.1.3) is reported and is referred to as the "best fit" structure. Figure 6.1.3 shows a plot of the fit standard deviation obtained with different test values of the angle φ.

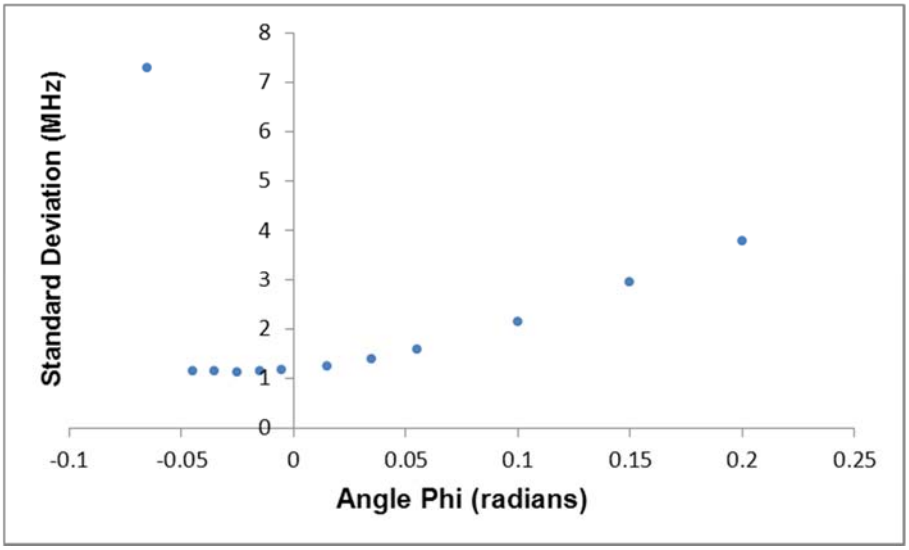

Figure 6.1.3 Plot showing the variation of the "best-fit" standard deviation for the nonlinear least squares structure fit with the angle φ. The variation of the angle φ represents the rotation of the FA moiety in the x-y Cartesian plane and changes the relative lengths of the two hydrogen bonds.

The standard deviation of the structure fit significantly increases after a value smaller than φ = -0.05 radians. At these small φ values, the FA moiety is rotated to an unreasonable position relative to the CPCA molecule and clearly does not correspond with experimental results as seen with the standard deviation. The deviation represents

the differences of the best fit structure's rotational constants with the experimentally fit values. The actual value of φ is less important compared with the differences in hydrogen bond lengths which are directly correlated with φ. Comparing the optimized equilibrium structure with the best fit structure obtained from the nonlinear least squares fit, the hydrogen bond lengths and center of mass separation of each monomer are listed in Table 6.1.5. The hydrogen bond lengths became very asymmetric in the best fit structure and the center of mass separations of the monomers only increased by 0.02 Å.

Table 6.1.5 Interatomic distances obtained by fitting the experimental rotational constants for six isotopologues in a nonlinear least squares fit. Hydrogen bond lengths and COM separations are in Å.

Interatomic Distance	Microwave Fit Value	Calculated (MP2) Value
$r(H_{12}\text{-}O_{14})$	1.36	1.67
$r(O_{11}\text{-}H_{13})$	2.25	1.62
COM Separation	4.11	4.09

6.1.6 DISCUSSION

The pure rotational spectrum of the doubly hydrogen bonded dimer formed between CPCA – FA has been measured using a PBFT microwave spectrometer and all the measured rotational transitions were assigned to be associated with the low energy conformer. Scans for the high energy conformer transitions for the dimer were unsuccessful. The predicted energy difference between the two conformers was only ~200 cm^{-1}, but may be larger as these high energy conformer transitions were not observed. There may be steric interactions of the FA hydrogen bonding to CPCA which

may prevent the CPCA molecule in the high energy form to form the hydrogen bonded dimer, even though this conformer of CPCA was observed with the monomer.

The Kraitchman calculated coordinates of the ^{13}C atoms and the D atom are in fair agreement with the best fit coordinates, with the exception of some coordinates varying by ~0.1 Å and more for the D substituted atom. The errors in some of the substituted coordinates are large, a result of the substituted atoms lying close to the principle axes or center of mass within the dimer. If we exclude the cyclopropane ring, the backbone structure of the dimer is planar. The hydrogen bond lengths in the best fit structure became very asymmetric compared with the theoretical computation and the separation of each of the monomers changes very little with the rotation angle φ. The asymmetry of the hydrogen bonds in the "best fit" structure may confirm these steric interactions of FA with the cyclopropane ring. A smaller asymmetry of the hydrogen bond lengths was found for the more symmetric doubly hydrogen bonded complex propiolic acid-formic acid and 1,2-cyclohexanedione-formic acid (next chapter).[109]

For the transitions measured of the CPCA – FA dimer, there appeared to be a small splitting within each transition and an example of this splitting can be observed in Figure 6.1.1. This is due to Doppler Effects commonly observed in spectra using PBFT spectrometers and likely not due to proton tunneling as was observed in other carboxylic acid dimers. The magnitude of the splitting increased with increasing frequency of the transitions, typical of Doppler type splittings. To confirm that these splittings were indeed Doppler splittings, a 50/50 argon/neon mixture was used as the carrier gas and, as expected with the presence of argon, these Doppler splittings decreased slightly. Tunneling splittings were not observed, most likely because the

dimer lacks the C_{2v}(M) symmetry, which may be necessary to create the symmetric double well potential, allowing for the protons to tunnel through the energy barrier. Because this dimer lacked C_{2v}(M) symmetry, the resulting potential energy surface is more asymmetric, “locking” the dimer in the lower of the tunneling configurations. The doubly hydrogen bonded dimers that exhibit this proton tunneling seem to have this symmetry, or very close to it.

6.2 1,2-CYCLOHEXANEDIONE (MONOENOLIC) – FORMIC ACID DIMER

6.2.1 INTRODUCTION

There has been substantial interest in doubly and triply hydrogen-bonded complexes since they provide simple models for the hydrogen bonding that exists between the complementary base pairs in DNA. These hydrogen-bonded dimers are not static structures and have been shown to exhibit proton tunneling dynamics in the gas phase. There have been several doubly hydrogen-bonded dimers in which the structure and proton tunneling have been studied. These dimers include complexes such as propiolic acid - formic acid and acetic acid - formic acid. 1,2-cyclohexanedione (1,2-CDO) exhibits tautomerization to the monoenolic form and this is the favorable tautomer for forming a dimer with formic acid. This results in a dimer structure capable of forming two hydrogen bonds similar the above dimers. Since 1,2-CDO is nonplanar, the dimer with formic acid is a bit more complex than the hydrogen-bonded dimers listed above and does not have a C_{2V}(M) symmetry. Due to the lack of symmetry in this dimer, the proton tunneling motion is not expected to be observed. Studying asymmetric dimers is still important as a tunneling case without a symmetric double well potential will be important to characterize and will be necessary to determine how asymmetric the dimers can be to still exhibit the proton tunneling.

6.2.2 MICROWAVE MEASUREMENTS

The microwave spectrum was measured in the 4.5-9 GHz range for the hydrogen bonded dimer between 1,2-cyclohexanedione (1,2-CDO) and formic acid (FA). Measurements were made using a pulsed-beam Fourier transform (PBFT) microwave

spectrometer. Four isotopologues were measured, including the parent, a single deuterium substitution at H12 on FA, a single deuterium substitution at H14 on 1,2-CDO, and a double deuterium substitution at H12 and H14 on FA and 1,2-CDO respectively. The atom numbering scheme is shown in Figure 6.2.1. There were 49 transitions measured in total; 19 for the parent isotopologue, 10 for the single deuterium substitution at H12 on FA, 10 for the single deuterium substitution at H14 on 1,2-CDO, and 10 for the double deuterium substitution at H12 on FA and H14 on 1,2-CDO. These transitions are all listed in Tables 6.2.1-3.

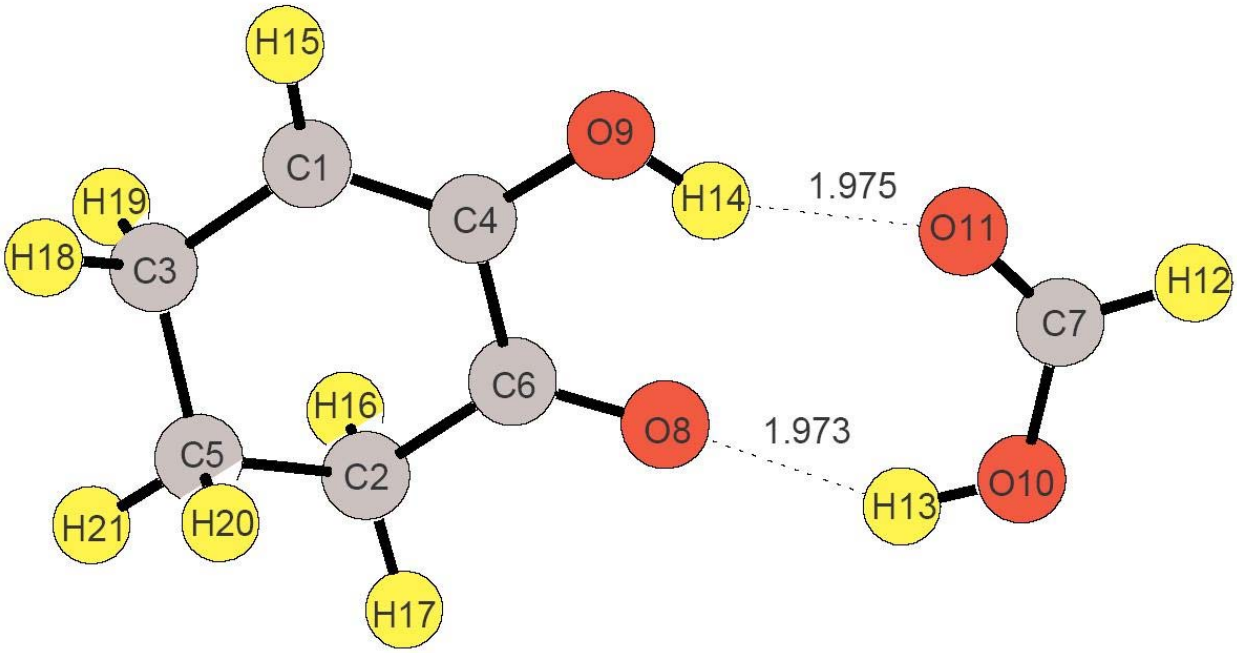

Figure 6.2.1. Best fit structure of the 1,2-CDO and FA hydrogen-bonded dimer.

Table 6.2.1 Results of the measurements and least squares fit calculations for 1,2-CDO/FA parent dimer isotopologue transitions. The standard deviation of the fit is 0.002 MHz. Frequencies are given in MHz.

$J'_{Ka'Kc'}$	$J''_{Ka''Kc''}$	ν_{obs}	ν_{o-c}
5_{15}	4_{14}	4732.9860	-0.002
5_{05}	4_{04}	4911.8100	-0.002
5_{24}	4_{23}	4969.4110	-0.001
5_{23}	4_{23}	5034.3650	0.001
5_{14}	4_{13}	5191.5510	0.002
6_{16}	5_{15}	5671.5780	-0.001
6_{06}	5_{05}	5860.6920	0.000
6_{25}	5_{24}	5957.2310	-0.000
6_{24}	5_{23}	6068.6140	0.001
6_{15}	5_{14}	6219.5780	0.002
7_{17}	6_{16}	6606.4180	0.002
7_{07}	6_{06}	6794.6320	-0.001
7_{26}	6_{25}	6941.7680	0.001
7_{25}	6_{24}	7114.4330	-0.003
7_{16}	6_{15}	7241.2990	-0.001
8_{18}	7_{17}	7537.3440	0.002
8_{08}	7_{07}	7714.6800	0.001
8_{27}	7_{26}	7922.5080	0.000
9_{09}	8_{08}	8623.3360	-0.001

Table 6.2.2 Results of the measurements and least squares fit calculations for 1,2-CDO/DFA parent dimer isotopologue transitions. The standard deviation of the fit is 0.003 MHz. Frequencies are given in MHz.

$J'_{Ka'Kc'}$	$J''_{Ka''Kc''}$	ν_{obs}	ν_{o-c}
4_{13}	3_{12}	4064.9410	0.002
5_{15}	4_{14}	4635.9410	0.001
5_{05}	4_{04}	4809.4060	-0.000
5_{24}	4_{23}	4862.0070	-0.000
5_{14}	4_{13}	5075.0680	0.001
6_{16}	5_{15}	5555.7840	-0.000
6_{06}	5_{05}	5740.5340	-0.001
6_{15}	5_{14}	6080.7580	-0.002
7_{07}	6_{06}	6657.6900	-0.001
8_{08}	7_{07}	7561.5940	0.001

Table 6.2.3 Results of the measurements and least squares fit calculations for 1,2-DCDO/FA and 1,2-DCDO/DFA dimer isotopologue transitions. Frequencies are given in MHz. The standard deviation of the fits are 0.003 MHz and 0.002 MHz respectively.

		1,2-DCDO/FA		1,2-DCDO/DFA	
$J'_{Ka'Kc'}$	$J''_{Ka''Kc''}$	ν_{obs}	ν_{o-c}	ν_{obs}	ν_{o-c}
5_{15}	4_{14}	4723.0850	-0.002	4626.7041	-0.001
5_{05}	4_{04}	4901.9722	0.004	4800.2813	0.002
6_{16}	5_{15}	5659.5898	-0.004	5544.6025	-0.001
6_{06}	5_{05}	5848.4570	-0.001	5729.1812	0.000
7_{17}	6_{16}	6592.3052	-0.001	6458.9888	-0.003
7_{07}	6_{06}	6779.8853	-0.001	6643.9844	-0.001
8_{18}	7_{17}	7521.0698	0.002	7369.7031	-0.001
8_{08}	7_{07}	7697.3687	0.000	7545.4683	-0.002
9_{19}	8_{18}	8445.8906	0.004	8276.7246	0.004
9_{09}	8_{08}	8603.4980	-0.000	8435.7979	0.001

The 1,2-CDO (97%) and FA (98%) samples were purchased from Sigma Aldrich and were used without further purification. The deuterated FA was purchased from CDN isotopes (99.2% D) and was also used without further purification. The deuterated 1,2-CDO sample was prepared by mixing equimolar quantities of 1,2-CDO (Sigma Aldrich, 97%) and MeOD (Cambridge Isotope Lab, Inc., 99%) and letting them exchange overnight. The remaining MeOH was removed from the mixture under reduced pressure and the deuterated 1,2-CDO crystallized in the flask and was then removed and transferred to a small vial to be used for the measurements.

The samples of 1,2-CDO and FA were transferred into separate glass sample cells. The cell containing 1,2-CDO was attached to the pulsed-valve (General Valve series 9) and was heated to ~35 °C. The cell containing FA was placed in the neon gas line leading to the cell containing 1,2-CDO. The FA sample was maintained at -10 °C

using a Peltier cooling system. The pressure inside the spectrometer was maintained at 10^{-6} to 10^{-7} Torr prior to the pulsed injection of the samples and the Ne carrier gas, which was maintained at ~1 atm. The valve was set to pulse at ~2 Hz. A similar set up was used to measure the transitions of all other isotoplogues, using the respective isotopic samples of either the deuterated 1,2-CDO or FA. An example of an observed transition is shown in Figure 6.2.2. Some small splittings of lines were observed but none are assigned to possible proton tunneling. These splittings are a result of the Doppler Effect, which is present in these pulsed beam experiments as was discussed in the previous chapter. The present complex does not possess a C_2 symmetry axis, so we would expect an asymmetric tunneling potential making it unlikely that concerted proton tunneling splittings would be observed.

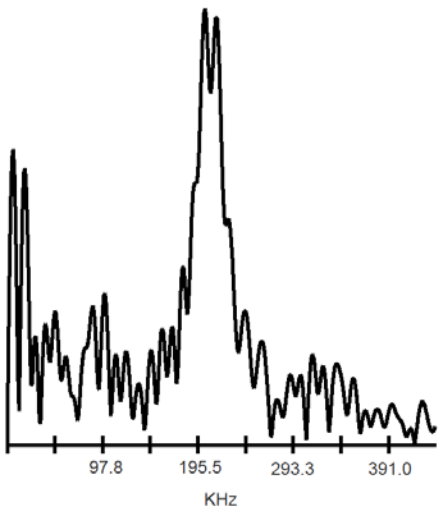

Figure 6.2.2 Example of observed transition for 1,2-CDO – FA parent (5_{05}-6_{06}, 245 pulsed-beam cycles) at stimulating frequency 5860.900 MHz. The horizontal axis represents the difference of the observed transition from the stimulating frequency, shown in KHz.

6.2.3 CALCULATIONS

Ab initio computations to obtain an optimized equilibrium structure were performed using Gaussian 09 suite using MP2 with a 6-311++G** basis set in order to obtain initial values of the rotational constants. The rotational constants from the optimized Gaussian structure were used to predict the a-dipole rotational transitions as the a-dipole moment component was predicted to be the largest leading to stronger transitions. The optimized values of the rotational constants were A=2413.722 MHz, B=544.074 MHz, and C=454.138 MHz. These calculated rotational constants fall within 0.6% of the experimental values, limiting the scan range of the experiment and aided in quantum number assignments of the rotational states involved in the measured transitions. A comparison of the hydrogen bond distances and the center of mass separations of the calculated Gaussian and experimental structure are shown in Table 6.2.4.

Table 6.2.4 Interatomic distances obtained by fitting the experimental rotational constants for four isotopologues. Hydrogen bond lengths and COM separations are in Å.

Interatomic Distance	Microwave Fit Value (Å)	Calculated Value (Å)
$r(H_{13}\text{-}O_8)$	1.973(30)	1.771
$r(H_{14}\text{-}O_{11})$	1.975(30)	1.886
COM Separation	4.591(2)	4.571

6.2.4 ROTATIONAL CONSTANTS

Experimental rotational and centrifugal distortion constants for the parent isotopologue of the dimer were determined using a nonlinear least-squares fitting program and are given in Table 6.2.5. A similar analysis was carried out for the remaining 3 isotopologues of the dimer, but the centrifugal distortion constants were held fixed to the values obtained from the parent isotopologue. The observed (o) and calculated (c) rotational transition frequencies from the fit rotational constants for each of the isotopologues are given in Tables 6.2.1-3.

Table 6.2.5 Atom Cartesian coordinates in a, b, c system for the best fit structure of 1,2-CDO/FA hydrogen bonded dimer, and the Kraitchman determined values (Krait.) for the isotopic substitutions.

Atom	a	b	c	|a| -Krait.	|b| -Krait.	|c| -Krait.
C1	2.236	0.100	1.290			
C2	1.676	0.257	-1.554			
C3	3.383	0.124	0.308			
C4	0.946	0.037	0.887			
C5	2.981	-0.394	-1.074			
C6	0.582	0.031	-0.543			
C7	-3.616	0.001	0.165			
O8	-0.608	-0.031	-0.846			
O9	-0.089	-0.103	1.753			
O10	-3.374	-0.001	-1.240			
O11	-2.840	0.000	0.943			
H12	-4.631	0.006	0.550	4.7(8)	0.06(1)	0.15(3)
H13	-2.459	0.014	-1.527			
H14	-0.884	-0.094	1.195	1.(1)	0.03(2)	1.(1)
H15	2.448	0.075	2.357			
H16	1.832	1.344	-1.616			
H17	1.341	-0.088	-2.536			
H18	4.245	-0.436	0.687			
H19	3.707	1.173	0.227			
H20	2.817	-1.477	-1.013			
H21	3.782	-0.221	-1.800			

6.2.5 MOLECULAR STRUCTURE

The rotational constants acquired from each of the microwave fits of the isotopologues were used in a nonlinear least squares fitting program to determine the experimental hydrogen bond lengths and the center of mass separation of the 1,2-CDO and FA monomers. In the fit, 1,2-CDO coordinates were held fixed to those obtained previously.[110] Structural parameters for formic acid were obtained from the work of Gerry[108] and were also held fixed. The coordinates of both monomers were initially set up in such a way that the sp^2 hybridized carbon atoms of 1,2-CDO (C1, C4, and C6) and FA (C7), as well as all oxygen atoms and the hydrogen atoms H12-15, were in the same plane (the x-y plane). There were two variable parameters assigned during the structure fit. These parameters represented the x - y coordinates for the center of mass of FA, with respect to the coordinate system of 1,2-CDO. A third fixed parameter, ϕ (phi), represented the rotation of the formic acid moiety in the x-y plane. The rotation of the FA moiety was held fixed to ϕ= -0.1047 radians, as this angle produced the best structure with the smallest deviation of its calculated rotational constants compared with the experimentally determined values obtained from assigning the transitions. The value of the angle ϕ is not as important as the hydrogen bond lengths that result and the COM separation changes very little with ϕ. The center of mass separation of the monomers was calculated using the parallel axis theorem resulting in the equation $I_{CC} = I_{CC}$(1,2-CDO) + I_{CC}(FA) + μR^2_{CM}. The calculated and experimental values for the hydrogen bond lengths and the center of mass separations are shown in Table 6.2.4.

The experimental A, B, and C rotational constants and the deviations from the best fit calculated values are listed in Table 6.2.6. Values of the atomic coordinates

obtained from the structure fit are shown in Table 6.2.5. Coordinates for the substituted atoms were also obtained by performing a Kraitchman analysis. We do not believe that all of the magnitudes of coordinates from the Kraitchman analysis are very accurate nor reliable due to the substitutions being in close proximity to the principal axes or center of mass of the dimer, but they are all included in Table 6.2.5 for reference.

Table 6.2.6 MEASURED rotational constants and the "best fit" CALCULATED values for rotational constants obtained from the structure fit. The standard deviation for the fit is 1.12 MHz. Also shown are the distortion constants (kHz) of the parent isotopologue, held fixed for all other isotopic substitutions.

ISOTOPOLOGUE		MEASURED	CALCULATED	(M. – C.)
Parent	A	2415.0439(179)	2417.1848	-2.1410
	B	543.6907(2)	543.7113	-0.0206
	C	451.6663(2)	450.8779	0.7884
	D_J	0.0220(13)		
	D_{JK}	0.119(31)		
CDO-DFA	A	2414.7543(379)	2413.7931	0.9613
	B	530.9216(2)	531.4466	-0.5250
	C	442.8253(3)	442.2975	0.5278
DCDO-FA	A	2399.6875(257)	2400.6990	-1.0115
	B	542.9527(9)	543.2486	-0.2959
	C	450.6175(3)	449.9907	0.6267
DCDO-DFA	A	2399.4147(226)	2397.5249	1.8897
	B	530.2502(7)	531.0291	-0.7789
	C	441.8415(2)	441.4666	0.3749

6.2.6 DISCUSSION

The pure rotational spectrum of the doubly hydrogen bonded dimer of 1,2-cyclohexanedione and formic acid has been measured using a PBFT microwave spectrometer and all measured rotational transitions were assigned. The experimental

rotational transitions are shown in Tables 6.2.1-3 and the best fit hydrogen bond lengths and center of mass separations and structural coordinates of the dimer are given in Tables 6.2.4 and 6.2.5 respectively. The best fit structure shown in Figure 6.2.1 produced more symmetric and slightly longer hydrogen bond lengths when compared with the Gaussian calculation. The experimental hydrogen bond lengths of 1.97 Å are a bit longer than the optimized (Gaussian) values of 1.77 Å and 1.89 Å. This difference is a bit larger than expected, but in the correct direction since the experimental values are r_0 and calculated values are for r_e. We believe that the average of the hydrogen-bond lengths is quite accurate (r_{OH} = 1.97(1)) but the uncertainty is perhaps a factor of 2 or 3 higher for the individual hydrogen bond lengths (r_{OH} = 1.97(3)) because the fit was not very sensitive to the angle ϕ. More isotopologue transitions need to be measured to determine a more complete and accurate gas phase structure for this dimer.

6.3 MALEIMIDE – FORMIC ACID DIMER

6.3.1 INTRODUCTION

Interest to study hydrogen bonded complexes has been growing over recent years to better understand these interactions. Hydrogen bonded systems are prevalent all throughout nature and can be seen in systems such as DNA, with the hydrogen bonding between base pairs, or in proteins as the secondary structure is highly dependent upon the amount of hydrogen bonding present. Hydrogen bonding interactions give rise to proton tunneling motions, and some of these tunneling motions may be associated with point mutations in DNA that may cause disease. In the gas phase, some of these hydrogen bonded dimers formed between two carboxylic acids have been shown to exhibit this proton tunneling motion. Information about the dynamics of this tunneling motion, such as the tunneling splitting, can be determined directly through the analysis of the microwave spectra. Further analysis of the structure and the tunneling splitting can yield information about the potential energy surface specifically the barrier height between the two tunneling configurations. Studying these systems is important to better understand these types of phenomena and provide benchmarks to help improve the accuracy of theoretical computations for larger systems.

Previously studied doubly hydrogen bonded carboxylic acid dimers that exhibited the tunneling motion maintained a C_{2v}(M) symmetry, allowing for a symmetric potential energy surface. One of these dimers is the propiolic acid – formic acid dimer. The double hydrogen bonded dimer formed between the monoenolic tautomer of 1,2-cyclohexanedione and formic acid (CDO-FA), discussed in the previous section, had

low symmetry and was not a dimer formed between two carboxylic acids; no proton tunneling was observed. In this study, the maleimide – formic acid (Mal-FA) doubly hydrogen bonded dimer, which also does not have C_{2v}(M) symmetry, was observed. It is important to study even the asymmetric hydrogen bonded dimers because if the tunneling motion is observed, then the C_{2v}(M) symmetry thought to be required may not be necessary to observe this tunneling effect. Furthermore, it will be important to characterize the tunneling splitting in dimers without a symmetric potential energy surface and answer an important question about how asymmetric can the dimers be and the tunneling still be present. Many of the dimers studied are formed between carboxylic acids or other similar oxygen containing species, as in the CDO-FA dimer, but it is important to also characterize the dimers with nitrogen containing groups, as there may be structural differences when compared to the complexes with the oxygen containing species.

6.3.2 CALCULATIONS, MICROWAVE MEASUREMENTS, AND DATA ANALYSIS

DFT computations were performed on the Mal-FA dimer in order to obtain preliminary rotational constants and quadrupole coupling strengths for this system, allowing for the pure rotational transitions to be predicted using Pickett's SPCAT program. A B3LYP method was used with an aug-cc-pVTZ basis using the Gaussian 09 suite on the HPC system at the University of Arizona. Additional predictive calculations were performed to predict the rotational constants of the deuterated isotopologues. These were performed by first determining the ratio, or scale factor, between the parent experimental and calculated rotational constants. The scale factor was then multiplied

by the calculated rotational constants of the deuterated isotopologue, which were recalculated using Kisiel's PMIFST program,[111] after changing the mass of the respective substituted H atom. Usually these corrected values of the rotational constants for the singly substituted isotopologues are very close to experimental values for ^{13}C substituted isotopologues. In the case of these D substituted isotopologues, the H atoms are distant from the principle axes, thus making the effect of changing the mass of H to D larger, resulting in predicted rotational constants that did not agree very well with the fit experimental values and so some searching was required to observe and measure these D substituted rotational transitions.

The rotational transitions were measured for the parent in the 4.9 – 10 GHz range using a Flygare-Balle type pulsed-beam Fourier transform microwave spectrometer that has been previously described. The maleimide sample was purchased from Sigma Aldrich (99%) and was used without further purification. The pressure inside the vacuum cavity was maintained at 10^{-6} to 10^{-7} Torr prior to the pulse of the molecular beam. The backing pressure of the Ne carrier gas was maintained at ~ 1 atm. In order to obtain sufficient vapor pressure of the maleimide sample, the sample cell and pulsed valve were heated to ~70 °C. To prepare the doubly hydrogen bonded dimer, the maleimide and formic acid samples were transferred to separate glass sample cells. Within the Ne gas line, the cooled formic acid (-8 °C) sample cell was placed before the maleimide sample cell and the temperature of the FA was maintained using a Peltier cooling device. This allowed the FA vapor to be seeded into the Ne carrier gas before picking up the gaseous maleimide sample. All measured rotational transitions for the parent are shown in Table 6.3.1 and the transitions measured of each

of the D substituted isotopologues are shown in Table 6.3.2. There was no evidence of the concerted proton tunneling motion as many b-type transitions were measured and used in the fits. If proton tunneling is present, the b-type transitions will be significantly split possibly by hundreds of MHz, due to these ro-vibrational transitions changing vibrational states.

Table 6.3.1 Measured rotational transitions of the maleimide – formic acid heterodimer and the differences ($\nu_{o\text{-}c}$) from the calculated values in the fit. Values shown are in MHz.

J′ Ka′ Kc′ F′	J″ Ka″ Kc″ F″	ν_{obs}	$\nu_{o\text{-}c}$
2 2 0 2	2 1 1 2	4907.953	0.006
4 1 4 5	3 1 3 4	5093.764	0.002
4 1 4 4	3 1 3 3	5093.864	-0.006
3 1 3 4	2 0 2 3	5287.475	0.005
3 1 3 3	2 0 2 2	5288.088	0.001
4 0 4 5	3 0 3 4	5353.787	-0.004
4 0 4 4	3 0 3 3	5353.961	0.003
4 2 3 3	3 2 2 2	5494.710	0.002
4 2 3 5	3 2 2 4	5494.768	0.006
4 2 3 4	3 2 2 3	5494.978	0.006
5 0 5 5	4 1 4 4	5632.969	-0.002
5 0 5 6	4 1 4 5	5633.204	-0.004
5 0 5 4	4 1 4 3	5633.323	-0.000
4 1 3 3	3 1 2 2	5856.487	-0.002
4 1 3 5	3 1 2 4	5856.553	0.005
4 1 3 4	3 1 2 3	5856.633	0.001
3 2 2 3	3 1 3 3	5764.425	-0.001
3 2 2 4	3 1 3 4	5765.572	0.004
5 1 5 6	4 1 4 5	6342.525	0.006
5 1 5 5	4 1 4 4	6342.597	-0.008
5 0 5 4	4 0 4 3	6593.400	-0.001
5 0 5 5	4 0 4 4	6593.573	0.001
5 2 4 5	5 1 5 5	6671.616	0.000
5 2 4 6	5 1 5 6	6672.609	-0.003
5 2 4 4	5 1 5 4	6672.816	0.001
5 2 4 6	4 2 3 5	6848.564	-0.000
5 2 4 5	4 2 3 4	6848.697	0.002

5	3	3	6	4	3	2	5	6930.662	-0.005
5	3	3	5	4	3	2	4	6930.853	-0.001
6	1	6	6	5	1	5	5	7578.725	0.001
6	0	6	7	5	0	5	6	7793.394	0.005
6	0	6	6	5	0	5	5	7793.556	-0.003
2	2	1	3	1	1	0	2	7837.498	-0.004
2	2	1	2	1	1	0	1	7837.952	-0.005
5	3	2	5	5	2	3	4	8267.066	0.002
5	3	2	5	5	2	3	6	8267.096	-0.008
5	3	2	6	5	2	3	6	8267.188	0.007
3	2	2	4	2	1	1	3	9022.316	-0.002
3	2	2	2	2	1	1	3	9022.316	-0.002
3	2	2	3	2	1	1	3	9022.316	-0.002
3	2	2	3	2	1	1	2	9022.830	-0.009
3	2	2	2	2	1	1	2	9022.830	-0.009
3	2	1	3	2	1	2	2	9676.429	-0.001
3	2	1	4	2	1	2	3	9677.607	0.007
3	2	1	2	2	1	2	1	9678.211	0.001

Table 6.3.2 Measured rotational transitions of the isotopologues of the Mal-FA dimer and the differences (ν_{o-c}) from the calculated values in the fit. Values shown are in MHz.

Rotational Transitions								Mal – (D)FA		Mal(ND) – FA		Mal – FA(OD)	
J′	K_a'	K_c'	F'	J″	K_a"	K_c"	F"	ν_{obs}	ν_{o-c}	ν_{obs}	ν_{o-c}	ν_{obs}	ν_{o-c}
2	2	0	1	2	1	1	1	4926.610	-0.001			4897.0811	-0.003
2	2	0	3	2	1	1	3	4926.645	0.000			4897.1440	0.005
4	1	4	5	3	1	3	4	4984.640	-0.006	5088.241	-0.006	5055.5005	-0.004
4	1	4	4	3	1	3	3	4984.742	-0.004	5088.347	-0.002	5055.6011	0.000
3	1	3	2	2	0	2	1	5217.600	0.010	5271.962	0.001	5256.7998	0.005
3	1	3	4	2	0	2	3	5217.708	-0.001	5272.074	-0.001	5256.9155	-0.003
3	1	3	3	2	0	2	2	5218.325	0.001				
4	0	4	5	3	0	3	4	5238.871	-0.006			5313.5459	-0.007
4	0	4	4	3	0	3	3	5239.036	0.000	5348.165	0.001	5313.7095	-0.003
5	0	5	5	4	1	4	4	5469.778	-0.002	5636.195	-0.005	5581.7734	0.004
5	0	5	6	4	1	4	5	5470.032	-0.002	5636.430	-0.002	5582.0132	0.001
5	0	5	4	4	1	4	3	5470.153	0.004	5636.546	0.004	5582.1284	0.006
4	1	3	3	3	1	2	2	5717.417	-0.007			5809.5996	-0.006
4	1	3	5	3	1	2	4	5717.487	0.004	5853.249	0.002	5809.6655	0.001
4	1	3	4	3	1	2	3	5717.567	0.008	5853.324	0.000		
5	1	5	6	4	1	4	5	6207.899	0.002	6335.367	0.000	6295.1514	0.002
5	1	5	4	4	1	4	3	6207.954	0.009	6335.420	0.006		
5	0	5	6	4	0	4	5			6585.264	-0.002		
5	0	5	4	4	0	4	3	6456.280	-0.007			6544.7793	-0.006

5 0 5 5	4 0 4 4	6456.449	-0.004	6585.437	-0.002	6544.9556	0.004
6 1 6 7	5 1 5 6			7569.764	0.003	7522.3765	0.009
6 1 6 5	5 1 5 4	7419.320	0.003	7569.798	0.005		
6 1 6 6	5 1 5 5	7419.359	0.004	7569.839	0.006	7522.4468	0.011
6 0 6 5	5 0 5 4	7635.267	-0.004	7782.922	0.004	7736.7603	-0.003
6 0 6 7	5 0 5 6	7635.267	0.002				
6 0 6 6	5 0 5 5	7635.427	-0.004	7783.064	-0.014	7736.9170	-0.005

The experimental rotational, quadrupole coupling (for ^{14}N) and centrifugal distortion constants were determined from the assigned rotational transitions for each of the isotopologues using Pickett's SPFIT program and these values are shown in Table 6.3.3. The quadrupole coupling strengths of D were not determined for those isotopologues with a D substitution as the D hyperfine structure was not resolved. The calculated values are within 0.1% of the experimental values. During the microwave fits for the isotopologues, the centrifugal distortion constants were held fixed to the values obtained from the parent. The experimental inertial defect was Δ = -0.528 amu Å^2, indicating the molecular structure is planar with a value close to zero. The small negative nonzero value of this inertial defect indicates the presence of out of plane vibrational motions within this dimer. Compared with the inertial defect of the maleimide monomer (Δ = -0.0536 amu Å^2),[112] the magnitude of the inertial defect of the dimer is larger, suggesting more out of plane vibrational modes.

Table 6.3.3 Fit rotational, centrifugal distortion, and quadrupole coupling constants of the Mal – FA dimer. Also shown is the B3LYP/aug-cc-pVTZ calculated values.

	Parent	B3LYP/aug -cc-pVTZ	-ND	D-FA	FA-OD
A/MHz	2415.0297(11)	2414.7720	2403.7960(43)	2402.0396(22)	2405.0404(22)
B/MHz	784.37494(41)	784.34024	784.16342(70)	764.72770(54)	777.87629(55)
C/MHZ	592.44190(36)	592.04019	591.65013(28)	580.42763(25)	588.13551(25)
$1.5\chi_{aa}$/MHz	2.083(15)	2.150	1.86(11)	1.860(44)	1.694(40)
$0.25(\chi_{bb}- \chi_{cc})$/MHz	1.1565(32)	1.1865	1.118(17)	1.136(10)	1.117(12)
D_J/kHz	0.0616(69)		0.0616*	0.0616*	0.0616*
D_{JK}/kHz	-0.118(38)		-0.118*	-0.118*	-0.118*
D_K/kHz	-1.38(16)		-1.38*	-1.38*	-1.38*
N	45		19	24	20
σ/kHz	4		5	5	5

* Centrifugal distortion constants were held fixed to the experimental parent isotopologue values during the microwave fits of each isotopologue.

From the rotational constants of the parent and each D substituted isotopologue, a nonlinear least squares fit was performed to determine the best fit gas phase structure of this hydrogen bonded dimer. This fitting program varies the Cartesian coordinates of the atoms within the molecules to obtain a structure that calculates rotational constants closest to the experimentally determined values obtained from assigning the measured transitions to the correct energy levels. During the fit, the atomic coordinates of Mal were held fixed to previously obtained values (discussed earlier in this dissertation) and the structure of formic acid was held fixed to what was obtained from the work of Gerry.[108] Because the structure of the Mal monomer is an averaged structure of both equilibrium and ground state atomic coordinates, the obtained structure of the dimer is also a vibrationally averaged structure. We believe the differences in these structures are small and this best fit structure reasonably represents this dimer in the ground state. There were 2 varied parameters during the structure fit which varied the coordinates of

FA in the molecular (a-b) plane. A third parameter, φ, was the rotation of the formic acid coordinates within this molecular plane. φ was not varied, but was set to a value that provided the smallest standard deviation in the structure fit, which was 1.09 MHz. This best fit structure can be seen in Figure 6.3.1 and the hydrogen bond lengths from the B3LYP calculation and the best fit structure are compared in Table 6.3.4. The best fit structure seemed to correlate with the formic acid moiety slightly rotated to increase the length of r(H_6-O_{13}) and decrease the length of r(O_{12}-H_{10}). The center of mass separation, determined through the use of the parallel axis theorem, of the monomer units remained unchanged from the calculation and the experimentally determined rotational constants.

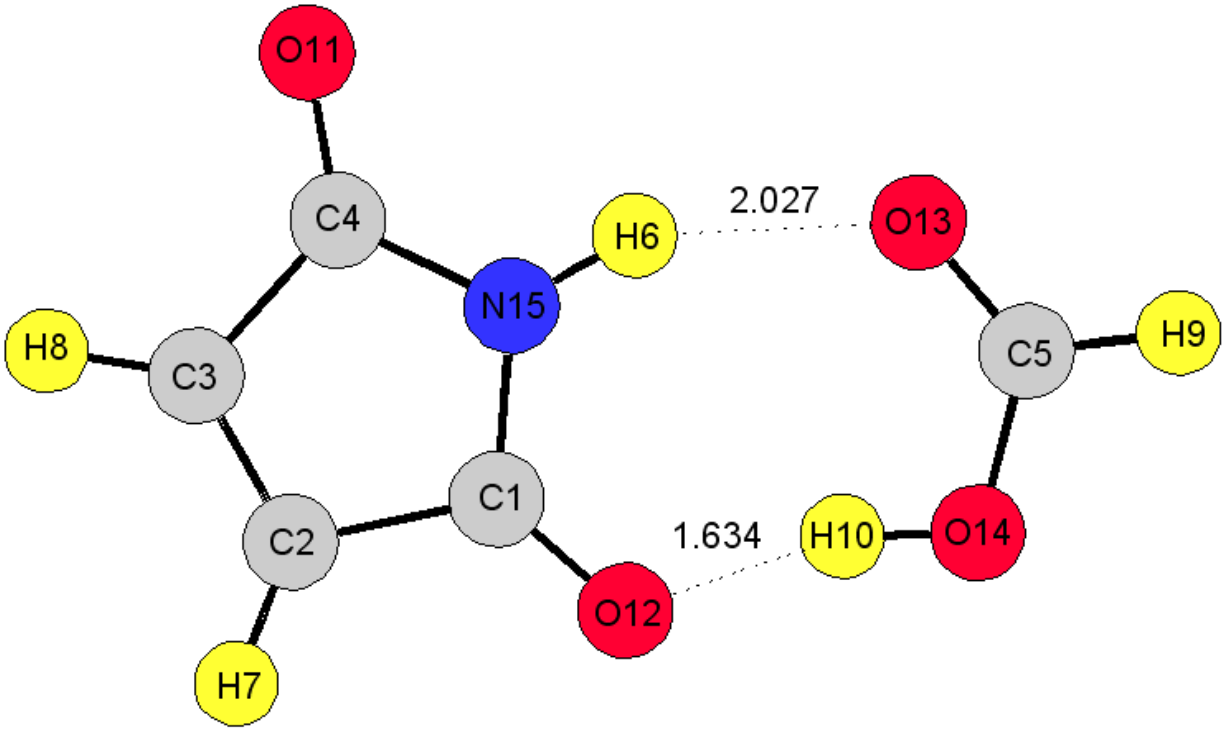

Figure 6.3.1 Best fit structure of the maleimide – formic acid dimer, showing the hydrogen bond distances in Å.

Table 6.3.4 Hydrogen bond distances and center of mass separation of the monomers in the best fit structure compared with the B3LYP/aug-cc-pVTZ calculated values, shown in Å.

Interatomic Distance	Microwave Fit Value	Calculated (B3LYP) Value
$r(H_6\text{-}O_{13})$	2.027	1.874
$r(O_{12}\text{-}H_{10})$	1.634	1.685
COM Separation	4.06	4.06

The principle axes coordinates of the best fit structure are shown in Table 6.3.5 along with the Kraitchman determined coordinates for the single D substituted H atoms, which were calculated using Kisiel's KRA program. The Kraitchman determined coordinates only give the magnitudes and so the absolute values of the coordinates are shown. The D substituted coordinates do not agree very well with the best fit structure, indicating a large change of the molecular structure upon the isotopic substitution. The change in structure upon substitution agrees with the fact that the rotational constants of these D isotopologues could not be predicted very accurately by changing the mass of each of these substituted atoms. Since the nonlinear least squares fitting program assumes the structure does not change upon isotopic substitution, this current structure can be refined with the measurement of transitions from singly substituted ^{13}C and ^{15}N isotopologues to obtain more accurate hydrogen bond distances.

Table 6.3.5 Best fit atomic coordinates (Å) of the best fit structure compared with the Kraitchman determined coordinates of the substituted D isotopes. The Kraitchman values only show the magnitudes of the COM coordinates.

Atom	a	b	Krait-|a|	Krait-|b|
C1	0.469	-1.006		
C2	1.868	-1.542		
C3	2.726	-0.481		
C4	1.908	0.775		
C5	-3.095	0.642		
H6	-0.200	1.007	0.4042(38)	0.9895(15)
H7	2.091	-2.601		
H8	3.808	-0.477		
H9	-4.143	0.944	4.06138(38)	1.0843(14)
H10	-2.005	-0.871	2.31736(66)	0.9384(16)
O11	2.313	1.918		
O12	-0.564	-1.642		
O13	-2.184	1.425		
O14	-2.958	-0.691		
N15	0.586	0.371		

6.3.3 CONCLUSIONS

Rotational transitions were measured for the maleimide – formic acid doubly hydrogen bonded dimer and three single D substituted isotopologues. There was no evidence of the double concerted proton tunneling in the measurement of the rotational transitions of this dimer, further suggesting that $C_{2v}(M)$ symmetry is required to observe this tunneling effect. The best fit gas phase structure is an averaged structure of equilibrium and ground state atomic coordinates, but is a reasonable representation of the ground state of this dimer. The current structure can be further refined with the measurement of additional isotopologue transitions.

6.4 TROPOLONE – FORMIC ACID DIMER

6.4.1 INTRODUCTION

Tropolone, or 2-hydroxy-2,4,6-cycloheptatriene-1-one, is a seven membered ring and a pseudoaromatic molecule.[113] The carbonyl and hydroxyl groups interact with each other to form a stabilizing intramolecular hydrogen bond. Tropolone has been previously studied and it was observed that the hydrogen atom on the hydroxyl group tunnels between the two oxygen atoms in the molecule. The structure after tunneling occurs is identical to the configuration before the tunneling motion. The tunneling motion is described by a symmetric potential energy surface that has a double well minima that is caused by the C_{2v}(M) symmetry along the proton tunneling coordinates. The proton tunneling effect has been extensively studied for other systems using microwave spectroscopy, rotationally resolved degenerate four-wave mixing,[114,115,116,117,118] matrix-isolated infrared spectroscopy,[119,120] laser-induced fluorescence (LIF) techniques,[121,122] and gaseous infrared spectroscopy.[123,124,125,126]

The magnitude of the splitting between ro-vibrational transitions can be affected by a number of factors. Some of these factors are the motion of the tunneling proton, displacement of nuclei during the tunneling motion, redistribution of electronic charge, energy and mode of the vibrational excitation, and asymmetric isotopic substitutions. The barrier height can also be influenced by intermolecular interactions, such as the van der Waals complexes formed with noble gases or hydrogen bonding.[127] Previous microwave studies reported the microwave spectrum of Ar-tropolone and H_2O-tropolone and found that the weak interactions both quench the proton tunneling motion.[128,129]

There also may have been other interactions with H_2O that may have quenched the tunneling.

Formic Acid is known to form doubly hydrogen bonded dimers with several carboxylic acids. Some of these dimers exhibit proton tunneling and some do not. The microwave spectra of cyclopropanecarboxylic acid – formic acid (CPCA-FA) dimer was previously discussed in chapter 6.1 and no tunneling was observed for this doubly hydrogen bonded dimer, due to its lack of symmetry. Due to the tropolone-formic acid doubly hydrogen bonded dimer possessing the C_{2V}(M) symmetry, the potential energy surface has a symmetric double well potential and the proton tunneling motion is expected to be observed in this study. An image of this dimer is shown below in Figure 6.4.1.

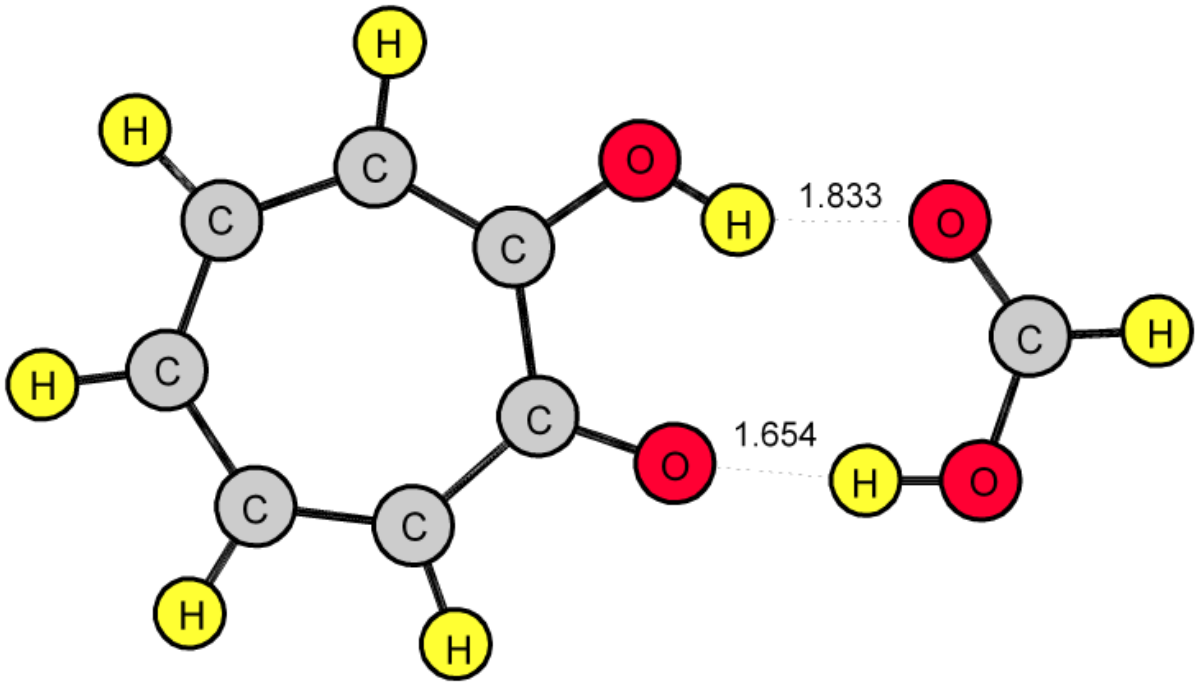

Figure 6.4.1 Calculated B3LYP/aug-cc-pVTZ structure of the Tropolone – Formic Acid doubly hydrogen bonded dimer. Hydrogen bond lengths are shown in Å.

6.4.2 MICROWAVE MEASUREMENTS

The microwave spectrum was measured for the tropolone – formic acid doubly hydrogen bonded dimer in the 4.7 – 9 GHz range and all assigned transitions are shown in Table 6.4.1.

Table 6.4.1 Measured a- and b-type rotational transitions of the tropolone – formic acid doubly hydrogen bonded dimer. Values are shown in MHz.

J′ Ka' Kc'	J″ Ka" Kc"	ν_{obs}	ν_{o-c}
$4_{1\,4}$	$3_{0\,3}$	4776.994	0.006
$6_{1\,6}$	$5_{1\,5}$	4879.911	-0.001
$6_{0\,6}$	$5_{0\,5}$	5051.614	-0.002
$6_{3\,3}$	$5_{3\,2}$	5169.534	0.000
$6_{2\,4}$	$5_{2\,3}$	5237.764	0.000
$5_{1\,5}$	$4_{0\,4}$	5444.692	-0.007
$7_{1\,7}$	$6_{1\,6}$	5683.893	0.004
$7_{0\,7}$	$6_{0\,6}$	5855.119	0.004
$7_{3\,5}$	$6_{3\,4}$	6030.552	0.001
$7_{3\,4}$	$6_{3\,3}$	6038.775	0.002
$6_{1\,6}$	$5_{0\,5}$	6089.936	0.003
$7_{2\,5}$	$6_{2\,4}$	6141.604	-0.005
$7_{1\,6}$	$6_{1\,5}$	6257.955	0.001
$8_{1\,8}$	$7_{1\,7}$	6484.354	0.001
$8_{0\,8}$	$7_{0\,7}$	6646.059	-0.001
$7_{1\,7}$	$6_{0\,6}$	6722.206	0.000
$8_{1\,7}$	$7_{1\,6}$	7133.512	0.003
$9_{1\,9}$	$8_{1\,8}$	7281.295	-0.003
$8_{1\,8}$	$7_{0\,7}$	7351.443	-0.001
$9_{0\,9}$	$8_{0\,8}$	7426.650	-0.002
$9_{1\,9}$	$8_{0\,8}$	7986.682	-0.001
$10_{0\,10}$	$9_{0\,9}$	8199.868	-0.003
$10_{1\,9}$	$9_{1\,8}$	8856.853	-0.003
$11_{1\,11}$	$10_{1\,10}$	8865.250	0.005
$11_{0\,11}$	$10_{0\,10}$	8968.743	0.000

These measurements were taken using a Flygare-Balle type pulsed-beam Fourier transform microwave spectrometer that has been previously described. The

tropolone (98%) and formic acid (98%) samples were both purchased from Sigma Aldrich and used without further purification. The samples were transferred to separate glass sample cells. The cell containing tropolone was placed in the Ne gas line just before the pulsed valve (General Valve Series 9) and was set to pulse at room temperature. The Ne backing pressure was maintained at about 1 atm. The tropolone sample was pulsed until there was a strong parent test signal recorded. Once the tropolone signal was sufficiently strong, the sample cell containing the formic acid was placed in the Ne gas line, before the tropolone sample and the formic acid vapor was passed over the tropolone sample with each molecular beam pulse. The sample of formic acid was brought to -8 °C before attaching to the Ne gas line and this temperature was maintained using a Peltier cooling device. The formic acid vapor was pulsed over the solid tropolone sample for about 15 minutes, and then was removed from the Ne gas line as this provided a sufficient concentration of formic acid to measure the dimer transitions in a single pulsed beam cycle. The high concentration of FA being pulsed into the cavity reduced the signal intensity of the dimer. The removal of formic acid was also crucial to the experiment as tropolone is very hygroscopic and was absorbing much of the water vapor within the formic acid sample.

6.4.3 CALCULATIONS AND ROTATIONAL CONSTANTS

DFT computations were performed on the HPC system at the University of Arizona using the Gaussian 09 suite with a B3LYP method and a aug-cc-pVTZ basis. The results from this calculation are shown in Table 6.4.2. The calculated rotational constants were used in the Pickett SPCAT program to predict the rotational transitions

expected to be observed. The calculated dipole moment components were 3.8 D along the a-axis and 0.6 D along the b-axis, so it was expected the a-type transitions would be strongest and these were the transitions that were initially searched for. The rotational and centrifugal distortion constants were determined from the 25 a- and b- type rotational transitions using the Pickett SPFIT program and these determined parameters are shown in Table 6.4.2 along with the calculated values.

Table 6.4.2 Experimental and calculated rotational constants of the tropolone – formic acid doubly hydrogen bonded dimer.

	Parent	B3LYP/aug-cc-pVTZ
A/MHz	2180.7186(98)	2191.3931
B/MHz	470.87390(25)	474.39567
C/MHZ	387.68984(22)	389.97457
D_J/kHz	0.0100(14)	
D_{JK}/kHz	0.102(28)	
D_K/kHz	13.2(81)	
N	25	
σ/kHz	3	

6.4.4 DISCUSSION

The rotational spectrum was measured for the tropolone – formic acid doubly hydrogen bonded dimer in the 4.7-9 GHz range using a pulsed-beam Fourier transform microwave spectrometer. It was expected that this doubly hydrogen bonded dimer would exhibit a concerted double proton tunneling motion as the dimer has a C_{2v}(M) symmetry resulting in a symmetric double well potential. This symmetry has been suggested as a requirement to observe the proton tunneling motion in the gas phase

and it has been present in numerous other hydrogen bonded dimers exhibiting observable tunneling splittings within the microwave spectra. When the doubly hydrogen bonded dimer exhibits proton tunneling, each rotational transition measured is split; the magnitude of this splitting ranges up to a few MHz for a-type transitions and can be hundreds of MHz for b-type transitions and is dependent on the barrier height and separation of the minima for the potential energy surface. When the splittings due to tunneling are observed, a vibration-rotation coupling analysis is performed to fit the spectra from the two tunneling states which are treated as two vibrational states. After measuring both a- and b-type transitions for this dimer, no splittings for any transition were observed indicating that this doubly hydrogen bonded dimer did not exhibit the concerted double proton tunneling motion.

To get an estimate of the barrier height in the potential energy surface to the transition state structure during the tunneling motion, the two tunneling protons were held fixed between the tropolone and formic acid molecules such that the distance of the proton between the two oxygens in each molecule was equivalent and a C2v symmetry was maintained. The energy of this structure was calculated using B3LYP/aug-cc-pVTZ and the difference in energy of the calculated equilibrium structure and this predicted transition state structure was about 15000 cm^{-1}. The distance that each proton was estimated to move during the tunneling process is about 0.8 Å, which is similar to what was found for the propiolic – formic acid dimer. The distance each proton moves was found by taking the transition state O-H bond lengths and subtracting the B3LYP optimized bond lengths and multiplying by 2 to get to the next tunneling state. The large barrier height between the two tunneling states may be why the

concerted double proton tunneling motion was not resolved for this doubly hydrogen bonded dimer as the estimated distance between the potential minima was similar to propiolic acid – formic acid in which the proton tunneling process was observed in the microwave spectra.

While measuring the rotational transitions from this dimer, the spectrum was congested with numerous other transitions that had significant intensity. From the optimization calculations, it was predicted that there are many low energy out of plane vibrational modes. The inertial defect calculated from the experimentally determined rotational constants is Δ = -1.46 amu Å^2. This is indicative of a planar structure with the magnitude not being significantly large, but because of the nonzero negative value, this is a confirmation that there is significant out of plane vibrational motion for this dimer. After measuring many transitions and attempting to make sense and assign the congested spectra, none of the additional transitions measured were able to be fit to an excited vibrational state. The additional transitions are most likely from other complexes formed with Formic Acid or water or a combination.

7. CONCLUDING REMARKS

Microwave spectroscopy is a very powerful technique that can be used to determine accurate gas phase molecular structure parameters as well as additional electronic structure information around nuclei that have a nuclear spin greater than one half. The importance of the structure of molecules is very well known to all types of chemists and this dissertation has studied and determined important structural parameters for a wide variety of different organic molecules and hydrogen bonded dimers. Not only are the determined structures in this dissertation important to understand the fundamental chemistry in certain systems, but these structures also supply theoretical chemists with excellent benchmarks on which to refine the theoretical models. Today in chemistry, all sub-disciplines within the field are relying more on the calculations to advance the research and understanding of chemical systems, so it is very critical to have theoretical models which accurately describe, for instance the hydrogen bonding in large systems such as in DNA or proteins and predict the quantum mechanical effects such as proton tunneling or other large amplitude motions that may occur. Even though the molecules discussed in this dissertation are considered small on most standards, the available theory still only does a fair job in accurately predicting the experimental spectra and molecular structure for the systems studied. The importance to refine theoretical models based on benchmarks of larger molecules, such as the ones discussed in this dissertation, is increasing to advance the understanding of chemical systems.

Chapter four focused on what is considered large molecules in the microwave spectroscopists' realm. These are cyclopropanecarboxylic acid and 1,2-

cyclohexanedione. Both of these molecules undergo some transformation to produce a new structure – cyclopropanecarboxylic acid is able to rotate the carboxylic acid group around the single bond with the cyclopropane ring, producing a high energy conformer which was observed and reported. In the case of 1,2-cyclohexanedione, the parent dione molecule was unable to be observed and it appeared that there was a complete tautomerization that occurred very readily under the experimental conditions to produce its monoenolic form, which was then studied further in a doubly hydrogen bonded dimer with formic acid, discussed in chapter 6. These two molecules provide great benchmarks for theoretical chemists and these microwave studies also provide some insight into the molecular dynamics within these molecules. Future work to study large molecules will depend on an efficient method to bring the samples into the gas phase, such as a laser ablation system. As these organic molecules become larger, the larger number intermolecular interactions decreases the vapor pressure and so the laser ablation source must be developed and implemented in the lab to study larger and more biologically relevant organic systems.

Much of the time, molecules may look very similar but produce very different microwave spectra. In the case of some molecules, if there is an atom that has a nuclear spin greater than one half, this produces a quadrupole moment around that nuclei which results in hyperfine interactions that give rise to the hyperfine structure within the microwave spectra. The analysis of the hyperfine structure is possible by measuring the high resolution microwave spectra obtained from the pulsed beam experiments used in this dissertation. This splitting caused by the electric quadrupole interactions within the molecules allows for additional electronic structure information to

be determined about the systems studied, directly providing details about the electric fields in these molecules. Chapter 5 studied a couple of molecules related to a number of different biochemical applications – maleimide and phthalimide. 4a,8a-azaboranaphthalene was also discussed in chapter 5 and because this molecule has two quadrupolar nuclei, there were increased splittings, providing a very rich spectrum with a nice hyperfine structure. From this analysis, the extent of the aromatic character was determined for this BN substituted naphthalene molecule by determining valence p-orbital occupations using a Townes-Dailey analysis. It was found that this molecule displays similar aromatic character when compared to other N-containing aromatic molecules, such as pyrrole. Future work on these BN substituted systems is important so this class of molecules can be characterized and implemented in chemical applications, such as hydrogen storage or other organic electronic devices such as LEDs. One such system that will need to be studied is the BN-cyclohexane molecule, which readily lost H_2 to produce a BN-cyclohexene molecule, a nice example of the hydrogen storage capabilities of such systems.

The pulsed-beam microwave technique utilized for all of the systems discussed in this dissertation lends itself as a great method to produce hydrogen bonded complexes that can be observed in the microwave spectrometer. Many hydrogen bonded complexes (dimer, trimers, etc.) are readily produced in the pulsed-beam and chapter 6 focused on the microwave spectra of doubly hydrogen bonded dimers. It has been shown in previous research that there is a concerted double proton tunneling motion between two molecules that make up a heterodimer if there is a $C_{2V}(M)$ symmetry with respect to the principal axes; this symmetry creates a symmetric double-

well potential that allows for the tunneling motion to be resolved. A couple of the central questions about these doubly hydrogen bonded dimers are: can the tunneling motion and splitting caused by this tunneling be observed in heterodimers that do not have the C_{2V}(M) symmetry? How asymmetric can the dimers be and proton tunneling still be observed? Cyclopropanecarboxylic acid – formic acid, the monoenolic tautomer of 1,2-cyclohexanedione – formic acid, maleiminde – formic acid, and tropolone – formic acid were all studied and detailed in this dissertation. The first three dimers do not have the C_{2V}(M) symmetry and no tunneling was observed in any of these dimers. It would be an extremely important result if splitting caused from this tunneling motion was observed for these asymmetric dimers as this has yet to be observed in such systems. The last dimer, formed with tropolone, does have the C_{2V}(M) symmetry about the a-principal axis, but splitting caused from the proton tunneling motion was not observed. This may have been due to a large barrier height in its potential energy surface as suggested by the calculations performed for this dimer, making the tunneling splitting very small and unable to be resolved in the spectra. The inertial defect calculated from the experimental parameters also indicated significant out of plane vibrations for the dimer, which may also quench the tunneling motion. Future work on hydrogen bonded complexes should be extended to larger systems containing more than two hydrogen bonds, additional dimers that exhibit the concerted proton tunneling (dimers with C_{2V}(M) symmetry), as well as organometallic doubly hydrogen bonded systems to observe the effects metal centers have on the structure of hydrogen bonding. Optimization calculations have been performed for the ferrocenecarboxylic acid – formic acid dimer (Fc-COOH – FA) and these optimized rotational constants are listed below in Table 7.1.

This will be the first hydrogen bonded dimer studied with an organometallic complex. Although this dimer is not expected to exhibit any proton tunneling due to its lack of C_{2v}(M) molecular symmetry, the large size and the effect of the metal center on the structure will be useful to use as a benchmark to advance theoretical computations, as the theoretical methods are less accurate for these organometallic systems. Additional systems which could be studied include other hydrogen bonded dimers that have the potential to exhibit proton tunneling (possessing the C_{2v}(M) symmetry): propiolic acid – nitric acid (PA – NA), benzoic acid – nitric acid (BzA – NA), and dimers with phenylpropiolic acid and formic (PPA – FA), propiolic acid (PPA – PA), or nitric acid (PPA – NA). The optimized rotational constants of these dimers are listed in Table 7.1.

Table 7.1. Optimized rotational constants for several doubly hydrogen bonded dimers using B3LYP/aug-cc-pVTZ.

Dimer	A /MHz	B /MHz	C /MHz
Fc-COOH – FA	893.465	253.520	233.789
PA – NA	6084.953	643.850	582.243
BzA – NA	2938.885	293.324	266.704
PPA – FA	2915.683	193.343	181.319
PPA – PA	2913.863	132.097	126.368
PPA – NA	2903.485	153.218	145.538

Many molecules and dimers were studied and discussed throughout this dissertation, but there is still much work to be done to advance research in the lab. A

laser ablation beam source needs to be constructed to allow for efficient vaporization of extremely low vapor pressure samples, such as organic molecules that have pharmaceutical implications or highly reactive, short-lived organometallic intermediates which can only be synthesized in the gas phase using ablation techniques. The ablation source will open the door for molecules that could not be put into the gas phase by the traditional method of heating the solenoid pulsed valve. Laser ablation could also be used to synthesize transient organometallic species, such as iron or chromium carbonyls with ligands such as butadiene, H_2 or N_2. Furthermore, the technique of chirped pulse microwave spectroscopy[130,131] will also be another invaluable tool in the lab to aid in the study of these complex molecules. Data from a large range of frequencies can be collected in a fraction of the time it takes the traditional pulsed beam spectrometer to scan the same range. Chirped pulsed microwave spectroscopy will allow strong rotational transitions to be found very quickly and the pulsed beam setup can be used to narrow in on the transitions to resolve the hyperfine splittings, allowing for more efficient use of the spectrometers and lab resources. Additionally, the chirped pulse microwave technique can also be used to probe chemical kinetics and dynamics,[132,133] opening the door for even more studies using microwave spectroscopy.

8. APPENDIX A

The following inputs are the examples of the formatted files needed to perform the least squares structure fitting routine, written in the programming language Fortran. The first file that follows is the input file, which introduces the rotational constants from each of the unique singly substituted isotopologues. The first line in this input file is the title, which can be anything the operator chooses. The following line is the indication of the number of varied parameters, rotational constants, and iterations the program is set to cycle through. The following line contains the initial values of the variable parameters used in the structure fitting routine. These variable parameters are set and allow the Cartesian coordinates of the molecule to be varied, which will provide a structure that calculates rotational constants closest to all of the experimentally determined values.

The second file following the input file is the file in which all the atomic masses and Cartesian coordinates are specified for the molecule or complex. This is the subroutine that cycles through the data, which are the sets of rotational constants determined for each of the isotopologues, and allows the designated coordinates to vary by the variable parameters assigned to the coordinates of the atoms. Following the adjustment of the coordinates within the structure, the rotational constants are calculated from the resulting structure and compared with the constants designated in the first file that were determined from the experimental spectra. The program will continue until the sum of squares for the data has the smallest value. The Cartesian coordinates and parameters are listed at the end of this file.

The final file is the output displaying the results of the sum of least squares fitting routine. The input file is reiterated and displayed in this file and the values of the varied

parameters in the structure fit are listed for each subsequent iteration of the program. At the end of the file are the final values of the varied parameters as well as all of the calculated rotational constants of the resulting best fit structure (lowest sum of squares), a comparison with the experimentally determined values listed in the input file (first file), and the differences between the values. The final values of the varied parameters must have errors smaller than the magnitudes of the parameters themselves, which indicates that these parameters have been determined. The second file and two additional Fortran programs (one is the main fitting program calling upon each subroutine and the other calculates rotational constants), which are not shown here, are compiled using g77 or a similar compiler which produces an executable for the specified information within the modified files. The program is initiated via UNIX commands using the standard input and output operators.

1,2-CDO FA DIMER

```
cdo-str1
2 12 1 18
 0.0001, 0.0001, 0.0001
2415.043869     0
543.6907091     0
451.6663339     0
2414.754335     0
530.9215857     0
442.8252644     0
2399.687491     0
542.9527044     0
450.6174626     0
2399.414692     0
530.2501681     0
441.8414584     0
0
0
1
```

```
0
0
0
0
0
0
```

```
INPUT
C  STRUCTURE FIT - BZZ1 - GSUB  - ftbz7.f
C  ** NEW FCNDP FOR
C  LINK - FTHCO, FITB1, ROTSUB, CFAC
          SUBROUTINE FCNDP(NP,ND,NV,NDATA,X1,P0,W,CM)
      IMPLICIT REAL*8(A-H,O-Z)
          DIMENSION X1(ND,NV),W(ND),P0(NP),CM(ND,NP)
          DIMENSION FO(21),ZO(21),YO(21),XO(21), PP(21)
      DIMENSION F(21),X(21),Y(21),Z(21)
      DIMENSION AN(21), BN(21), CN(21)
      NCYC = NCYC + 1
      DELTA = 1.0D-05
      N=21  !no atoms
      ISW=0
      SYM=2
C     NX = 0
CCC-----MASSES-----------
      DMO = 2.004245
      DMC = 1.0033544
      DMD = 1.006277
      MASSH = 1.007825
      FMC = 13.0033544
      FMD = 2.014102
      FMO = 15.994915
C**********ASSIGN MASSES TO STRUCTURE***************
      DO 17, I=1,7
          FO(I)=12.000000
 17   F(I)=12.000000
      DO 18, I=8,11
          FO(I) = 15.994915
 18   F(I) = 15.994915
      DO 19, I=12,21
          FO(I)=1.007825
 19   F(I)=1.007825
C---------------------------------------
C*********USE PARAMATERS TO OBTAIN GEOMETRY********
C        DO 21, I=1,3
```

```
C        PP(I)= 0.0
21      CONTINUE
       DO 50, I=1,3
         PP(I)=P0(I)
50      CONTINUE
         CALL GSUB(NP,PP,X,Y,Z)
         DO 20, L=1,N
          XO(L)=X(L)
          YO(L)=Y(L)
          ZO(L)=Z(L)
20      CONTINUE
C**********CYCLE THROUGH DATA SETS*****************************
         DO 100, NQ=1,13,3
        DO 60, L=1,N  !CYCLE THRU DATA SET
          F(L)=FO(L)
60       CONTINUE
       IF(NQ.EQ.4) F(12)=FMD
       IF(NQ.EQ.7) F(14)=FMD
       IF(NQ.EQ.10) F(12)=FMD
       IF(NQ.EQ.10) F(14)=FMD
C        IF(NQ.EQ.16) F(9)=FMO + DMO
C      IF(NQ.EQ.19) F(10)=FMO + DMO
      ISW=1
          IF(NCYC.EQ.9)ISW=1
      CALL ROTCONST(N,SYM,F,X,Y,Z,A,B,C,ASYMK,ISW)
          ISW=0
          W(NQ)=A
          W(NQ+1)=B
          W(NQ+2)=C
          DO 40, K=1,10
           PP(K)=P0(K)+DELTA  !MOVE ATOMS
           CALL GSUB(NP,PP,X,Y,Z)
        PP(K)=P0(K)
62       CONTINUE
       IF(NQ.EQ.4) F(12)=FMD
       IF(NQ.EQ.7) F(14)=FMD
       IF(NQ.EQ.10) F(12)=FMD
       IF(NQ.EQ.10) F(14)=FMD
C        IF(NQ.EQ.16) F(9)=FMO + DMO
C      IF(NQ.EQ.19) F(10)=FMO + DMO
           CALL ROTCONST(N,SYM,F,X,Y,Z,AN(K),BN(K),CN(K),ASYMK,ISW)
40       CONTINUE
          DO 70, L=1,N
           X(L)=XO(L)
           Y(L)=YO(L)
           Z(L)=ZO(L)
```

```
70       CONTINUE
         DO 30, K=1,10
          CM(NQ,K)=(AN(K)-A)/DELTA
          CM(NQ+1,K)=(BN(K)-B)/DELTA
          CM(NQ+2,K)=(CN(K)-C)/DELTA
30       CONTINUE
100     CONTINUE
      RETURN
      END

     SUBROUTINE GSUB(NP,PP,X,Y,Z)
     IMPLICIT REAL*8(A-H,O-Z)
     DIMENSION X(21),Y(21),Z(21),PP(21)
        DO 2, I1=1,21
 2    Z(I1) = 0.0
C      Z(1)=PP(1)
C##########################################
       XCM = PP(1) - 4.57
       YCM = PP(2) - 0.07792
       PHI = -0.1047
C       PHI = 0.000
C       THT = 0.05
C       GAM = PP(3)
C       EPP = 0.0
C       RH = 0.99
C       RHH= RH
Cnnnnnnnnnnnnnnnnnnnnnnnnnnnnnnnnnnnnnnnnnnnnnnnn
X(1) = 0.477797
Y(1) = 1.468200
Z(1) = 0.100057
X(2) = 0.799835
Y(2) = -1.411894
Z(2) = 0.257327
X(3) = 1.867282
Y(3) = 0.877927
Z(3) = 0.124422
X(4) = -0.631010
Y(4) = 0.695567
Z(4) = 0.036638
X(5) = 1.900146
Y(5) = -0.560958
Z(5) = -0.394258
X(6) = -0.547667
Y(6) = -0.777189
Z(6) = 0.030727
X(8) = -1.590489
```

```
Y(8) = -1.424860
Z(8) = -0.031032
X(9) = -1.878412
Y(9) = 1.209461
Z(9) = -0.102649
X(14) = -2.468724
Y(14) = 0.438582
Z(14) = -0.094158
X(15) = 0.358277
Y(15) = 2.549623
Z(15) = 0.075462
X(16) = 0.967381
Y(16) = -1.423781
Z(16) = 1.344453
X(17) = 0.776653
Y(17) = -2.449404
Z(17) = -0.088033
X(18) = 2.575221
Y(18) = 1.498641
Z(18) = -0.436158
X(19) = 2.200818
Y(19) = 0.897604
Z(19) = 1.173445
X(20) = 1.725406
Y(20) = -0.552873
Z(20) = -1.477181
X(21) = 2.882578
Y(21) = -1.012511
Z(21) = -0.220758
X(7) = (-0.408196*DCOS(PHI) + 0.084999*DSIN(PHI)) + XCM !FA
Y(7) = (-0.408196*DSIN(PHI) + 0.084999*DCOS(PHI)) + YCM
Z(7) = 0.000579
X(10) = (0.121604*DCOS(PHI) - 1.132562*DSIN(PHI)) + XCM !FA
Y(10) = (0.121604*DSIN(PHI) - 1.132562*DCOS(PHI)) + YCM
Z(10) = -0.001207
X(11) = (0.210238*DCOS(PHI) + 1.131568*DSIN(PHI)) + XCM !FA
Y(11) = (0.210238*DSIN(PHI) + 1.131568*DCOS(PHI)) + YCM
Z(11) = -0.000458
X(12) = (-1.503153*DCOS(PHI) + 0.032243*DSIN(PHI)) + XCM !FA
Y(12) = (-1.503153*DSIN(PHI) + 0.032243*DCOS(PHI)) + YCM
Z(12) = 0.005667
X(13) = (1.096936*DCOS(PHI) - 1.028534*DSIN(PHI)) + XCM !FA
Y(13) = (1.096936*DSIN(PHI) - 1.028534*DCOS(PHI)) + YCM
Z(13) = 0.013845
C-------------------------------
      RETURN
```

```
      END
```

```
OUTPUTFILE
DATE =  4- 23- 2014
 cdo-str1                          20140423
         2    12     1    18
            0.0001
            0.0001

       2415.0439   0.0
        543.6907   0.0
        451.6663   0.0
       2414.7543   0.0
        530.9216   0.0
        442.8253   0.0
       2399.6875   0.0
        542.9527   0.0
        450.6175   0.0
       2399.4147   0.0
        530.2502   0.0
        441.8415   0.0

 GIVE: 1 - TO ENTER SD(Y), 1 - TO SUPP. STAT. OF PARAMS.
 1 - TO SUPP. STAT.(Y), 1 - TO SUPP. DER., 1 - TO SUPP. CORR. MAT.

   IV, NOVP, NOVC, NOCOUT, NOCORR
         0     0     1     0     0
 CYCLE NUMBER    1
           P0                  P1                  P1 - P0
    0.10000000000D-03    0.22277235720D-01    0.22177235720D-01
    0.10000000000D-03   -0.28893702439D+01   -0.28894702439D+01
 CYCLE NUMBER    2
           P0                  P1                  P1 - P0
    0.22277235720D-01    0.13991872691D+00    0.11764149119D+00
   -0.28893702439D+01   -0.12972614552D+01    0.15921087887D+01
 CYCLE NUMBER    3
           P0                  P1                  P1 - P0
    0.13991872691D+00    0.22073231777D+00    0.80813590851D-01
   -0.12972614552D+01   -0.14209497996D+01   -0.12368834439D+00
 CYCLE NUMBER    4
           P0                  P1                  P1 - P0
    0.22073231777D+00    0.22103865096D+00    0.30633319485D-03
   -0.14209497996D+01   -0.14163467322D+01    0.46030674394D-02
 CYCLE NUMBER    5
```

```
          P0                P1              P1 - P0
  0.22103865096D+00  0.22103930990D+00  0.65893427087D-06
 -0.14163467322D+01 -0.14163449076D+01  0.18245971096D-05
CYCLE NUMBER   6
          P0                P1              P1 - P0
  0.22103930990D+00  0.22103930967D+00 -0.22248786630D-09
 -0.14163449076D+01 -0.14163449075D+01  0.12962591226D-09
CYCLE NUMBER   7
          P0                P1              P1 - P0
  0.22103930967D+00  0.22103930967D+00  0.62811837494D-12
 -0.14163449075D+01 -0.14163449075D+01 -0.16524500184D-11
CYCLE NUMBER   8
          P0                P1              P1 - P0
  0.22103930967D+00  0.22103930968D+00  0.22115728228D-11
 -0.14163449075D+01 -0.14163449075D+01 -0.38187188125D-11
CYCLE NUMBER   9
          P0                P1              P1 - P0
  0.22103930968D+00  0.22103930967D+00 -0.26123210449D-11
 -0.14163449075D+01 -0.14163449075D+01  0.57538844699D-11
CYCLE NUMBER  10
          P0                P1              P1 - P0
  0.22103930967D+00  0.22103930967D+00 -0.10168986130D-11
 -0.14163449075D+01 -0.14163449075D+01  0.54184644716D-11
CYCLE NUMBER  11
          P0                P1              P1 - P0
  0.22103930967D+00  0.22103930968D+00  0.58627913436D-11
 -0.14163449075D+01 -0.14163449075D+01 -0.15900929920D-10
CYCLE NUMBER  12
          P0                P1              P1 - P0
  0.22103930968D+00  0.22103930967D+00 -0.35611516124D-11
 -0.14163449075D+01 -0.14163449075D+01  0.11209571425D-10
CYCLE NUMBER  13
          P0                P1              P1 - P0
  0.22103930967D+00  0.22103930967D+00 -0.17245218625D-11
 -0.14163449075D+01 -0.14163449075D+01 -0.13708987052D-11
CYCLE NUMBER  14
          P0                P1              P1 - P0
  0.22103930967D+00  0.22103930967D+00 -0.10537043629D-11
 -0.14163449075D+01 -0.14163449075D+01  0.24392305692D-11
CYCLE NUMBER  15
          P0                P1              P1 - P0
  0.22103930967D+00  0.22103930967D+00 -0.32226538526D-12
 -0.14163449075D+01 -0.14163449075D+01  0.45376270377D-11
CYCLE NUMBER  16
          P0                P1              P1 - P0
  0.22103930967D+00  0.22103930967D+00 -0.48938464829D-12
```

```
  -0.14163449075D+01   -0.14163449075D+01    0.88048758532D-12
 CYCLE NUMBER  17
         P0                P1              P1 - P0
    0.22103930967D+00    0.22103930967D+00    0.33435425643D-11
   -0.14163449075D+01   -0.14163449075D+01   -0.11010899233D-10
 CYCLE NUMBER  18
         P0                P1              P1 - P0
    0.22103930967D+00    0.22103930967D+00   -0.31614138923D-11
   -0.14163449075D+01   -0.14163449074D+01    0.13488119104D-10


 *** FINAL VALUES OF THE PARAMETERS AND STANDARD DEVIATIONS ***

          I          P0(I)-PARAMETER        S.D.(PARAM)
          1          0.22103930967D+00    0.31247004707D-02
          2         -0.14163449074D+01    0.56979328075D-02


        YMEAS             YCALC              DEV.
      2415.0439         2417.1848          -2.1410
       543.6907          543.7113          -0.0206
       451.6663          450.8779           0.7884
      2414.7543         2413.7931           0.9613
       530.9216          531.4466          -0.5250
       442.8253          442.2975           0.5278
      2399.6875         2400.6990           -1.0115
       542.9527          543.2486          -0.2959
       450.6175          449.9907           0.6267
      2399.4147         2397.5249            1.8897
       530.2502          531.0291          -0.7789
       441.8415          441.4666           0.3749

  SUM OF SQUARED RESIDUES =  0.12505837899D+02

  STANDARD DEVIATION FOR FIT =  0.11182950370D+01


 THE VALUES IN THE FINAL MATRIX OF DERIVATIVES:
0
  -0.261409D+02   0.827665D+02
   0.167262D+03   0.528275D+02
   0.114112D+03   0.392077D+02
  -0.267200D+02   0.856229D+02
   0.163463D+03   0.510108D+02
   0.112324D+03   0.382072D+02
  -0.295460D+02   0.940284D+02
```

```
  0.166761D+03   0.524003D+02
  0.113383D+03   0.392573D+02
 -0.300366D+02   0.967196D+02
  0.162999D+03   0.506198D+02
  0.111635D+03   0.382642D+02
0
 VARIANCE-COVARIANCE MATRIX OF PARAMETERS
0
  0.780736D-05  -0.660423D-05
 -0.660423D-05   0.259610D-04
0
 CORRELATION COEFFICIENT MATRIX OF PARAMETERS
0
  0.100000D+01  -0.463884D+00
 -0.463884D+00   0.100000D+01
0
 TYPE 1 IF THERE ARE MORE DATA TO BE FITTED:

        0
```

The following is the input file needed of the molecular structure Cartesian coordinates (or Z-matrix) of the molecular species of interest (shown are the coordinates of ferrocenecarboxylic acid) to start an optimization computation in the Gaussian program. The first two lines in the file are where the memory and number of processors are specified. The third line is where the keywords of the computation are specified (for example if it is an optimization, a scan of the potential energy surface by rotating a bond or whether or not vibrational frequencies are calculated, then these keywords are opt, scan, and freq – the keywords can be found on the Gaussian website and are described in great detail). This line is also where the computational method and basis set of the computation are chosen, in this case CCSD is the method with a basis set of cc-pVDZ (these methods and basis set keywords are also given in the Gaussian documentation with great detail). The fifth line is the title line. The following line, the 0

and 1 represent the charge and multiplicity of the molecular species of interest, in this case the charge is zero and the molecule is in a singlet state with zero unpaired electrons. Following these specifications, the molecular coordinates or Z-matrix of the molecular are written.

```
%Mem=2GB
%NProcs=8
#P CCSD/cc-pVDZ opt NoSymm output=pickett

FcA nosym using cc-pVDZ/cc-pVDZ

0 1
C                -1.385554    0.551631    0.024903
C                -0.769884    1.161139    1.162709
C                -0.806665    1.127488   -1.151147
H                -0.994594    0.923197    2.187902
C                 0.171356    2.106648    0.689604
H                -1.058517    0.867689   -2.164422
C                 0.148857    2.086393   -0.735071
H                 0.810775    2.720587    1.301502
H                 0.767365    2.683207   -1.384470
C                 0.981888   -1.857185   -0.002714
H                0.199479   -2.597696   -0.005868
C                 1.566841   -1.268926    1.152034
C                 1.579821   -1.268048   -1.150498
H                 1.310051   -1.492225    2.173825
C                 2.528429   -0.314663    0.717658
H                 1.337173   -1.491411   -2.175785
C                 2.536433   -0.313847   -0.704690
H                 3.129623    0.312978    1.353924
H                 3.145012    0.314152   -1.333496
Fe                 0.648003    0.194722   -0.003301
C                -2.410875   -0.493067    0.101862
O                -2.870971   -0.950745    1.121884
O                -2.825705   -0.910106   -1.124867
H                -3.502503   -1.584009   -0.968624
```

The following is the PBS script file needed to submit Gaussian jobs into the queueing system that will run jobs on the high performance computing system at the University of Arizona. The file shown is to specifically run jobs on the ocelote system. This script file where the input file is specified and the memory and time needed to run the computation are designated. Lines preceding with ### are commented out of the file and will not be read by the system. Comments have been left throughout the script file to indicate what each line represents.

```
#!/bin/csh
### Refer to docs.hpc.arizona.edu website for more detailed system documentation
### Set the job name
#PBS -N FcCOOH
### Request an email be sent when computation job begins and ends
#PBS -m bea
### Specify the email address to use for these notifications
#PBS -M pejlovas@email.arizona.edu
### Specify the PI (principle investigator) of the research group for the computation
#PBS -W group_list=kukolich
### Set the queue for the computation on windfall or standard systems (adjust with ###
### and # to comment out and read which system to run)
#PBS -q standard
###PBS -q windfall
### Set the number of cores/cpus and memory that will be used for the job
### When specifying memory, request less than 2GB memory per ncpus for standard
### node. Some memory needs to be reserved for the Linux system processes
#PBS -l select=1:ncpus=28:mem=168gb:pcmem=6gb
#PBS -l place=pack:shared
#PBS -l pvmem=23gb
#PBS -l walltime=100:00:00
#PBS -l cput=1000:00:00
### Specify "wall clock time" required for the computation, hhh:mm:ss
### Specify total cpu time required for the computation, hhh:mm:ss (total cputime =
###walltime * ncpus)
### Load required modules/libraries if needed and se "module avail" command to list all
###available modules
module load gaussian/g09-D.01
module list
### Your jobname.o file will show the path to the execution directory
```

```
echo $GAUSS_EXEDIR
### set your scratch space file location
set SCR = /rsgrps/kukolich/
setenv GAUSS_ARCDIR    $SCR
setenv GAUSS_SCRDIR    $SCR
### Be sure the following path is your execution directory
### The last item on the next line is the input file for the Gaussian computation
###(FcCOOH.inp)
date
time $GAUSS_EXEDIR/g09 FcCOOH.inp
date

echo exit status = $?
```

The following are the various files needed to run Dr. Herb Pickett's SPCAT and SPFIT programs. The first file listed is the .int file and is needed to run SPCAT. This is the file where the calculated dipole moment components (from the Gaussian optimization) and value of the rotational partition function (shown as 1527.9640) are specified, depending on what temperature is chosen (right most number in the second lines, shown as 1.0 K). The rotational partition function is calculated using the rotational constants designated in the .var file and can be adjusted once the program is initiated and ran for the first time. The partition function and dipole moment component values are needed in order for the intensities of each of the transitions to be predicted. The second file is called the .var file and this file is also needed to run SPCAT. This is the file where the optimized values of the rotational constants are specified, as well as additional information such as the nuclear spin of quadrupolar nuclei in the molecule. The input of these rotational constants can be provided by the Gaussian optimization if the keyword "output=Pickett" is designated on the keyword line, described previously. The errors listed for each of the constants specified in the .var file are typically set very small (10^{-30}) as these are calculated values and are shown as zero if the input is taken

from the Gaussian optimization. After performing the microwave fits of the measured spectra (using SPFIT) the .var file is updated with the new updated values for the constants, as well as errors, so the transitions can be predicted more accurately if they are assigned correctly.

The third file listed is needed for SPFIT and this is the .par file. This has the same formatting as the .var file, but now the number of parameters to be fit needs to be specified as well as how many rotational transitions are to be used in the fit. The errors for each of the specified constants are typically set very large (10^{30}) when the parameter is set to be fit from the data. The remaining file needed to run SPFIT is the .lin file. This file is where the quantum number assignments for each rotational energy level are assigned. There are three .lin files shown for reference: the first shows the formatting of the quantum numbers when there are two quadrupolar nuclei, the second file is when there is only one quadrupolar nucleus, and the last is when there are no quadrupolar nuclei present. The formatting for all of these files is essential to run the programs correctly.

```
BNnaphthalene
0112 00001 1527.9640  0  10   -8.0  -8.0  11.0  1.0
   2     1.6   /b dipole
```

```
BNnaphthalene 11B                                Fri JThu Nov 12 09:36:56 2015
  8   73   50    0    0.0000E+000    1.0000E+016    1.0000E+000 1.0000000000
'a'   34    1    0   15    0    2    1    1         0    1
       10000  3.042712752532214E+003 4.82859920E-004 /  A  /
       20000  1.202706572964331E+003 3.86452065E-004 /  B  /
       30000  8.622201276096232E+002 4.04395535E-004 /  C  /
   110010000 -3.922079665937628E+000 8.38534541E-003 /  (17 B-11
   110040000 -9.068881718801244E-001 2.76689206E-003 /  (17 B-11
```

220010000 2.578113459404607E+000 6.85316189E-003 / (18 N-14
220040000 -1.184730921187949E-001 1.93472338E-003 / (18 N-14
200 -5.647561432827691E-005 1.07823178E-005 / -DJ

BNnaphthalene 11B Fri JThu Nov 12 09:36:56 2015
8 73 50 0 0.0000E+000 1.0000E+016 1.0000E+000 1.0000000000
'a' 34 1 0 15 0 2 1 1 0 1
10000 3.042712752532214E+003 1.00000000E+037 / A /
20000 1.202706572964331E+003 1.00000000E+037 / B /
30000 8.622201276096232E+002 1.00000000E+037 / C /
110010000 -3.922079665937628E+000 1.00000000E+037 / (17 B-11
110040000 -9.068881718801244E-001 1.00000000E+037 / (17 B-11
220010000 2.578113459404607E+000 1.00000000E+037 / (18 N-14
220040000 -1.184730921187949E-001 1.00000000E+037 / (18 N-14
200 -5.647561432827691E-005 4.33624533E+036 / -DJ

Line file from BN-naphthalene (2 quadrupolar nuclei)

1	1	0	3	2	1	0	1	1	1	2179.7240	0.005
1	1	0	1	1	1	0	1	3	2	2179.7813	0.005
1	1	0	1	1	1	0	1	2	1	2179.9329	0.005
1	1	0	3	2	1	0	1	3	3	2179.9571	0.005
1	1	0	2	3	1	0	1	1	2	2180.2341	0.005
1	1	0	3	4	1	0	1	3	4	2180.3198	0.005
1	1	0	3	4	1	0	1	2	3	2180.8807	0.005
1	1	0	2	3	1	0	1	3	2	2181.1696	0.005
2	0	2	2	1	1	1	1	3	2	2246.0699	0.005
2	0	2	3	4	1	1	1	3	4	2246.1470	0.005
2	0	2	2	3	1	1	1	2	3	2246.6648	0.005
2	0	2	2	2	1	1	1	1	1	2246.7358	0.005
2	0	2	4	4	1	1	1	3	4	2247.3151	0.005
2	0	2	1	2	1	1	1	1	1	2247.4661	0.005
2	1	1	4	3	2	0	2	1	2	2562.9129	0.005
2	1	1	2	3	2	0	2	1	2	2563.1467	0.005
2	1	1	2	3	2	0	2	4	4	2563.3627	0.005
2	1	1	3	4	2	0	2	4	5	2563.9003	0.005
2	1	1	3	2	2	0	2	2	3	2563.9272	0.005
2	1	1	3	2	2	0	2	2	1	2563.9517	0.005
2	1	1	1	2	2	0	2	2	3	2563.9928	0.005
2	1	1	3	3	2	0	2	4	3	2564.0394	0.005
2	1	1	3	4	2	0	2	2	3	2564.1451	0.005
2	1	1	2	3	2	0	2	3	2	2564.7382	0.005
2	1	1	3	3	2	0	2	3	3	2564.8827	0.005

1	1	1	3	3	0	0	0	2	2	3904.6352	0.005
1	1	1	2	2	0	0	0	2	3	3904.6973	0.005
1	1	1	2	3	0	0	0	2	2	3904.9352	0.005
1	1	1	3	4	0	0	0	2	3	3905.0188	0.005
1	1	1	3	2	0	0	0	2	3	3905.4868	0.005
3	0	3	3	2	2	1	2	2	1	4484.1528	0.005
3	0	3	4	5	2	1	2	3	4	4484.4399	0.005
3	0	3	5	4	2	1	2	4	3	4484.5142	0.005
3	0	3	4	4	2	1	2	3	3	4484.5903	0.005
3	0	3	2	2	2	1	2	1	1	4484.6792	0.005
3	0	3	3	2	2	1	2	3	2	4484.7446	0.005
5	2	3	4	4	5	1	4	4	4	5011.6021	0.005
5	2	3	6	7	5	1	4	7	8	5011.7275	0.005
5	2	3	6	5	5	1	4	7	6	5011.7778	0.005
3	2	1	2	2	3	1	2	2	3	5248.8096	0.005
3	2	1	4	4	3	1	2	4	3	5249.3145	0.005
6	2	4	5	4	6	1	5	5	4	5302.4146	0.005
6	2	4	8	9	6	1	5	8	9	5302.4692	0.005
2	2	0	1	2	2	1	1	2	1	5562.0176	0.005
2	2	0	4	4	2	1	1	3	3	5562.1392	0.005
2	2	0	1	1	2	1	1	1	2	5562.2998	0.005
2	2	0	1	1	2	1	1	3	2	5562.3691	0.005
2	2	0	4	3	2	1	1	3	3	5562.4224	0.005
2	2	0	1	1	2	1	1	1	1	5562.4722	0.005
2	2	0	4	4	2	1	1	4	3	5562.7515	0.005
2	2	0	2	1	2	1	1	2	1	5563.0088	0.005
2	1	2	2	3	1	0	1	3	2	5629.4268	0.005
2	1	2	5	4	1	0	1	3	4	5629.5298	0.005
2	1	2	4	4	1	0	1	3	4	5629.6841	0.005
3	2	2	2	3	3	1	3	2	2	7076.6250	0.005
3	2	2	2	3	3	1	3	2	3	7076.8428	0.005
3	1	3	3	3	2	0	2	2	3	7201.3242	0.005
3	1	3	2	2	2	0	2	1	2	7201.3672	0.005
4	2	3	4	5	4	1	4	3	4	7800.8184	0.005
4	2	3	4	3	4	1	4	3	2	7800.9487	0.005
4	1	4	4	4	3	0	3	5	4	8675.9053	0.005
4	1	4	3	2	3	0	3	2	1	8676.3770	0.005
5	1	5	5	5	4	0	4	4	4	10128.1406	0.005
5	1	5	6	5	4	0	4	5	4	10128.2158	0.005
5	1	5	4	4	4	0	4	3	4	10128.6934	0.005
5	1	5	7	6	4	0	4	5	5	10128.7666	0.005
5	3	3	6	7	5	2	4	7	6	10397.6445	0.005
5	3	3	4	4	5	2	4	4	3	10397.6816	0.005
5	3	3	6	6	5	2	4	6	6	10397.8994	0.005
5	3	3	7	6	5	2	4	5	6	10397.9766	0.005
5	3	3	5	4	5	2	4	5	4	10398.0127	0.005

5	3	3	5	5	5	2	4	5	6	10398.0547	0.005
5	3	3	6	7	5	2	4	6	7	10398.0947	0.005

Line file from maleimide (one quadrupolar nucleus)

1	1	0	1	1	0	1	1	5059.7046	0.005
1	1	0	1	1	0	1	2	5060.1914	0.005
1	1	0	2	1	0	1	1	5060.7686	0.005
1	1	0	1	1	0	1	0	5060.9170	0.005
1	1	0	2	1	0	1	2	5061.2568	0.005
1	1	0	0	1	0	1	1	5062.3672	0.005
2	1	1	2	2	0	2	2	5725.5610	0.005
2	1	1	2	2	0	2	3	5726.1904	0.005
2	1	1	3	2	0	2	3	5726.8076	0.005
2	1	1	1	2	0	2	1	5727.4976	0.005
3	1	2	3	3	0	3	3	6827.3027	0.005
3	1	2	4	3	0	3	3	6827.7744	0.005
3	1	2	2	3	0	3	3	6827.9375	0.005
3	1	2	3	3	0	3	4	6828.1113	0.005
3	1	2	3	3	0	3	2	6828.4028	0.005
3	1	2	4	3	0	3	4	6828.5864	0.005
3	1	2	2	3	0	3	2	6829.0381	0.005
3	0	3	2	2	1	2	2	8214.5664	0.005
3	0	3	4	2	1	2	3	8215.9912	0.005
3	0	3	2	2	1	2	1	8216.3369	0.005
3	0	3	3	2	1	2	3	8216.7988	0.005
4	1	3	4	4	0	4	4	8466.0400	0.005
4	1	3	5	4	0	4	5	8467.4316	0.005
4	1	3	3	4	0	4	3	8467.7949	0.005
1	1	1	0	0	0	0	1	8568.6826	0.005
1	1	1	2	0	0	0	1	8569.5527	0.005
1	1	1	1	0	0	0	1	8570.1250	0.005
5	2	3	5	5	1	4	5	11862.7266	0.005
5	2	3	6	5	1	4	6	11862.7617	0.005
4	0	4	4	3	1	3	3	12726.9668	0.005
4	0	4	5	3	1	3	4	12727.2832	0.005
4	0	4	3	3	1	3	2	12727.4932	0.005
4	2	2	3	4	1	3	3	12191.2578	0.005
4	2	2	5	4	1	3	5	12191.2920	0.005

Line file from cyclopropanecarboxylic acid (no quadrupolar nuc)

1	0	1	0	0	0	5204.936	0.005
2	1	2	1	1	1	10035.056	0.005

2 0 2 1 0 1	10388.154	0.005
2 1 1 1 1 0	10784.638	0.005
1 1 1 0 0 0	9867.375	0.005
1 1 0 1 0 1	5037.232	0.005
2 1 1 2 0 2	5433.717	0.005
3 1 2 3 0 3	6068.218	0.005
2 0 2 1 1 1	5725.706	0.005
4 1 3 4 0 4	6984.654	0.005

---

9. WORKS CITED

1. Legon, A.C. Pulsed-Nozzle, Fourier-Transform Microwave Spectroscopy of Weakly Bound Dimers. *Ann. Rev. Phys. Chem.* 34 (**1983**) 275-300.

2. P. R. Bunker and P. Jensen, Molecular Symmetry and Spectroscopy, 2nd ed., NRC Research Press, Ottawa, **2006**.

3. R. E. Bumgarner and S. G. Kukolich. Microwave Spectra and Structure of HI-HF Complexes. *J. Chem Phys.* 86 (**1987**) 1083.

4. B. S. Tackett, C. Karunatilaka, A. M. Daly, and S. G. Kukolich. Microwave Spectra and Gas-Phase Structural Parameters of Bis(η^5-cyclopentadienyl)tungsten Dihydride. *Organometallics* 26/8 (**2007**) 2070-2076. http://dx.doi.org/10.1021/om061027f

5. Daly, A. M. Gas Phase Structures and Molecular Constants of Dimers and Molecules Determined Using Microwave Spectroscopy. Ph.D. Dissertation. The University of Arizona **2010**.

6. Gordy, W.; Cook, R. L. *Microwave Molecular Spectra*; Chemical Applications of Spectroscopy IX; John Wiley & Son Inc.: New York, **1968** and **1970**.

7. H.W. Kroto. Molecular Rotation Spectra. Dover Publications, Inc. New York, 1992.

8. H.M. Pickett, *J. Mol. Spectrosc*. 148 (**1991**) 371.
http://spec.jpl.nasa.gov/ftp/pub/calpgm/spinv.html

9. R. A. Fiesner, R. B. Murphy, M. D. Beachy, M. N. Ringualda, W. T. Pllard, B.D. Dunietz and Y. Cao J.Phys. Chem. A. 18 (**1999**) 1913.

10. Frisch, M.J.; Trucks, G.W.; Schlegel, H.B.; Scuseria, G.E.; Robb, M.A.; Cheeseman, J.R.; Scalmani, G.; Barone, V.; Mennucci, B.; Petersson, G.A., et al. Gaussian 09, Revision A.02, Gaussian, Inc., Wallingford CT, **2009**.

11. Kimura, T.; Hattori, Y.; Momochi, H.; Nakaya, N.; Satoh, T. *Synlett*. 24 (**2013**) 483-486.

12. Duncombe, W.G.; Rising, T.J. *Biochem. J.* 109 (**1968**) 449-455.

13. Aratani, T. *Pure & Appl. Chem.* 57/12 (**1985**) 1839-1844.

14. Hirao, T.; Harano, Y.; Yamana, Y.; Hamada, Y. *Bull. Chem. Soc. Jpn.* 59 (**1986**) 1341-1347.

15. H.M. Badawi. A.A. Al-Saadi. M.A.A. Al-Khaldi. S.A. Al-Abbad. Z.H.A. Al-Sunaidi. *Spectrochimica Acta Part A.* 71 (**2008**) 1540–1546.

16. de Boer, J. S. A. M.; Stam, C.H. *Recueil des Travaux Chimiques des Pays-Bas.* 111/9 (**1992**) 407-410.

17. Maillols, J.; Tabacik, V.; Sportouch, S. *Journal of Molecular Structure.* 32 (**1976**) 173-190.

18. Marstokk, K. M.; Møllendal, H.; Samdal, S. *Acta Chemica Scandinavica.* 45 (**1991**) 37-45.

19. A.M. Pejlovas, K. Li, S.G. Kukolich. Microwave measurements of cyclopropanecarboxylic acid and –OD isotopologue. *Journal of Molecular Spectroscopy.* 313 (**2015**) 1-3.

20. A.M. Pejlovas, W.Lin, and S.G. Kukolich. Microwave Spectrum for a Second Higher Energy Conformer of Cyclopropanecarboxylic Acid and Determination of the Gas Phase Structure of the Ground State. *J. Phys. Chem. A*. 119/39 (**2015**) 10016-10021.

21. Z. Kisiel , <http://www.ifpan.edu.pl/~kisiel/struct/struct.htm#kra>

22. Antoniotti, S.; Duñach, E. Studies on the Catalytic Oxidation of Epoxides to α-diketones by Bi(0)/O2 in DMSO. *J. of Mol. Catal. A: Chem*. 208 (**2004**) 135-145.

23. Antoniotti, S.; Duñach, E. Novel and Catalytic Oxidation of Internal Epoxides to α-diketones. *Chem. Commun.* 24 (**2001**) 2566-2567.

24. Simpkins, C.M.; Hunt, D.A. The Michael Addition of 1,2-cyclohexanedione to β-nitrostyrenes (I): The Synthesis of 3-aryl-5,6-dihydrobenzofuran-7(4H)-ones. *Tetrahedron Lett.* 54 (**2013**) 3371-3373.

25. Wolt, J., Flavoring Foodstuffs with a Mixture Containing 1,2-Cyclohexanedione. US Patent 3,875,307. April 1, **1975**.

26. Montazeri, N.; Oliveira, A.C.M.; Himelbloom, B.H.; Leigh, M.B.; Crapo, C.A. Chemical Characterization of Commercial Liquid Smoke Products. *Food Sci. and Nutr*. 1 (**2013**) 102-115.

27. Patthy, L.; Smith, E.L. Reversible Modification of Arginine Residues: Application to Sequence Studies by Restriction of Tryptic Hydrolysis to Lysie Residues. *J. of Biol. Chem*. 250 (**1975**) 557-564.

28. Heiland, I.; Wittmann-Liebold, B. Amino Acid Sequence of the Ribosomal Protein L21 of Escherichia Coli. *Biochemistry.I* 18 (**1979**) 4605-4612.

29. De Borger, L.; Anteunis, M.; Lammens, H.; Verzele, M. 1,2-Cyclohexanedione. *Bull. Soc. Chim.* 73 (**1964**) 73-80.

30. Shen, Q.; Traetteberg, M.; Samdal, S. The Molecular Structure of Gaseous 1,2-Cyclohexanedione. *J. of Mol. Struct*. 923 (**2009**) 94-97.

31. Samanta, A.K.; Pandey, P.; Bandyopadhyay, B.; Chakraborty, T. Keto-enol Tautomers of 1,2-Cyclohexanedione in Solid, Liquid, Vapour and a Cold Inert Gas Matrix: Infrared Spectroscopy and Quantum Chemistry Calculation. *J. of Mol. Struct*. 963 (**2010**) 234–239.

32. Bumgarner, R.E. Microwave Spectroscopy of Weakly Bound Complexes and High Resolution Infrared Studies of the v_6 and v_8 Bands of Formic Acid. Ph.D. Dissertation. Department of Chemistry, University of Arizona. (**1988**) 221-227.

33. Frogner, M.; Johnson, R. D.; Hedberg, L.; Hedberg, K., *J. Phys. Chem A.* 117 (**2013**) 11101-11106

34. Blanco, Susana; Lesarri, Alberto; Lopez, Juan C.; Alonso, Jose L. *J. Am. Chem. Soc.* 126 (**2004**) 11675.

35. S.G. Kukolich, M. Sun, A.M. Daly, W. Luo, L.N. Zakharov, S. Liu. Identification and characterization of 1,2-BN cyclohexene using microwave spectroscopy. *Chem. Phys. Lett.* 639 (**2015**) 88-92. http://dx.doi.org/10.1016/j.cplett.2015.09.009

36. W. Gordy, and R.L. Cook, Microwave Molecular Spectra, Wiley-Interscience, New York, **1984**.

37. Lauer, M.H. Drekener, R.L. Correia, C.R. and Gehlen, M.H. *Photochem. Photobiol. Sci.* 13 (**2014**) 859

38. Benkova, B. *Journal of Chromatography B.* 870/1 (**2008**) 103-108.

39. Thale, P.B. Borase, P.N. and Shankarling, G.S. *RSC Advances,* 4/103 (**2014**) 59454-59461.

40. Osby, J. O. Martin, M. G. and Ganem, B. *Tetrahedron Lett.* 25 (**1984**) 2093–2096.

41. Mathur, P. Joshi, R.K. Rai, D.K. Jhaa. B. and Mobinb, S.M. *Dalton Trans.* 41 (**2012**) 5045.

42. Lin, K.F. Lin, J.S. Cheng, C.H. *Polymer.* 37/21 (**1996**) 4729–4737.

43. Matheus, M. Sirqueira, A.S. and Soares, B.G. *Polymer Testing.* 29/7 (**2010**) 840-848.

44. Birkinshaw, J. H. Kalyanpur, M.G. and Stickings, C.E. *Biochem. J.* 86 (**1963**) 237–243.

45. Roberts, M.J. Bentley, M.J. and Harris, J. M. *Advanced drug delivery reviews.* 64 (**2012**) 116-127.

46. Moore, E. and Pickelman, D. *Industrial & Engineering Chemistry Product Research and Development.* 25/4 (**1986**) 603-609.

47. Rinkes, I.J. *Rec. Trav. Chim*. 48 (**1929**) 961.

48. Taherpour, A. Abramian, A. Kardanyazd, H. *Asian Journal of Chemistry* 18/3 (**2006**) 2401-2403.

49. Baltá-Calleja, F. J. Ramos, J. G. and Barrales-Rienda, J. M. *Kolloid-Zeitschrift und Zeitschrift für Polymere.* 250/5 (**1972**) 474-481.

50. Harsányi, L. Vajda, E. and Hargittai, I. *Journal of molecular structure.* 129/3 (**1985**) 315-320.

51. T. Oka. *Journal of Molecular Structure.* 352/353 (**1995**) 225-233.

52. M.A. Motaleb, L.Y. Abdel-Ghaney, H.M. Abdel-Bary, H.A. Shamsel-Din. *J. Radioanal. Nucl. Chem.* 307/1 (**2015**) 363-372. DOI:10.1007/s10967-015-4140-3.

53. Kishida, K. Aoyama, A. Hasimoto, Y. Miyachi, H. *Chem. Pharm. Bull.* 58. 11 (**2010**) 1525-1528.

54. T. W. Green, P. G. M. Wuts, “Protective Groups in Organic Synthesis,” Wiley-Interscience, New York. (**1999**) 564-566, 740-743.

55. L.J. Winters and W.E. McEwen. *Tetrahedron*. 19 (**1963**) 49-56.

56. W. A. Noyes and P. K. Porter. *Org. Syn*. 2 (**1922**) 75.

57. M.A.V. Ribeiro da Silva. Claudia P.F. Santos. M.J.S. Monte. C.A.D. Sousa. *J. Therm. Anal. Cal.* 83 (**2006**) 533-539.

58. Matzat, E. *Acta. Cryst*. B28 (**1972**) 415-418.

59. Binev, I.G. Stamboliyska, B.A. Binev, Y.I. Velcheva, E.A. Tsenov, J.A. *Journal of Molecular Structure*. 513 (**1999**) 231-243.

60. Choudhury M. Zakaria. John N. Low. Christopher Glidewell. *Acta. Cryst*. C58 (**2002**) o9-o10

61. A. Staubitz, A.P.M. Robertson, I. Manners. *Chem. Rev*. 110 (**2010**) 4079.

62. Z. Huang, T. Autrey. *Energy Environ. Sci*. 5 (**2012**) 9257.

63. (a) M. Bowden, S.T. Autrey, I. Brown, M. Ryan, Curr. *Appl. Phys*. 8 (**2008**) 498; (b) W.J. Shaw, J.C. Linehan, N.K. Szymczak, D.J. Heldebrant, C. Yonker, D.M.Camaioni, R.T. Baker, T. Autrey, Angew. *Chem. Int. Ed. Engl*. 47 (**2008**) 7493.

64. (a) T.M. Douglas, A.B. Chaplin, A.S. Weller. *J. Am. Chem. Soc*. 130 (**2008**) 14432; (b) M.C. Denney, V. Pons, T.J. Hebden, D.M. Heinekey, K.I. Goldberg. *J. Am. Chem. Soc*. 128 (**2006**) 12048; (c) N. Blaquiere, S. Diallo-Garcia, S.I. Gorelsky, D.A. Black, K. Fagnou. *J. Am. Chem. Soc.* 130 (**2008**) 14034; (d) M.E. Sloan, A. Staubitz, T.J. Clark, C.A. Russell, G.C. Lloyd-Jones, I. Manners. *J. Am. Chem. Soc*. 132 (**2010**) 3831; (e) D.W. Himmelberger, C.W. Yoon, M.E. Bluhm, P.J. Carroll, L.G. Sneddon. *J. Am. Chem. Soc*. 131 (**2009**) 14101.

65. G. Chen, L.N. Zakharov, M.E. Bowden, A.J. Karkamkar, S.M. Whittemore, E.B.Garner, T.C. Mikulas, D.A. Dixon, T. Autrey, S.-Y. Liu. *J. Am. Chem. Soc*. 137 (**2015**) 134.

66. P.G. Campbell, L.N. Zakharov, D.J. Grant, D.A. Dixon, S.-Y. Liu. *J. Am. Chem. Soc.*132 (**2010**) 3289.

67. (a) W. Luo, P.G. Campbell, L.N. Zakharov, S.-Y. Liu. *J. Am. Chem. Soc*. 133 (**2011**) 19326; (b) W. Luo, D. Neiner, A. Karkamkar, K. Parab, E.B. Garner, D.A. Dixon, D. Matson,T. Autrey, S.-Y. Liu. *Dalton Trans*. 42 (**2013**) 611.

68. P.G. Campbell, J.S.A. Ishibashi, L.N. Zakharov, S.-Y. Liu. *Aust. J. Chem*. 67 (**2013**) 521.

69. Forrest, S. R.; Thompson, M. E. *Chem. Rev*. 107 (**2007**) 923.

70. (a) Bencini, A.; Lippolis, V. Coord. *Chem. Rev*. 256 (**2012**) 149; (b) Formica, M.; Fusi, V.; Giorgi, L.; Micheloni, M. Coord. *Chem. Rev*. 256 (**2012**) 170; (c) Wade, C. R.; Brooms grove, A. E. J.; Aldridge, S.; Gabbaï, F. P. *Chem. Rev*. 110 (**2010**) 3958.

71. (a) Hatakeyama, T.; Hashimoto, S.; Seki, S.; Nakamura, M. *J. Am. Chem. Soc*. 133 (**2011**) 18614; (b) Hatakeyama, T.; Hashimoto, S.; Oba, T.; Nakamura, M. *J. Am. Chem. Soc*. 134 (**2012**) 19600; (c) Wang, X.; Lin, H.; Lei, T.; Yang, D.; Zhuang, F.; Wang, J.; Yuan, S.; Pei, J. *Angew. Chem., Int. Ed*. 52 (**2013**) 3117; (d) Lepeltier, M.; Lukoyanova, O.; Jacobson, A.; Jeeva, S.; Perepichka, D. F. *Chem. Commun*. 46 (**2010**) 7007; (e) Zhou, Z.; Wakamiya, A.; Kushida, T.; Yamaguchi, S. *J. Am. Chem. Soc*. 134 (**2012**) 4529.

72. (a) Neue, B.; Araneda, J. F.; Piers, W. E.; Parvez, M. *Angew. Chem., Int. Ed*. 52 (**2013**) 9966; (b) Jaska, C. A.; Emslie, D. J. H.; Bosdet, M. J. D.; Piers, W. E.; Sorensen, T. S.; Parvez, M. *J. Am. Chem. Soc*. 128 (**2006**) 10885; (c) Bosdet, M. J. D.; Piers, W. E.; Sorensen, T. S.; Parvez, M. *Angew. Chem., Int. Ed*. 46 (**2007**) 4940; (d) Wisniewski, S. R.; Guenther, C. L.; Argintaru, O. A.; Molander, G. A. *J. Org. Chem*. 79 (**2014**) 365.

73. F. Sun; L. Lv; M. Huang; Z. Zhou; X. Fang. *Organic Letters*. 16 (**2014**) 5024-5027.

74. W. Luo, L.N. Zakharov, S.-Y. Liu. *J. Am. Chem. Soc*. 133 (**2011**) 13006.

75. S.G. Kukolich; M. Sun; A.M. Daly; W. Luo; L.N. Zakharov; Shih-Yuan Liu. *Chemical Physics Letters*. 639 (**2015**) 88-92.

76. A.M. Daly, C. Tanjaroon, A.J.V. Marwitz, S.-Y. Liu, S.G. Kukolich. *J. Am. Chem. Soc*. 132/15 (**2010**) 5501.

77. Abbey, E. R.; Zakharov, L. N.; Liu, S.-Y. *J. Am. Chem. Soc.* 130 (**2008**) 7250–7252.

78. Novick, S.E. *Journal of Molecular Spectroscopy*. 267 (**2011**) 13-18.

79. Kang, L.; Sunahori, F.; Minei, A. J.; Clouthier, D. J.; Novick, S. E. *J. Chem. Phys.* 130 (**2009**) 124317.

80. C. Tanjaroon, A. Daly, A.J.V. Marwitz, S.-Y. Liu, S. Kukolich. *J. Chem. Phys.* 131/22 (**2009**) 224312/1.

81. A. Konovalov, H. Mollendal, J.-C. Guillemin. *J. Phys. Chem. A*. 113/29 (**2009**) 8337.

82. D. Fujiang, P.W. Fowler, A.C. Legon. *J. Chem. Soc. Chem. Commun*. 1 (**1995**) 113.

83. Legon, A. C.; Warner, H. E. *J. Chem. Soc., Chem. Commun.* (**1991**) 1397–1399.

84. L.R. Thorne, R.D. Suenram, F.J. Lovas. *J. Chem. Phys*. 78/1 (**1983**) 167.

85. M. Sugie, H. Takeo, C. Matsumura. *Chem. Phys. Lett*. 64 (**1979**) 573.

86. Vormann, K.; Dreizler, H.; Doose, J.; Guarnieri, A. *Z. Naturforsch. A.* 46 (**1991**) 770–776.

87. F.J. Lovas, D.R. Johnson. *J. Chem. Phys*. 59 (**1973**) 2347.

88. T.S. Briggs, W.D. Gwinn, W.L. Jolly, L.R. Thorne. *J. Am. Chem. Soc*. 100 (**1978**) 7762.

89. Reeve, S. W.; Burns, W. A.; Lovas, F. J.; Suenram, R. D.; Leopold, K. R. *J. Phys. Chem.* 97 (**1993**) 10630–10637.

90. X. Fang; H. Yang; J.W. Kampf; M.M.B. Holl, A.J. Ashe III. *Organometallics*. 25 (**2006**) 513-518.

91. Rohr, A. D.; Kampf, J. W.; Ashe, A. J. III. *Organometallics*. 33 (**2014**) 1318.

92. S.G. Kukolich and L.C. Sarkozy. *Rev. Sci. Instrum.* 82 (**2011**) 094103; http://dx.doi.org/10.1063/1.3627489

93. Bohn, R. K.; Hillig, K. W., II; Kuczkowski, R. L. *J. Phys. Chem.* 93 (**1989**) 3456–3459.

94. P. O. Löwdin. *Adv. Quantum Chem*. 2 (**1965**) 213.

95. J. Catalan, M. Kasha*, J. Phys. Chem. A*. 104 (**2000**) 10812.

96. Daly, A. M.; Bunker, P. R.; Kukolich, S. G. *J. Chem. Phys*. 132/20 (**2010**) 201101/1.

97. Daly, A. M.; Bunker, P. R.; Kukolich, S. G. *J. Chem. Phys*. 133/7 (**2010**) 079903/1.

98. Daly, A. M.; Douglass, K. O.; Sarkozy, L. C.; Neill, J. L.; Muckle, M. T.; Zaleski, D. P.; Pate, B. H.; Kukolich, S. G. *J. Chem. Phys*. 135 (**2011**) 154304/1−154304/12.

99. Tayler, M. C. D.; Ouyang, B.; Howard, B. J. *J. Chem. Phys*. 134 (**2011**) 054316/1−054316/9.

100. Pejlovas, A.M. Barfield, Michael. Kukolich, Stephen G. *Chemical Physics Letters*. 613 (**2014**) 86-89.

101. Birer, O.; Havenith, M. *Annu. Rev. Phys. Chem*. 60 (**2009**) 263−275.

102. Rowe, W. F.; Duerst, R. W.; Wilson, E. B. *J. Am. Chem. Soc*. 98 (**1976**) 4021−4023.

103. Baughcum, S. L.; Duerst, R. W.; Rowe, W. F.; Smith, Z.; Wilson, E. B. *J. Am. Chem. Soc*. 103 (**1981**) 6296−6303.

104. Baughcum, S. L.; Smith, Z.; Wilson, E. B.; Duerst, R. W. *J. Am. Chem. Soc*. 106 (**1984**) 2260−2265.

105. Turner, P.; Baughcum, S. L.; Coy, S. L.; Smith, Z. *J. Am. Chem. Soc*. 106 (**1984**) 2265−2267.

106. K. Tanaka, H. Honjo, T. Tanaka, H. Kohguchi, Y. Ohshima, and Y. Endo. *J. Chem. Phys*. 110 (**1999**) 1969.

107. Keske, J. C.; Lin, W.; Pringle, W. C.; Novick, S. E.; Blake, T. A.; Plusquellic, D. F. *J. Chem. Phys*. 124 (**2006**) 074309.

108. R.W. Davis, A.G. Robiette, M.C.L. Gerry, E. Bjarnov, G. Winnewisser. *J. Mol. Spec*. 81 (**1980**) 93.

109. Kukolich, S. G.; Mitchell, E. G.; Carey, S. J.; Sun, M.; and Sargus, B. A. *J. Phys. Chem. A.* 117/39 (**2013**) 9525–9530.

110. A.M. Pejlovas, M. Barfield, S.G. Kukolich. *Journal of Physical Chemistry A*. 119 (**2015**) 1464-1468.

111. Z. Kisiel , < http://www.ifpan.edu.pl/~kisiel/struct/struct.htm#pmifst>

112. A.M. Pejlovas, O. Oncer, L. Kang, and S.G. Kukolich. *Journal of Molecular Spectroscopy*. 319 (**2016**) 26-29.

113. A.K. Chandra. Introductory Quantum Chemistry. 4th Ed. Tata McGraw-Hill Publishing Company Limited. (**1994**).

114. A. E. Bracamonte and P. H. Vaccaro. *J. Chem. Phys.* 120 (**2003**) 4638.

115. L. A. Burns, D. Murdock, and P. H. Vaccaro. *J. Chem. Phys.* 124 (**2006**) 204307.

116. D. Murdock, L. A. Burns, and P. H. Vaccaro. *J. Chem. Phys.* 127 (**2007**) 081101.

117. L. A. Burns, D. Murdock, and P. H. Vaccaro. *J. Chem. Phys*. 130 (**2009**) 144304.

118. D. Murdock, L. A. Burns, and P. H. Vaccaro. *Phys. Chem. Chem. Phys.* 12 (**2010**) 8285.

119. R. L. Redington, and T. E. Redington. *J. Mol. Spectrosc.* 78 (**1979**) 229.

120. R. L. Redington, and T. E. Redington. *J. Chem. Phys*. 122 (**2005**) 124304.

121. R. Rossetti, and L. E. Brus. *J. Chem. Phys.* 73 (**1980**) 1546.

122. Y. Tomioka, M. Ito, and N. Mikami. *J. Phys. Chem.* 87 (**1983**) 4401.

123. R. L. Redington. *J. Chem. Phys.* 113 (**2000**) 2319.

124. R. L. Redington, and R. L. Sams. *J. Phys. Chem. A.* 106 (**2002**) 7494.

125. R. L. Redington, T. E. Redington, and R. L. Sams. *J. Phys. Chem. A.* 110 (**2006**) 9633.

126. R. L. Redington, T. E. Redington, and R. L. Sams. *J. Phys. Chem. A.* 112 (**2008**) 1480.

127. H. Sekiya, T. Nakajima, H. Ujita, T. Tsuji, S. Ito, Y. Nishimura. *Chem. Phys. Lett*. 215 (**1993**) 499.

128. W. Lin, W. C. Pringle, S. E. Novick, T. A. Blake. *J. Phys. Chem. A.* 113 (**2009**) 13076.

129. J. C. Keske, and D. F. Plusquellic, International Symposium of Molecular Spectroscopy, TD10, Columbus, OH. (**2003**).

130. G. G. Brown, B. C. Dian, K. O. Douglass, S. M. Geyer, S. T. Shipman, and B. H. Pate. *Rev. Sci. Instrum*. 79 (**2008**) 053103. https://doi.org/10.1063/1.2919120

131. G. G. Brown, B. C. Dian, K. O. Douglass, S. M. Geyer, and B. H. Pate. *J. Mol. Spectrosc*. 238 (**2006**) 200. https://doi.org/10.1016/j.jms.2006.05.003

132. K. Prozument, Y. V. Suleimanov, B. Buesser, J. M. Oldham, W. H. Green, A. G. Suits, and R. W. Field. *J. Phys. Chem. Lett*. 5 (**2014**) 3641. https://doi.org/10.1021/jz501758p

133. C. Abeysekera, B. Joalland, N. Ariyasingha, L. N. Zack, I. R. Sims, R. W. Field, and A. G. Suits. *J. Phys. Chem. Lett*. 6 (**2015**) 1599. https://doi.org/10.1021/acs.jpclett.5b00519